

Equation of State of Superdense Matter
and
Neutron Star Properties

Dissertation

der Fakultät fuer Physik

der Ludwig-Maximilians-Universität München

vorgelegt von
Kwang Won Lee
aus Korea

20. März 1998

Gutachter: Prof. Dr. M. Weigel
Gutachter: Prof. Dr. V. Mukhanov
Tag der muendlichen Pruefung: 25. Juli 2000

Abstract

The behaviour of the equation of state of superdense matter is studied. The relativistic Hartree and Hartree-Fock approximations are introduced to determine the equation of state of dense baryonic matter in the relativistic Green's function approach. We find that the standard ground state, in which fields are occupied up to their Fermi momenta in momentum space, is unstable due to appearances of instability modes for pure neutron matter or asymmetric nuclear matter at high densities. In those systems a phase transition may occur from the standard ground state to a new stable ground state. However, for the system, which is composed of symmetric nuclear matter or in which baryons are in β -equilibrium with leptons, the standard ground state still remains stable. The results show that energetically the symmetrization process and β -equilibrium phase are favourable. The equations of state of superdense matter are also applied to calculate the physical properties of neutron stars. It is found that the phase transition for neutron matter or asymmetric nuclear matter has the small effects on the bulk properties of neutron stars at all densities.

Zusammenfassung

In dieser Arbeit wird das Verhalten der Zustandsgleichung superdichter Materie untersucht. Die relativistische Hartree und Hartree-Fock Naehierungen werden eingefuehrt, um die Zustandsgleichung dichter Baryonenmaterie im Formalismus der Greenschen Funktionen zu bestimmen. Wir finden, dass der Standardgrundzustand, in dem die Felder bis zum Fermi-Impuls im Impulsraum besetzt sind, instabil ist, aufgrund der Erscheinungen der Instabilitaet der reinen Neutronenmaterie oder der asymmetrischen Kernmaterie bei den hohen Dichten. In diesen Systeme koennte Phasenuebergang zu einem neuen stabilen Grundzustand auftreten. Aber fuer das System, das aus der symmetrischen Kernmaterie besteht oder in dem Baryonen im β -Gleichgewicht mit Leptonen sind, bleibt der Standardgrundzustand noch stabil. Die Resultate zeigen, dass der Prozess der Symmetrization und die β -Gleichgewichtsphase energetisch guenstig sind. Die Zustandsgleichungen superdichter Materie wird auch angewendet, um die physikalischen Eigenschaften der Neutronensterne zu berechnen. Dabei wurde gefunden, dass der Phasenuebergang der Neutronenmaterie oder der asymmetrischen Kernmaterie die geringen Auswirkungen auf die physikalischen Eigenschaften der Neutronensterne hat.

Contents

1	Introduction	6
2	Theory	8
2.1	Relativistic field equations	8
2.2	Propagator	9
2.3	Solution of the field equations	11
3	Model	15
3.1	Self-energy	15
3.2	The baryonic matter equation of state	17
3.3	The equation of state of lepton	19
3.4	Coupling constants of the Hartree-Fock approximation	21
4	Phase transition of superdense matter	22
4.1	Neutron matter	24
4.2	Asymmetric nuclear matter	26
5	Hadronic phase in β-equilibrium and quark matter phase	28
5.1	Hadronic Phase	28
5.2	Quark-Gluon Phase	33
6	Application to celestial objects	36
6.1	General theory of relativity	36
6.2	Non-rotating neutron star	36
6.3	Rotating neutron star	37
6.3.1	Perturbation solution	38
6.3.2	Kepler frequency	41
6.4	Matter in neutron star	43
6.5	Neutron star properties	46
6.5.1	Non-rotating neutron star	46
6.5.2	Rotating neutron star	47
7	Summary	49
A	Appendix A	50
B	Appendix B	64
C	Appendix C	72
D	Appendix D	75

1 Introduction

The equation of state is the basic quantity for determining the physical evolution of a system. Particularly the equation of state of nuclear matter provides detailed understanding for the stellar structure and evolution. The equation of state below neutron drip[1], where $\rho_{drip} \approx 4.3 \times 10^{11} g/cm^3$, and at densities above neutron drip but below the saturation density of nuclear matter[2] is relatively well known. But the physical properties of matter at high densities, above the saturation density($\rho_0 \approx 2.5 \times 10^{14} g/cm^3$), are still uncertain and the associated equation of state is only poorly understood[3]. The determination of the equation of state of superdense baryonic matter is one of the most challenging problems in modern physics [4,5,6,30,31,32]. Such superdense matter is encountered in high-energy heavy ion reactions and in the interior of the compact stars. For instance, a neutron star has a diameter of only 10 – 15km but has the same mass as the sun, resulting in a central density, which may be as dense as $10^{14} g/cm^3$. Since it is impossible to mimic such densities in a terrestrial laboratory over a time period large in comparison with the characteristic time of the weak interaction(= $10^{-12} sec$), one is confronted in so-called neutron stars with exotic matter, i.e. so-called neutron star matter, which is rather asymmetric and has to obey the constraints of charge neutrality and generalized β -equilibrium. The simplest model for a description of this kind of matter is pure neutron matter. For a more improved description of neutron star matter(NSM), which gives lower energies, one has used either the relativistic Hartree- or Hartree-Fock approximation[7], where NSM consists of neutrons, protons, and leptons in β -equilibrium. So far one has used in this scheme the standard assumption that the particles fill the states up to their corresponding Fermi momenta. However, it has been suggested by Horowitz and Serot that a phase transition occurs for pure neutron matter at high densities in the relativistic Hartree-Fock-approximation[8]. Such a phase transition, as already described in another context by Landau and Lifschitz, is characterized by a redistribution of the occupation, replacing the standard Fermi sphere by shell structure, which leads to a lower energy state. A former investigation, in which very simplified dynamics was used, which is not realistic for asymmetric systems, has found such an effect[8,9]. It is one of the main aims of this investigation to reexamine the situation for more realistic Lagrangian and compositions, and to study the possibility of such a phase transition and to investigate further possible impacts on the properties of neutron stars. The basic input quantity, whose knowledge is necessary in order to solve the stellar structure equations for neutron stars, is the equation of state, i.e. the functional dependence of pressure on density, $P(\epsilon)$. For neutron stars the density of matter spans an enormous range, from high densities of $\rho \approx (10 - 20)\rho_0$ in the core down to zero at the star's edge. But the star's atmosphere is so thin that the crust of neutron stars contributes negligibly to the bulk properties of the stars like mass, radius, and moment of inertia[10]. Most of the bulk properties of neutron stars are sensitive to the equation of state at high densities above neutron drip. For that reason the high density part of the equation of state plays the decisive role in deter-

mining the physical properties of neutron stars. Physically the phases and the chemical compositions of a system must change as the density increases. Such changes have the effects on the fundamental interactions and the equations of state. For instance, in the neutron stars, depending on the star's central densities, the phase transition may occur to form the new phases from pure neutron matter. For pure neutron matter or asymmetric nuclear matter without leptons, one of the possible phase transitions may be forming a new stable ground state, shell distribution of the states, in momentum space. However, the possibility of such phase transition is relatively weak because of appearances of the unphysical phenomena at high densities, above critical density. Instead, in the cores of neutron stars, the phase may be rather an electrically charged neutral system of either interacting baryons and/or quarks in generalized β -equilibrium with leptons. In β -equilibrium phase, other ingredients soften the equation of state considerably at all densities. This behaviour of the equation of state has direct impacts on the properties of neutron stars. Another interesting issue is the formation of quark matter in the cores of neutron stars. Since a phase transition of hadronic matter to the quark-gluon phase has been suggested[26], in the cores of neutron stars such a phase transition is predicted by a theory(see Ref.[3] for a proper discussion of the phase transition in neutron stars). But the critical density at which the phase transition might occur is still poorly understood. Recently, concerning the interpretation of pulsars, which are accepted as fast rotating neutron stars, the quark matter phase in the cores of neutron stars and the pure quark stars are also suggested[3]. One of the recent reports related to these issues suggests that such a phase transition may be detected from observations of the changes of the pulsar's bulk properties at critical density[12]. The neutron star bulk properties, which are determined by theories, depend on the equation of state taken into account. In return, the pulsar's bulk properties estimated from observations, particularly the mass of neutron stars and rotational frequency of fast pulsars, constrain the equation of state at high densities. As a result the improved astronomical observations provide better understanding of the fundamental interactions and the physical properties of superdense matter. This work is organized as follows. In Chapter 2 and 3 the treatment of the many-body problems in the framework of the relativistic Green's function method is summarized. In Chapter 4 we discuss the phase transition from the spherical distribution to the shell distribution in the ground state. Baryon phase in generalized β -equilibrium with leptons is discussed in Chapter 5. In Chapter 5 the numerical results for quark-gluon phase in the nuclear domain are shown. In Chapter 6 we discuss neutron star matter and the physical properties of neutron stars. A summary is given in Chapter 7. In Appendix the numerical results, which are graphically depicted, are listed for the properties of neutron matter (Appendix A), asymmetric nuclear matter (Appendix B), and the properties of non-rotating (Appendix C) and rotating (Appendix D) neutron stars.

2 Theory

In the framework of quantum field theory we have studied the equation of state of superdense matter. In this system superdense baryonic matter and free leptons are in β -equilibrium. Baryons interact with each other through the exchange of mesons. The most important contribution comes from the exchange of $\pi(J^\pi, T = 0^-, 1), \sigma(0^+, 0), \omega(1^-, 0)$, and $\rho(1^-, 1)$ mesons [cf. Table 3.4].

2.1 Relativistic field equations

Dynamics of the system is determined by Hamilton's principle[11]

$$\delta \int L(x) d^4x = 0 \quad (2.1)$$

where $L(x)$ is the Lagrangian density. Hamilton's principle, Eq.(2.1), yields the Euler-Lagrange equation for field $\psi(x)$:

$$\frac{\partial}{\partial x^\mu} \left(\frac{\partial L(x)}{\partial (\frac{\partial \psi(x)}{\partial x^\mu})} \right) - \frac{\partial L(x)}{\partial \psi(x)} = 0. \quad (2.2)$$

The Lagrangian density for the present model has the form[3]

$$L(x) = \sum_{B=p,n} L_B^0(x) + \sum_{M=\sigma,\omega,\pi,\rho} L_M^0(x) + \sum_{B=p,n} \sum_{M=\sigma,\omega,\pi,\rho} L_{BM}(x). \quad (2.3)$$

The full Lagrangian density is given by [13,3]

$$\begin{aligned} L(x) = & \sum_{B=p,n} \bar{\psi}_B(x) (i\gamma^\mu \partial_\mu + g_\sigma \sigma(x) - g_\omega \gamma^\mu \omega_\mu(x) - \frac{f_\omega}{4m_B} \sigma^{\mu\nu} F_{\mu\nu}(x) \\ & - \frac{f_\pi}{m_\pi} \gamma^5 \gamma^\mu (\partial_\mu \vec{\tau} \vec{\pi}(x)) - g_\rho \gamma^\mu \vec{\tau} \vec{\rho}_\mu(x) - \frac{f_\rho}{4m_B} \sigma^{\mu\nu} \vec{\tau} \vec{G}_{\mu\nu}(x)) \psi_B(x) + \\ & \frac{1}{2} (\partial^\mu \sigma(x) \partial_\mu \sigma(x) - m_\sigma^2 \sigma^2(x)) - \frac{1}{4} F^{\mu\nu}(x) F_{\mu\nu}(x) + \frac{1}{2} m_\omega^2 \omega^\nu(x) \omega_\nu(x) + \\ & \frac{1}{2} (\gamma^\mu \vec{\pi}(x) \gamma_\mu \vec{\pi}(x) - m_\pi^2 \vec{\pi}(x) \vec{\pi}(x)) - \frac{1}{4} \vec{G}^{\mu\nu}(x) \vec{G}_{\mu\nu}(x) + \frac{1}{2} m_\rho^2 \vec{\rho}^\mu(x) \vec{\rho}_\mu(x). \end{aligned} \quad (2.4)$$

The tensor fields $F_{\mu\nu}(x)$ and $\vec{G}_{\mu\nu}(x)$ of Eq.(2.4) are defined by

$$F_{\mu\nu}(x) = \partial_\mu \omega_\nu(x) - \partial_\nu \omega_\mu, \quad \vec{G}_{\mu\nu}(x) = \partial_\mu \vec{\rho}_\nu(x) - \partial_\nu \vec{\rho}_\mu(x). \quad (2.5)$$

The quantity $\sigma^{\mu\nu}$ in Eq.(2.4) is defined by [14]

$$\sigma^{\mu\nu} = \frac{i}{2} [\gamma^\mu, \gamma^\nu] \quad (2.6)$$

where γ^μ denotes the Dirac matrices.

From the Euler-Lagrange equation, Eq.(2.2), and Lagrangian density, Eq.(2.4), the field equations for baryons and mesons are given by

$$\begin{aligned} (i\gamma^\mu \partial_\mu - m_B) \psi_B(x) = & -g_\sigma \psi_B(x) \sigma(x) + g_\omega \gamma^\mu \omega_\mu(x) \psi_B(x) + \\ & \frac{f_\omega}{4m_B} \sigma^{\mu\nu} F_{\mu\nu}(x) \psi_B(x) - \frac{f_\pi}{m_\pi} \gamma^5 \gamma^\mu (\partial_\mu \vec{\tau} \vec{\pi}(x)) \psi_B(x) + \\ & g_\rho \gamma^\mu \vec{\tau} \vec{\rho}_\mu(x) \psi_B(x) + \frac{f_\rho}{4m_B} \sigma^{\mu\nu} \vec{\tau} \vec{G}_{\mu\nu}(x) \psi_B(x), \end{aligned} \quad (2.7)$$

$$(\partial^\mu \partial_\mu + m_\sigma^2)\sigma(x) = \sum_{B=p,n} g_\sigma \bar{\psi}_B(x)\psi_B(x), \quad (2.8)$$

$$\begin{aligned} \partial^\mu F_{\mu\nu}(x) + m_\omega^2 \omega^\nu(x) &= \sum_{B=p,n} g_\omega \bar{\psi}_B(x)\gamma^\nu \psi_B(x) - \\ \sum_{B=p,n} \frac{f_\omega}{2m_B} \partial^\mu (\bar{\psi}_B(x)\sigma_{\mu\nu}\psi_B(x)), \end{aligned} \quad (2.9)$$

$$(\partial^\mu \partial_\mu + m_\pi^2)\vec{\pi}(x) = \sum_{B=p,n} \frac{f_\pi}{m_\pi} \partial^\mu (\bar{\psi}_B(x)\gamma_5 \gamma_\mu \vec{\tau}\psi_B(x)), \quad (2.10)$$

$$\begin{aligned} \partial^\mu \vec{G}_{\mu\nu}(x) + m_\rho^2 \vec{\rho}_\nu(x) &= \sum_{B=p,n} g_\rho \bar{\psi}_B(x)\vec{\tau}\gamma_\nu \psi_B(x) - \\ \sum_{B=p,n} \frac{f_\rho}{2m_B} \gamma^\mu (\bar{\psi}_B(x)\vec{\tau}\sigma_{\mu\nu}\psi_B(x)). \end{aligned} \quad (2.11)$$

2.2 Propagator

Before we solve the field equations, (2.7)-(2.11), we define the propagators for baryons and mesons respectively.

The $2n$ -point Green's function is defined by the ground state expectation value of the time ordered product of the baryon field operators ψ_B , in the form [15,16,33]

$$\begin{aligned} G_{\xi_1 \dots \xi_n \xi'_1 \dots \xi'_n}(x_1, \dots, x_n; x'_1, \dots, x'_n) &= \\ (i)^n \langle \phi_0 | T(\psi_{\xi_1}(x_1) \dots \psi_{\xi_n}(x_n) \bar{\psi}_{\xi'_1}(x'_1) \dots \bar{\psi}_{\xi'_n}(x'_n)) | \phi_0 \rangle. \end{aligned} \quad (2.12)$$

The quantity $|\phi_0\rangle$ denotes the ground state of infinite matter. The symbols $(\xi_1 \dots \xi_n)$ stand for spin-isospin quantum numbers of baryons B_1, \dots, B_n . The quantity T stands for the time-ordering operator. For the calculation of the properties of the many-body system the two-point Green's function, $G_{\xi\xi'}(x, x')$, is sufficient. It is convenient to decompose the two-point Green's function in the following way:

$$G_{\xi\xi'}^{BB'}(x, x') = i \langle \phi_0 | T(\psi_\xi^B(x) \bar{\psi}_{\xi'}^{B'}(x')) | \phi_0 \rangle \quad (2.13)$$

$$= \theta(x_0 - x'_0) G_{>}^{BB'}(x, \xi : x', \xi') + \theta(x'_0 - x_0) G_{<}^{BB'}(x, \xi : x', \xi'). \quad (2.14)$$

Here the auxiliary Green's functions $G_{>}$ and $G_{<}$ are given by

$$G_{>}^{BB'}(x, \xi : x', \xi') = i \langle \psi_\xi^B(x) \bar{\psi}_{\xi'}^{B'}(x') \rangle, \quad (2.15)$$

$$G_{<}^{BB'}(x, \xi : x', \xi') = -i \langle \bar{\psi}_{\xi'}^{B'}(x') \psi_\xi^B(x) \rangle. \quad (2.16)$$

The Heaviside's step function is defined by

$$\theta(x_0 - x'_0) = \frac{i}{2\pi} \int \frac{e^{-i\omega(x_0 - x'_0)}}{\omega + i\eta} d\omega. \quad (2.17)$$

From the Fourier transformation

$$g(x) = \frac{1}{(2\pi)^4} \int g(p) e^{-ipx} d^4p \quad (2.18)$$

$$g(p) = \int g(x) e^{ipx} d^4x \quad (2.19)$$

the momentum space representation of the Green's function can be written in the form [7,16,17]:

$$G_{\xi\xi'}^B(p) = \int \frac{a_{\xi\xi'}^{B'}(\omega, \vec{p})}{\omega - (p^0 - \mu_B)(1+i\eta)}. \quad (2.20)$$

Here the quantity μ_B denotes the chemical potential of baryons of type B . The spectral function $a_{\xi\xi'}^{B'}(\omega, \vec{p})$ of Eq.(2.20) is given by the cut of the analytically continued propagator, $\tilde{G}_{\xi\xi'}^B(z, \vec{p})$, along the real axis.

It is written by

$$\tilde{G}_{\xi\xi'}^B(z, \vec{p}) = \int \frac{a_{\xi\xi'}^{B'}(\omega, \vec{p})}{\omega - z} d\omega. \quad (2.21)$$

Using the relation

$$\frac{1}{x \pm i\eta} = \frac{P}{x} \mp \pi\delta(x) \quad (2.22)$$

the spectral function $a_{\xi\xi'}^{B'}(\omega, \vec{p})$ can be rewritten as

$$a_{\xi\xi'}^B(\omega, \vec{p}) = \frac{\tilde{G}_{\xi\xi'}^{B'}(\omega+i\eta, \vec{p}) - \tilde{G}_{\xi\xi'}^{B'}(\omega-i\eta, \vec{p})}{2\pi i}. \quad (2.23)$$

The two-point Green's function for mesons are defined analogously to Eq.(2.13) in the following:

For σ -meson:

$$\Delta(x, x') = i \langle \phi_0 | T(\sigma(x)\sigma(x')) | \phi_0 \rangle. \quad (2.24)$$

For ω -meson:

$$\Delta^{\mu\nu}(x, x') = i \langle \phi_0 | T(\omega^\mu(x)\omega^\nu(x')) | \phi_0 \rangle. \quad (2.25)$$

For π -meson:

$$\Delta_{rr'}(x, x') = i \langle \phi_0 | T(\pi_r(x)\pi_{r'}(x')) | \phi_0 \rangle. \quad (2.26)$$

For ρ -meson:

$$\Delta_{rr'}^{\mu\nu}(x, x') = i \langle \phi_0 | T(\rho_r^\mu(x)\rho_{r'}^\nu(x')) | \phi_0 \rangle. \quad (2.27)$$

The momentum space representation of the propagators of mesons are given in the form:

For σ -meson:

$$\Delta^0(p) = -\frac{1}{p^2 - m_\sigma^2 + i\eta}. \quad (2.28)$$

For ω -meson:

$$\Delta_{\mu\nu}^0(p) = (g_{\mu\nu} - \frac{P_\mu P_\nu}{m_\omega^2}) (-\frac{1}{p^2 - m_\omega^2 + i\eta}). \quad (2.29)$$

For π -meson:

$$\Delta_{rr'}^0(p) = -\delta_{rr'} \frac{1}{p^2 - m_\pi^2 + i\eta}. \quad (2.30)$$

For ρ -meson:

$$\Delta_{\mu\nu,rr'}^0(p) = \delta_{rr'} (g_{\mu\nu} - \frac{P_\mu P_\nu}{m_\rho^2}) (-\frac{1}{p^2 - m_\rho^2 + i\eta}). \quad (2.31)$$

Here $r = 1, 2, 3$ refers to isospin indices.

2.3 Solution of the field equations

From the definition of the Green's function the Eq.(2.7) may be written in the form:

$$G_1^{0B}(1, 1') = G_1^{0B}(1, 1') + i \int G_1^{0B}(1, 1'') \langle 1'' 2 | v^{BB'} | 34 \rangle G_2^{B'B}(34, 2+1'). \quad (2.32)$$

Here integers $1 \equiv (x_1^0, \vec{x}_1; \xi_1), \dots, n \equiv (x_n^0, \vec{x}_n; \xi_n)$ stand for the space-time coordinates (denoted by $x_1 = (x_1^0, \vec{x}_1), \dots, x_n = (x_n^0, \vec{x}_n)$) as well as the spin-isospin quantum number (ξ_1, \dots, ξ_n) of baryons B_1, \dots, B_n . The quantity G_1^0 denotes the free two-point baryon propagator which satisfies

$$G_1^{0B}(x - x')_{\xi\xi'}^{-1} = (-i\gamma^\mu \partial_\mu + m_B)_{\xi\xi'} \delta^4(x - x'). \quad (2.33)$$

The quantity $v^{BB'}$ is a two-body potential term and it contains the baryon-meson vertices. The matrix elements of $v^{BB'}$ are given by[3]:

$$\langle 12 | v^{BB'} | 34 \rangle \equiv \sum_{M=\sigma, \omega, \pi, \rho} \langle 12 | V_M^{BB'} | 34 \rangle \quad (2.34)$$

$$\equiv \sum_{M=\sigma, \omega, \pi, \rho} \delta^4(x_1 - x_3) \delta^4(x_2 - x_4) \Gamma_{\xi_1 \xi_3}^{M:B} \Gamma_{\xi_2 \xi_4}^{M:B'} \Delta_M^0(x_1, x_2). \quad (2.35)$$

The function Δ_M^0 in Eq.(2.35) is the single particle propagator of free meson fields of type M . The scalar, pseudo-vector, and vector meson-baryon vertices $\Gamma^{M:B}$ of Eq.(2.35) are given respectively by:

$$\Gamma_{\xi_1 \xi_3}^{\sigma:B} = i g_\sigma \delta_{\xi_1 \xi_3} \text{ (scalar)}, \quad (2.36)$$

$$\Gamma_{\xi_1 \xi_3}^{\pi:B} = -i \frac{f_\pi}{m_\pi} (i \gamma_5 \gamma_\mu \partial_1^\mu)_{\xi_1 \xi_3} \text{ (pseudo-vector)}, \quad (2.37)$$

$$\Gamma_{\xi_1 \xi_3}^{\omega, \rho:B} = (g_{\omega, \rho} \gamma_\mu + \frac{i}{2} \frac{f_{\omega, \rho}}{2m_{\omega, \rho}} \partial^\kappa [\gamma_\kappa, \gamma_\mu])_{\xi_1 \xi_3} \text{ (vector)}. \quad (2.38)$$

By introducing the reducible T-matrix in the form [3,13]

$$\int_{3,4:B'} \langle 12|v^{BB'}|34 \rangle G_2^{B'B}(34,1'2') = \int_{3,4:B'} \langle 12|T^{BB'}|34 \rangle G_1^{B'}(3,1')G_1^B(4,2'), \quad (2.39)$$

and the mass operator (self-energy) Σ

$$\Sigma^B(1,2) = -i \int_{3,4:B'} \langle 13|T^{BB'}|42 \rangle G_1^{B'}(4,3^+), \quad (2.40)$$

equation (2.32) leads to the Dyson's equation

$$G_1^B(1,1') = G_1^{0B}(1,1') - \int_{3,4} G_1^{0B}(1,3)\Sigma^B(3,4)G_1^B(4,1'), \quad (2.41)$$

whereby we introduce the notation $\int_{1:B} \equiv \sum_B \int d^4x_1$.

Equivalently the momentum-space representation of the Dyson's equation is given by:

$$(\gamma^\mu P_\mu - m_B - \Sigma^B(p))_{\xi_1\xi_3} G_1^B(p)_{\xi_3\xi_2} = -\delta_{\xi_1\xi_2}. \quad (2.42)$$

For each baryon of type B , the corresponding Green's function \tilde{G}^B of Eq.(2.21) solves the analytically continued Dyson equation following from Eq.(2.42) ($\hat{p} \equiv \frac{\vec{p}}{|\vec{p}|}$):

$$[(m_B + \tilde{\Sigma}_s^B(z, \vec{p})) + (|\vec{p}| + \tilde{\Sigma}_v^B(z, \vec{p}))\vec{\gamma}\hat{p} + (\tilde{\Sigma}_0^B(z, \vec{p}) + (z + \mu^B))\gamma^0]\tilde{G}^B(z, \vec{p}) = 1. \quad (2.43)$$

In Eq.(2.43), Σ^B has been decomposed into a scalar, vector, and time-like part according to

$$\Sigma_{\xi\xi'}^B = \Sigma_s^B(1)_{\xi\xi'} + \Sigma_v^B(\vec{\gamma}\hat{p})_{\xi\xi'} + \Sigma_0^B\gamma_{\xi\xi'}^0. \quad (2.44)$$

By means of Cauchy's integral formular one can derive the spectral representation for $\tilde{\Sigma}$ [3]:

$$\tilde{\Sigma}_{\xi\xi'}^B(z, \vec{p}) = \Sigma_{\xi\xi'}^{B(\infty)} + \int \frac{\sigma_{\xi\xi'}^B(\omega, \vec{p})}{\omega - z} d\omega \quad (2.45)$$

where

$$\Sigma_{\xi\xi'}^{B(\infty)} = (\gamma_\mu p^\mu - m_B)_{\xi\xi'}. \quad (2.46)$$

From Eq.(2.45) one derives for the real and imaginary part of $\tilde{\Sigma}^B$:

$$Re\tilde{\Sigma}(\omega + i\eta, \vec{p}) = Re\tilde{\Sigma}(\omega - i\eta, \vec{p}), \quad (2.47)$$

$$Im\tilde{\Sigma}(\omega + i\eta, \vec{p}) = -Im\tilde{\Sigma}(\omega - i\eta, \vec{p}). \quad (2.48)$$

Note that the unitary matrix of Eq.(2.44) consists of the Dirac and an isospin part. It therefore has the explicit form

$$(1)_{\xi\xi'} \equiv (1^{Dirac} \otimes 1^{iso})_{\xi\xi'} = \delta_{\alpha\alpha'} \delta_{ii'} \quad (2.49)$$

where ξ, ξ' denote the spin (α, α') and isospin (i, i') indices, i.e. $\xi = (\alpha, i)$ and $\xi' = (\alpha', i')$.

Inversion of Eq.(2.43) yields[7]

$$\tilde{G}^B(z, \vec{p}) = \frac{(m_B + \tilde{\Sigma}_s^B(z, \vec{p})) - (|\vec{p}| + \tilde{\Sigma}_v^B(z, \vec{p}))\vec{\gamma}\hat{p} - (\tilde{\Sigma}_0^B(z, \vec{p}) + (z + \mu^B))\gamma^0}{(m_B + \tilde{\Sigma}_s^B(z, \vec{p}))^2 + (|\vec{p}| + \tilde{\Sigma}_v^B(z, \vec{p}))^2 - (\tilde{\Sigma}_0^B(z, \vec{p}) + (z + \mu^B))^2}. \quad (2.50)$$

The physical baryon propagators G^B and baryon self energy Σ^B are connected to the analytically continued functions \tilde{G}^B and $\tilde{\Sigma}^B$ by the following boundary values ($j = s, v, 0$):

$$G_{\xi\xi'}^B(p) = \tilde{G}_{\xi\xi'}^B((p^0 - \mu^B)(1 + i\eta), \vec{p}), \quad (2.51)$$

$$\Sigma_{j\xi\xi'}^B(p) = \tilde{\Sigma}_{j\xi\xi'}^B((p^0 - \mu^B)(1 + i\eta), \vec{p}). \quad (2.52)$$

From Eq.(2.48) and Eq.(2.52) one finds

$$Im\tilde{\Sigma}_{j\xi\xi'}^B(\omega - \mu^B \pm i\eta, \vec{p}) = \mp sgn(\mu^B - \omega)\Gamma_{\xi\xi'}^B(\omega, \vec{p}). \quad (2.53)$$

The self-energy Σ_j^B is split into its real and imaginary parts, denoted by Λ_j^B and Γ_j^B respectively. The latter quantities define the following function[13,16]:

$$\Gamma^B(\omega, \vec{p}) = 2(\Gamma_s^B(\omega, \vec{p})[m_B + \Lambda_s^B(\omega, \vec{p})] + \Gamma_v^B(\omega, \vec{p})[|\vec{p}| + \Lambda_v^B(\omega, \vec{p})] - \Gamma_0^B(\omega, \vec{p})[\Lambda_0^B(\omega, \vec{p}) - \omega]). \quad (2.54)$$

In the case of the Hartree-Fock the imaginary part of Σ^B vanishes[13], and therefore $\Gamma^B(\omega, \vec{p}) \rightarrow 0$. Eqs.(2.50)-(2.54) lead to a spectral function of single-particle structure,

$$a^B(\omega, \vec{p}) = \delta[D^B(\omega + \mu^B, \vec{p})sgn[-\omega\tilde{\Gamma}^B(\omega + \mu^B)]][[m_B + \Lambda_s^B(\omega, \vec{p})] - [|\vec{p}| + \Lambda_v^B(\omega, \vec{p})]\vec{\gamma}\hat{p} - [\Lambda_0^B(\omega, \vec{p}) - \omega]\gamma^0], \quad (2.55)$$

with the definition

$$D^B(\omega, \vec{p}) = [m_B + \Lambda_s^B(\omega, \vec{p})]^2 + [|\vec{p}| + \Lambda_v^B(\omega, \vec{p})]^2 - [\Lambda_0^B(\omega, \vec{p}) - \omega]^2. \quad (2.56)$$

Eq.(2.55) can be decomposed into a baryon and an anti-baryon part. We neglect the anti-baryon part. The spectral function is rewritten by[13]

$$a_{\xi\xi'}^B(\omega, \vec{p}) = \delta(\omega + \mu^B - \omega^B(\vec{p}))a_{\xi\xi'}^B(\vec{p}) \quad (2.57)$$

with

$$a_{\xi\xi'}^B(\vec{p}) = \frac{(m_B + \Sigma_s^B)(1)_{\xi\xi'} - (|\vec{p}| + \Sigma_v^B)(\vec{\gamma}\hat{p})_{\xi\xi'} + (\omega^B(\vec{p}) - \Sigma_0^B)\gamma_{\xi\xi'}^0}{|\frac{\partial D^B(\omega, \vec{p})}{\partial \omega}|_{\omega=\omega^B(\vec{p})}} \quad (2.58)$$

$$\equiv a_s^B 1_{\xi\xi'} + a_v^B (\vec{\gamma}\hat{p})_{\xi\xi'} + a_0^B \gamma_{\xi\xi'}^0. \quad (2.59)$$

The derivative of the function D^B follows immediately from Eq.(2.56):

$$\frac{\partial D^B(\omega, \vec{p})}{\partial \omega} = 2[[m_B + \Sigma_s^B(\omega, \vec{p})] \frac{\partial \Sigma_s^B}{\partial \omega} + [|\vec{p}| + \Sigma_v^B(\omega, \vec{p})] \frac{\partial \Sigma_v^B}{\partial \omega} + [\Sigma_0^B(\omega, \vec{p}) - \omega](1 - \frac{\partial \Sigma_0^B}{\partial \omega})]. \quad (2.60)$$

The baryon energy-momentum relation in matter is given by the zeros of Eq.(2.56),

$$\omega^B(\vec{p}) = \Sigma_0^B(\omega, \vec{p}) + \sqrt{[m_B + \Sigma_s^B(\omega, \vec{p})]^2 + [|\vec{p}| + \Sigma_v^B(\omega, \vec{p})]^2}. \quad (2.61)$$

The chemical potentials of baryons having Fermi momenta $P_{F:B}$ are obtained from

$$\mu^B = \omega^B(p_{F:B}). \quad (2.62)$$

In the non-interacting case one has $\Sigma \equiv 0$, and then Eq.(2.57) and (2.61) are written by

$$\omega^B(\vec{p}) = \sqrt{m_B^2 + \vec{p}^2}, \text{ and } a^B(\vec{p}) = (\omega^B(\vec{p})\gamma^0 - \vec{\gamma}\cdot\vec{p} + m_B)/(2\omega^B(\vec{p})). \quad (2.63)$$

In the non-relativistic treatment the self-energies of Eq.(2.44) is given by[18]:

$$\Sigma_s(p) \rightarrow 0, \Sigma_v(p) \rightarrow 0, \Sigma_0(p) \rightarrow \Sigma(p) \quad (2.64)$$

which leads to the replacements

$$m_B^* \rightarrow m_B, p^* \rightarrow p, W \rightarrow \sqrt{m_B^2 + \vec{p}^2} \approx m_B + \frac{\vec{p}^2}{2m_B}. \quad (2.65)$$

The relativistic energy-momentum relation of Eq.(2.61) is to be replaced by

$$\omega^B(\vec{p}) \rightarrow \omega^B(\vec{p}) - m_B \equiv E^B(\vec{p}) = \frac{\vec{p}^2}{2m_B} + \Sigma(E^B(\vec{p}) - \mu^B, \vec{p}). \quad (2.66)$$

The spectral function $a^B(\vec{p})$ of Eq.(2.57) plays the role of a momentum density function, i.e.

$$a^B(p^0, \vec{p}) = n^B(|\vec{p}|) \delta(p^0 - E^B(\vec{p}) + \mu^B), \quad (2.67)$$

with

$$n^B(|\vec{p}|) \equiv |1 - \frac{\partial \Sigma}{\partial \omega}|_{\omega^B = E^B(\vec{p})}^{-1}. \quad (2.68)$$

3 Model

Here we apply the Hartree-Fock model to the determination of self-energy. The anti-symmetrized Hartree-Fock T-matrix has the form [13,3]

$$\langle 12|T^{HF,BB'}|34\rangle = \langle 12|v^{BB'}|34\rangle - \langle 12|v^{BB'}|43\rangle \quad (3.1)$$

where the first and second term refer to the direct (i.e. Hartree) and exchange (Fock) contribution respectively. This leads for the baryon self-energy of Eq.(2.40) to the following Hartree ($\Sigma^{H,B}$) and Fock ($\Sigma^{F,B}$) terms

$$\Sigma^{H,B}(1,1') = i \sum_{B'} \langle 12|v^{BB'}|1'3\rangle G_1^{B'}(3,2^+), \quad (3.2)$$

$$\Sigma^{F,B}(1,1') = i \sum_{B'} \langle 12|v^{BB'}|31'\rangle G_1^{B'}(3,2^+) \quad (3.3)$$

which give the total contribution:

$$\Sigma^{HF,B}(1,1') = \Sigma^{H,B}(1,1') + \Sigma^{F,B}(1,1'). \quad (3.4)$$

3.1 Self-energy

The self-energies arising from σ , ω , π , and ρ -meson after a lengthy calculation are given by

$$\Sigma_{\xi_1\xi'_1}^{H,B}(p)|_\sigma = -i\delta_{\xi_1\xi'_1}\Delta^0(0)g_\sigma^2 \sum_{B'} \int_{q^4} e^{iq^0} \delta_{\xi_2\xi_3} G_{\xi_3\xi_2}^{B'}(q), \quad (3.5)$$

$$\Sigma_{\xi_1\xi'_1}^{F,B}(p)|_\sigma = ig_\sigma^2 \int_{q^4} e^{iq^0} \Delta^0(p-q)(1 \otimes G^B(q) \otimes 1)_{\xi_1\xi'_1}, \quad (3.6)$$

$$\Sigma_{\xi_1\xi'_1}^{H,B}(p)|_\omega = i\gamma_{\xi_1\xi'_1}^\mu \Delta_{\mu\nu}^0(0)g_\omega^2 \sum_{B'} \int_{q^4} e^{iq^0} Tr(\gamma^\nu G^{B'}(q)), \quad (3.7)$$

$$\Sigma_{\xi_1\xi'_1}^{F,B}(p)|_\omega = -ig_\omega^2 \int_{q^4} e^{iq^0} \gamma_{\xi_1\xi_3}^\mu \Delta_{\mu\nu}^0(p-q)G_{\xi_3\xi_2}^B(q)\gamma_{\xi_2\xi'_1}^\nu, \quad (3.8)$$

$$\Sigma_{\xi_1\xi'_1}^{H,B}(p)|_\pi = 0, \quad (3.9)$$

$$\begin{aligned} & \Sigma_{\xi_1\xi'_1}^{F,B}(p)|_\pi = \\ & i\left(\frac{f_\pi}{m_\pi}\right)^2 \int_{q^4} e^{iq^0} (\gamma_5\gamma\nu)_{\xi_1\xi_3}(p-q)^\mu(p-q)^\nu \Delta^0(p-q)G_{\xi_3\xi_2}^B(q)(\gamma_5\gamma\nu)_{\xi_2\xi'_1}, \end{aligned} \quad (3.10)$$

$$\begin{aligned} & \Sigma_{\xi_1\xi'_1}^{H,B}(p)|_\rho = i \sum_{B'} \int_{q^4} e^{iq^0} (g_\rho\gamma_\mu - i\frac{f_\rho}{2m_B}(p-q)^\lambda\sigma_{\lambda\mu})_{\xi_1\xi'_1} \Delta^{0,\mu\nu}(0) \\ & Tr[(g_\rho\gamma_\nu + i\frac{f_\rho}{2m_B}(p-q)^\kappa\sigma_{\kappa\nu})G^{B'}(q)], \end{aligned} \quad (3.11)$$

$$\begin{aligned} \Sigma_{\xi_1 \xi'_1}^{F,B}(p)|_\rho &= -i \int_{q^4} e^{i\eta q^0} (g_\rho \gamma_\mu - i \frac{f_\rho}{2m_B} (p-q)^\lambda \sigma_{\lambda\mu})_{\xi_1 \xi_3} \Delta^{0,\mu\nu}(p-q) \\ G_{\xi_3 \xi_2}^B(q) (g_\rho \gamma_\nu + \frac{f_\rho}{2m_B} (p-q)^\kappa \sigma_{\kappa\nu})_{\xi_2 \xi'_1}. \end{aligned} \quad (3.12)$$

Here the symbols “ H and “ F refer to the Hartree and Fock terms respectively. Via substituting G^B , from Eq.(2.20), in Eqs.(3.5)-(3.12) and subsequent contour integrations over the variable G^0 , one obtains for self-energy:

$$\Sigma_{\xi_1 \xi'_1}^{H,B}(p)|_\sigma = -2\delta_{\xi_1 \xi'_1} (\frac{g_\sigma}{m_\sigma})^2 \sum_{B'} (2J_{B'} + 1) \int_{\vec{q}^3} a_s^{B'}(\vec{q}) \Theta^{B'}(\mu^{B'} - \omega^B(\vec{q})), \quad (3.13)$$

$$\begin{aligned} \Sigma_{\xi_1 \xi'_1}^{F,B}(p)|_\sigma &= g_\sigma^2 \int_{\vec{q}^3} [\delta_{\xi_1 \xi'_1} a_s^B(\omega^B(\vec{q}), \vec{q}) + (\vec{\gamma}\hat{p})_{\xi_1 \xi'_1} (\hat{p}\hat{q}) a_v^B(\omega^B(\vec{q}), \vec{q}) + \\ \gamma_{\xi_1 \xi'_1}^0 a_0^B(\omega^B(\vec{q}), \vec{q})] \Delta^0(p^0 - \omega^B(\vec{q}), \vec{p} - \vec{q}) \Theta^B(\mu^B - \omega^B(\vec{q})), \end{aligned} \quad (3.14)$$

$$\Sigma_{\xi_1 \xi'_1}^{H,B}(p)|_\omega = 2\gamma_{\xi_1 \xi'_1}^0 (\frac{g_\omega}{m_\omega})^2 \sum_{B'} (2J_{B'} + 1) \int_{\vec{q}^3} a_0^{B'}(\vec{q}) \Theta^{B'}(\mu^{B'} - \omega^B(\vec{q})), \quad (3.15)$$

$$\begin{aligned} \Sigma_{\xi_1 \xi'_1}^{F,B}(p)|_\omega &= g_\omega^2 \int_{\vec{q}^3} [-\delta_{\xi_1 \xi'_1} [4 - \frac{(p^0 - \omega^B(\vec{q}))^2 - (\vec{p} - \vec{q})^2}{m_\omega^2}] a_s^B(\omega^B(\vec{q}), \vec{q}) + (\vec{\gamma}\hat{p})_{\xi_1 \xi'_1} [(2|\vec{q}\hat{p}\hat{q} - \\ \vec{p}^2 + \vec{q}^2 + (p^0 - \omega^B(\vec{q}))^2) \frac{2|\vec{p}||\vec{q}|}{m_\omega^2} a_v^B(\omega^B(\vec{q}), \vec{q}) - \frac{2}{m_\omega^2} \hat{p}(\vec{p} - \vec{q})(p^0 - \omega^B(\vec{q})) a_0^B(\omega^B(\vec{q}), \vec{q})] + \\ \gamma_{\xi_1 \xi'_1}^0 [\frac{2}{m_\omega^2} \hat{q}(\vec{p} - \vec{q})(p^0 - \omega^B(\vec{q})) a_v^B(\omega^B(\vec{q}), \vec{q}) + (2 + \frac{(p^0 - \omega^B(\vec{q}))^2 - (\vec{p} - \vec{q})^2}{m_\omega^2}) a_0^B(\omega^B(\vec{q}), \vec{q})] \Delta^0(p^0 - \\ \omega^B(\vec{q}), \vec{p} - \vec{q}) \Theta^{B'}(\mu^{B'} - \omega^B(\vec{q})), \end{aligned} \quad (3.16)$$

$$\Sigma_{\xi_1 \xi'_1}^{H,B}(p)|_\pi = 0, \quad (3.17)$$

$$\begin{aligned} \Sigma_{\xi_1 \xi'_1}^{F,B}(p)|_\pi &= (\frac{f_\pi}{m_\pi})^2 \int_{\vec{q}^3} [\delta_{\xi_1 \xi'_1} [-(p^0 - \omega^B(\vec{q}))^2 + (\vec{p} - \vec{q})^2] a_s^B(\omega^B(\vec{q}), \vec{q}) + (\vec{\gamma}\hat{p})_{\xi_1 \xi'_1} [(2|\vec{q}\hat{p}\hat{q} - \\ |\vec{p}|)(|\vec{p}|\hat{p}\hat{q} - |\vec{q}|) - (p^0 - \omega^B(\vec{q}))^2 - (\vec{p} - \vec{q})^2] \hat{p}\hat{q}) a_v^B(\omega^B(\vec{q}), \vec{q}) + 2(|\vec{q}\hat{p}\hat{q} - |\vec{p}|)(p^0 - \\ \omega^B(\vec{q})) a_0^B(\omega^B(\vec{q}), \vec{q}) + \gamma_{\xi_1 \xi'_1}^0 [2(|\vec{p}|\hat{p}\hat{q} - |\vec{q}|)(p^0 - \omega^B(\vec{q})) a_v^B(\omega^B(\vec{q}), \vec{q}) + ((p^0 - \omega^B(\vec{q}))^2 + \\ (\vec{p} - \vec{q})^2) a_0^B(\omega^B(\vec{q}), \vec{q})] \Delta^0(p^0 - \omega^B(\vec{q}), \vec{p} - \vec{q}) \Theta^{B'}(\mu^{B'} - \omega^B(\vec{q})), \end{aligned} \quad (3.18)$$

$$\Sigma_{\xi_1 \xi'_1}^{H,B}(p)|_\rho = 2\gamma_{\xi_1 \xi'_1}^0 (\frac{f_\rho}{m_\rho})^2 \sum_{B'} (2J_{B'} + 1) I_{3B'} \int_{\vec{q}^3} a_0^{B'}(\vec{q}) \Theta^{B'}(\mu^{B'} - \omega^B(\vec{q})), \quad (3.19)$$

$$\begin{aligned} \Sigma_{\xi_1 \xi'_1}^{F,B}(p)|_\rho &= g_\rho^2 \int_{\vec{q}^3} [\delta_{\xi_1 \xi'_1} (-4 + \chi_1^B ((p^0 - \omega^B(\vec{q}))^2 - (\vec{p} - \vec{q})^2) a_s^B(\omega^B(\vec{q}), \vec{q}) + \frac{3f_\rho}{m_B g_\rho} (\hat{q}(\vec{p} - \\ \vec{q}) a_v^B(\omega^B(\vec{q}), \vec{q}) + (p^0 - \omega^B(\vec{q})) a_0^B(\omega^B(\vec{q}), \vec{q})) + (\vec{\gamma}\hat{p})_{\xi_1 \xi'_1} [\frac{3f_\rho}{m_B g_\rho} (|\vec{p}| - |\vec{q}|\hat{p}\hat{q}) a_s^B(\omega^B(\vec{q}), \vec{q}) + \\ (2\hat{p}\hat{q} + |\vec{p}||\vec{q}|(\hat{p}\hat{q})^2 (\chi_2^B - 2\chi_3^B) + |\vec{p}||\vec{q}|\chi_2^B - (\vec{p}^2 + \vec{q}^2)\hat{p}\hat{q}(\chi_2^B - \chi_3^B) - \chi_3^B (p^0 - \\ \omega^B(\vec{q}))^2 \hat{p}\hat{q}) a_v^B(\omega^B(\vec{q}), \vec{q}) + \chi_2^B (p^0 - \omega^B(\vec{q})) (|\vec{q}\hat{p}\hat{q} - |\vec{p}|) a_0^B(\omega^B(\vec{q}), \vec{q}) + \gamma_{\xi_1 \xi'_1}^0 [-\frac{3f_\rho}{m_B g_\rho} (p^0 - \\ \omega^B(\vec{q})) a_s^B(\omega^B(\vec{q}), \vec{q}) + \chi_2^B (p^0 - \omega^B(\vec{q})) \vec{q}(\vec{p} - \vec{q}) a_v^B(\omega^B(\vec{q}), \vec{q}) + ((\chi_2^B - \chi_3^B) (p^0 - \\ \omega^B(\vec{q}))^2 + \\ \chi_3^B (\vec{p} - \vec{q})^2 + 2) a_0^B(\omega^B(\vec{q}), \vec{q})] \Delta^0(p^0 - \omega^B(\vec{q}), \vec{p} - \vec{q}) \Theta^{B'}(\mu^{B'} - \omega^B(\vec{q})). \end{aligned} \quad (3.20)$$

The following abbreviations have been introduced in Eq.(3.20):

$$\chi_1^B \equiv \frac{1}{m_\rho^2} - \frac{3}{(2m_B)^2} \left(\frac{f_\rho}{g_\rho}\right)^2, \quad (3.21)$$

$$\chi_2^B \equiv \frac{2}{m_\rho^2} + \frac{1}{(m_B)^2} \left(\frac{f_\rho}{g_\rho}\right)^2, \quad (3.22)$$

$$\chi_3^B \equiv \frac{1}{m_\rho^2} + \frac{1}{(2m_B)^2} \left(\frac{f_\rho}{g_\rho}\right)^2. \quad (3.23)$$

The quantity $2J_B + 1$ in Eqs.(3.13), (3.15), and (3.19) denotes the spin degeneracy factor of baryons of type B .

3.2 The baryonic matter equation of state

The baryonic matter equations of state, the pressure P and energy E as a function of density, are determined by the expectation value of the energy-momentum tensor defined by [11]

$$T_{\mu\nu}(x) = \sum_B \partial^\nu \psi_B(x) \frac{\partial L(x)}{\partial (\partial_\mu \psi_B(x))} - g_{\mu\nu} L(x) \quad (3.24)$$

for field $\psi_B(x)$. The use of one previous expression of the Lagrangian density leads to

$$\begin{aligned} T_{\mu\nu}(x) = & \sum_B \bar{\psi}_B(x) [i\gamma^\lambda \partial_\nu - g_{\mu\nu} [i\gamma^\lambda \partial_\lambda - m_B + g_\sigma \sigma(x) - g_\omega \gamma^\lambda \omega_\lambda(x) - g_\rho \gamma^\lambda \vec{\tau} \vec{\rho}_\lambda(x) - \\ & \frac{f_\rho}{4m_B} \sigma^{\lambda\kappa} \vec{\tau} \vec{G}_{\lambda\kappa}(x) - \frac{f_\pi}{m_\pi} \gamma^5 \gamma^\lambda (\partial_\lambda \vec{\tau} \vec{\pi}(x))] \psi_B(x) - g_{\mu\nu} [-\frac{\sigma(x)}{2} (\partial_\lambda \partial^\lambda + m_\sigma^2) \sigma(x) + \frac{1}{2} \partial_\lambda (\sigma(x) \partial^\lambda \sigma(x)) - \\ & \frac{1}{2} \partial_\lambda (\omega_\kappa(x) F^{\lambda\kappa}(x)) + \frac{\omega_\lambda}{2} [\partial_\kappa F^{\kappa\lambda}(x) + m_\omega^2 \omega^\lambda(x)] - \frac{1}{2} \partial_\lambda (\vec{\rho}_\kappa(x) \vec{G}^{\lambda\kappa}(x)) + \frac{\vec{\rho}_\lambda(x)}{2} [\partial_\kappa \vec{G}^{\kappa\lambda}(x) + \\ & m_\rho^2 \vec{\rho}^\lambda(x)] - \frac{\vec{\pi}(x)}{2} (\partial_\lambda \partial^\lambda + m_\pi^2) \vec{\pi}(x) + \frac{1}{2} \partial_\lambda (\vec{\pi}(x) \partial^\lambda \vec{\pi}(x))] + \partial_\mu \sigma(x) \partial_\nu \sigma(x) + \partial_\nu \omega^\lambda(x) F_{\lambda\mu} + \\ & \partial_\nu \vec{\rho}^\lambda(x) \vec{G}_{\lambda\mu}(x) + \partial_\mu \pi(x) \partial_\nu \pi(x) + \\ & \sum_B [\frac{f_\rho}{2m_B} \bar{\psi}_B(x) \sigma_{\mu\lambda} \vec{\tau} \partial_\nu \vec{\rho}^\lambda(x) \psi_B(x) - \frac{f_\pi}{m_\pi} \bar{\psi}_B(x) \gamma_5 \gamma_\mu \vec{\tau} \partial_\nu \vec{\pi}(x) \psi_B(x)]. \end{aligned} \quad (3.25)$$

By means of the two-point Green's functions G^B , one can express the expectation value of the energy-momentum tensor of Eq.(3.25) as

$$\begin{aligned} \langle \phi_0 | T_{\mu\nu} | \phi_0 \rangle = & - \lim_{x' \rightarrow x^+} \partial_\nu \sum_B Tr \gamma_\mu G^B(x, x') - \\ & \frac{1}{2} g_{\mu\nu} \sum_B \int dy Tr \Sigma^B(x, y) G^B(y, x'). \end{aligned} \quad (3.26)$$

Here the limit $x' \rightarrow x^+$ ensures the infinitesimal proper time ordering of operators ($x^+ \equiv (x^0 + \eta, \vec{x}), \eta > 0$).

The energy density and pressure are determined respectively by

$$E = \langle \phi_0 | T_{00}(x) | \phi_0 \rangle, \quad (3.27)$$

$$P = \frac{1}{3} \sum_1^3 \langle \phi_0 | T_{ii}(x) | \phi_0 \rangle, \quad (3.28)$$

from which one calculates

$$E = - \lim_{x' \rightarrow x^+} \sum_B \partial_0 \int_{q^4} e^{-iq(x-x')} \gamma_{\xi\xi'}^0 G_{\xi'\xi}^B(q) - \frac{i}{2} \sum_B \int_{q^4} e^{iq^0 \eta} \Sigma_{\xi\xi'}^B(q), \quad (3.29)$$

and

$$P = \frac{i}{3} \sum_B \int_{q^4} e^{iq^0 \eta} (\vec{\gamma}\vec{q})_{\xi\xi'} G_{\xi'\xi}^B(q) + \frac{i}{2} \sum_B \int_{q^4} e^{iq^0 \eta} \Sigma_{\xi\xi'}^B(q) G_{\xi'\xi}^B(q). \quad (3.30)$$

By means of inserting the spectral decomposition of Eq.(2.20) into Eqs.(3.29) and (3.30), the energy and pressure densities can be written as

$$E = \sum_B (2J_B + 1) \int_{\vec{q}^3} [2[m_B a_s^B(\vec{q}) - |\vec{q}| a_v^B(\vec{q})] + [\Sigma_s^B(\omega^B(\vec{q}), \vec{q}) a_s^B(\vec{q}) - \Sigma_v^B(\omega^B(\vec{q}), \vec{q}) a_v^B(\vec{q}) + \Sigma_0^B(\omega^B(\vec{q}), \vec{q}) a_0^B(\vec{q})] \Theta^{B'}(\mu^{B'} - \omega^B(\vec{q}))], \quad (3.31)$$

and

$$P = \sum_B (2J_B + 1) \int_{\vec{q}^3} [\Sigma_s^B(\omega^B(\vec{q}), \vec{q}) a_s^B(\vec{q}) - [\Sigma_v^B(\omega^B(\vec{q}), \vec{q}) + \frac{2}{3} |\vec{q}|] a_v^B(\vec{q}) + \Sigma_0^B(\omega^B(\vec{q}), \vec{q}) a_0^B(\vec{q})] \Theta^{B'}(\mu^{B'} - \omega^B(\vec{q})). \quad (3.32)$$

The density of baryons of type B is obtained as follows:

$$\varrho^B \equiv \frac{N^B}{V} = \frac{1}{V} \int_V d\vec{x}^3 \langle \phi_0 | \psi_B^\dagger(x) \psi_B(x) | \phi_0 \rangle_{|x^0=0}, \quad (3.33)$$

$$= i \lim_{x' \rightarrow x^+} \gamma_{\xi\xi'}^0 G_{\xi'\xi}^B(x, x'), \quad (3.34)$$

$$= i \gamma_{\xi\xi'}^0 \int_{q^4} e^{i\eta q^0} G_{\xi'\xi}^B(q), \quad (3.35)$$

$$= 2(2J_B + 1) \int_{\vec{q}^3} a_0^B(\vec{q}) \Theta^{B'}(\mu^{B'} - \omega^B(\vec{q})). \quad (3.36)$$

The total number density, ϱ^B , is obtained from

$$\varrho^B = \sum_B \varrho^B. \quad (3.37)$$

In the nonrelativistic case, using Eqs.(2.64) - (2.67) the energy density, pressure and baryon density are written by

$$E = 2 \int_{\vec{q}^3} \left[\frac{\vec{q}^2}{2m_B} + \frac{1}{2} \Sigma(E^B(\vec{q}) - \mu^B, \vec{q}) \right] n^B(|\vec{q}|) \Theta^B(|\vec{q}|), \quad (3.38)$$

$$P = 2 \int_{\vec{q}^3} \left[\frac{1}{3} \left[\frac{\vec{q}^2}{2m_B} + \frac{1}{2} \Sigma(E^B(\vec{q}) - \mu^B, \vec{q}) \right] n^B(|\vec{q}|) \Theta^B(|\vec{q}|), \quad (3.39)$$

and

$$\varrho = 2 \int_{\vec{q}^3} n^B(|\vec{q}|) \Theta^B(|\vec{q}|). \quad (3.40)$$

For the shell structure the chemical potential is calculated from the thermodynamic relation

$$P = \varrho^2 \frac{\partial}{\partial \varrho} \left(\frac{E}{A} \right). \quad (3.41)$$

From Eq.(3.41) the chemical potential is given by

$$\mu = \frac{1}{\varrho} (\varepsilon + P). \quad (3.42)$$

3.3 The equation of state of lepton

To calculate the equations of state for lepton matter we begin with the Lagrangian density of free leptons. The Lagrangian density of free leptons is given by[3]

$$L_{lep}^0(x) = \sum_{\lambda=e^-, \mu^-} \bar{\psi}_\lambda(x) (i\gamma^\mu \partial_\mu - m_\lambda) \psi_\lambda(x). \quad (3.43)$$

From Eq.(3.24) and Eq.(3.43) we obtain the energy-momentum density tensor of Leptons

$$T_{\mu\nu}^{lep}(x) = \sum_{\lambda=e^-, \mu^-} \bar{\psi}_\lambda(x) [i\gamma_\mu \partial_\nu - g_{\mu\nu} (i\gamma^\sigma \partial_\sigma - m_\lambda)] \psi_\lambda(x). \quad (3.44)$$

The expectation value of the energy-momentum tensor becomes

$$\langle \phi_0 | T_{\mu\nu}^{lep} | \phi_0 \rangle = - \lim_{x' \rightarrow x^+} \sum_{\lambda=e^-, \mu^-} \partial_\nu \text{Tr}(\gamma_\mu G^\lambda(x, x')), \quad (3.45)$$

$$= - \lim_{x' \rightarrow x^+} \partial_\nu \sum_{\lambda=e^-, \mu^-} \int \frac{d^4 q}{(2\pi)^4} e^{-iq(x-x')} \text{Tr}(\gamma_\mu G^\lambda(q)). \quad (3.46)$$

in analogy to Eq.(2.20), the momentum-space representation of the lepton propagator, denoted by G_λ , is given by (α and α' refer to spin quantum numbers)

$$G_{\alpha\alpha'}^\lambda(p) = \int d\omega \frac{\Gamma_{\alpha\alpha'}^\lambda(\omega, \vec{p})}{\omega - (p^0 - \mu^\lambda)(1+i\eta)}. \quad (3.47)$$

The free leptonic spectral functions are

$$\Gamma_i^\lambda(\omega, \vec{p}) = \delta(\omega + \mu^\lambda - \omega^\lambda(\vec{p})) \Gamma_i^\lambda(\vec{p}), \quad i = s, v, 0, \quad (3.48)$$

with

$$\omega^\lambda(\vec{p}) = \sqrt{m_\lambda^2 + \vec{p}^2}, \quad (3.49)$$

$$\Gamma_s^\lambda(\vec{p}) = \frac{m_\lambda}{2\sqrt{m_\lambda^2 + \vec{p}^2}}, \quad (3.50)$$

$$\Gamma_v^\lambda(\vec{p}) = -\frac{|\vec{p}|}{2\sqrt{m_\lambda^2 + \vec{p}^2}}, \quad (3.51)$$

$$\Gamma_0^\lambda(\vec{p}) = \frac{1}{2}. \quad (3.52)$$

The calculation of the lepton density, ϱ^λ , can be performed analogously to Eq.(3.33). By denoting the leptonic distribution function with

$$\Theta^\lambda(\vec{q}) \equiv \Theta(P_{F,\lambda} - |\vec{q}|), \quad (3.53)$$

one gets

$$\varrho^\lambda = i \lim_{x' \rightarrow x^+} \gamma_{\xi\xi'}^0 G_{\xi'\xi}^\lambda(x, x') \quad (3.54)$$

$$= i \int_{q^4} e^{iq^0} \gamma_{\xi\xi'}^0 G_{\xi'\xi}^\lambda(q) \quad (3.55)$$

$$= 2(2J_B + 1) \int_{\vec{q}^3} \Gamma_0^\lambda(\vec{q}) \Theta^\lambda(\vec{q}) \quad (3.56)$$

$$= \frac{2J_B + 1}{2} \frac{P_{F,\lambda}^3}{3\pi^2}. \quad (3.57)$$

The total number density of leptons, ϱ^{lep} , is given by

$$\varrho^{lep} \equiv \sum_{\lambda=e^-, \mu^-} \varrho^\lambda. \quad (3.58)$$

The energy density and pressure contributions are obtained from Eq.(3.46):

$$E_{lep} \equiv \langle T_{00}^{lep}(x) \rangle = \frac{1}{\pi^2} \sum_{\lambda=e^-, \mu^-} (2J_B + 1) \int_0^{P_{F,\lambda}} dq \bar{q}^2 \sqrt{m_\lambda^2 + \bar{q}^2}, \quad (3.59)$$

and

$$P_{lep} \equiv \frac{1}{3} \sum_i \langle T_i^{lep}(x) \rangle = \frac{1}{6\pi^2} \sum_{\lambda=e^-, \mu^-} (2J_B + 1) \int_0^{P_{F,\lambda}} dq \frac{\bar{q}^4}{\sqrt{m_\lambda^2 + \bar{q}^2}}. \quad (3.60)$$

The quantity $2J_B + 1$ in the Eq.(3.59) and Eq.(3.60) refers to the spin degeneracy factor of leptons of type λ (see Table 3.1). The Fermi momenta of leptons of type λ are denoted by $P_{F,\lambda}$.

Table 3.1: Masses, spin quantum numbers and electric charges of leptons included in the determination of the equations of state of neutron star matter.

Lepton(λ)	$m_\lambda(MeV)$	J_λ	q_λ
e^-	0.511	$\frac{1}{2}$	-1
μ^-	106	$\frac{1}{2}$	-1

3.4 Coupling constants of the Hartree-Fock approximation

The coupling constants of the Lagrangian of Eq.(2.3) are not determined by the nucleon-nucleon interaction in free space, but must be adjusted to the bulk properties of nuclear matter at the saturation density[19]. These are binding energy, effective mass, compression modules, and symmetry energy. The baryon and meson masses usually are taken to be equal to their physical values[20], except for the hypothetical σ -meson, which is introduced to simulate the correlated 2π exchange. The π - and ρ -meson coupling constants, f_π and g_ρ , can be deduced from the description of the nucleon-nucleon interactions[11], and the ratio of the tensor to the vector coupling strength, f_ρ/g_ρ , can be obtained from the vector-dominance model which leads to $f_\rho/g_\rho \approx 3.7$ [3]. Two coupling strengths, g_σ and g_ω , are adjusted to the above mentioned ground state properties of nuclear matter. In this work we have adopted the parameter sets adjusted by Jetter et al.[19]. The parameter sets are summerized in Table 3.2.

Table 3.2: $m_\sigma = 550MeV$, $m_\omega = 783MeV$, $m_\pi = 138MeV$, $m_\rho = 770MeV$, $m_N = 939MeV$, $B.E = -15.75MeV$, $a_4 = 33.6MeV$.

model	$P_F(fm^{-1})$	$\frac{g_\sigma^2}{4\pi}$	$\frac{g_\omega^2}{4\pi}$	$\frac{f_\pi^2}{4\pi}$	$\frac{g_\rho^2}{4\pi}$	$\frac{f_\rho}{g_\rho}$
$(\sigma, \omega)_H$	1.42	7.3052	10.8621	—	—	—
$(\sigma, \omega, \rho)_H$	1.42	7.3052	10.8621	—	2.9231	—
$(\sigma, \omega)_{HF}$	1.42	6.6268	8.6136	—	—	—
$(\sigma, \omega, \pi^{Dv})_{HF}$	1.42	7.2262	8.0901	0.08	—	—
$(\sigma, \omega, \pi^{Dv}, \rho)_{HF}$	1.42	5.8594	4.7138	0.08	0.55	6.6

Table 3.3: Masses, electric charge(q_B) and quantum numbers (spin(J_B), isospin(I_B), strangeness(S_B), hypercharge(Y_B), third component of isospin(I_{3B})) of the baryons.

Baryon(B)	$m_B(MeV)$	J_B	I_B	S_B	Y_B	I_{3B}	q_B
n	939.6	$\frac{1}{2}$	$\frac{1}{2}$	0	1	$-\frac{1}{2}$	0
p	938.3	$\frac{1}{2}$	$\frac{1}{2}$	0	1	$\frac{1}{2}$	1

Table 3.4: quantum numbers(spin(J_M), parity(π), and isospin(T_M)) of Meson M and coupling of the meson exchange model for nucleon-nucleon interaction.

Meson(M)	J_M^π	T_M	coupling
σ	0^+	0	scalar
ω	1^-	0	vector
π	0^-	1	pseudo-vector
ρ	1^-	1	vector

4 Phase transition of superdense matter

A possible phase transition of superdense matter have been proposed to understand the instability modes of the ground state at high densities[8]. According to this suggestion, the states of the fields may redistribute in momentum space as the density increases. This redistribution of the states may change the microscopic properties of the ground state of the system. Normally the states of the particles are occupied up to their Fermi momenta in the ground state. But at high densities the standard spherical distribution may be unstable, because of the fluctuation in the patterns of the energy spectrum. For that reason another distribution of the states, shell structure, has been suggested and some results have been reported [8,9]. But earlier calculations have been carried out only for neutron matter using the simple dynamics, only taking σ - and ω -mesons into account. In this work we have studied more general cases, that is, asymmetric nuclear matter. The shell distribution function is given by

$$n^B(p) = \begin{cases} 1 & P_{min}^B \leq p \leq P_{max}^B \\ 0 & P < P_{min}^B, P > P_{max}^B \end{cases}, \quad (4.1)$$

where the quantities P_{min}^B and P_{max}^B satisfy the following relation:

$$P_{F,B}^3 = P_{max,B}^3 - P_{min,B}^3. \quad (4.2)$$

Here $P_{F,B}$ denotes the Fermi momenta of baryon B in the ground state. P_{min}^B and P_{max}^B are the lowest and highest momentum state occupied by baryon B respectively. In the ground state the energy density of the spherical and shell distribution are given respectively by

$$E_{sp} = \frac{1}{V} \sum_B \int_0^{P_{F,B}} H_{sp}^B(p) d\vec{p}^3, \quad (4.3)$$

and

$$E_{sh} = \frac{1}{V} \sum_B \int_{P_{min}^B}^{P_{max}^B} H_{sh}^B(p) d\vec{p}^3, \quad (4.4)$$

where the quantity $H(p)$ denotes the sum of the kinetic energy and potential energy of a single particle. The quantity V is the volume in momentum space, $V = \frac{4}{3}\pi P_F^3$. We now define the order parameter to describe the phase transition in the following way:

$$\Delta E = E_{sp} - E_{sh}. \quad (4.5)$$

At the certain density, ϱ_c , the order parameter ΔE changes:

$$\Delta E = \begin{cases} \leq 0 & \varrho < \varrho_c \\ > 0 & \varrho \geq \varrho_c \end{cases}. \quad (4.6)$$

The difference of the order parameter may be interpreted as the evidence for the phase transition. Above the critical density, ϱ_c , the shell structure may be a more stable ground state than sphere structure. We illustrate in Fig. 1 the density dependence of the order parameter. We will continue this topic more in detail in Section 4.1 and 4.2.

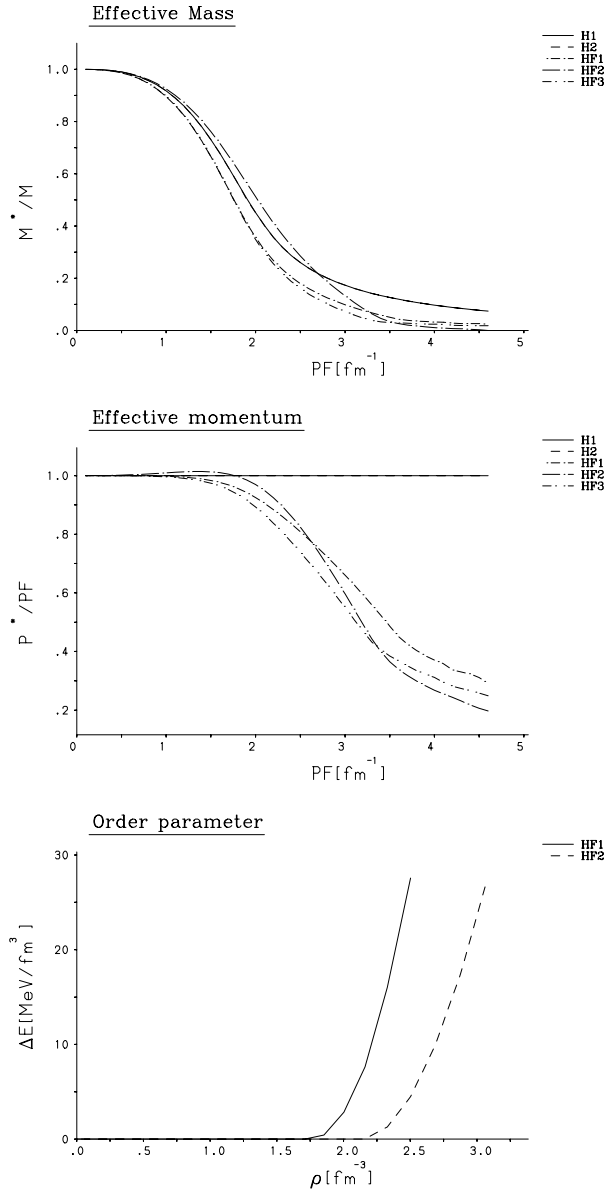


Figure 1: Effective mass, effective momentum and order parameter as a function of density for neutron matter in the Hartree and Hartree - Fock approximations.

4.1 Neutron matter

To determine the physical properties of neutron matter, the self-consistent Hartree-Fock approximation is introduced. The exchange corrections to the Hartree calculation lead to a phase transition to a new ground state at high densities(Fig. 1). The results, which are obtained from different models, are compared and shown in Fig. 6 - Fig. 18 in Appendix A. The equation of state for the H1(σ, ω) model shows the local minimum and there is a phase transition similar to the liquid-gas transition at low densities(Fig. 12), which are below the nuclear saturation density. But in the H2(σ, ω, ρ) ρ -meson stiffens the equation of state and the local minimum disappears. In the HF1(σ, ω) and HF2($\sigma, \omega, \pi, \rho$) the exchange terms modify the low density equation of state and the self-consistent exchange corrections remove also the local minimum. In these density ranges Fock terms, which are contributed from π and ρ -meson, soften the equations of state relatively. At intermediate densities($\rho_0 < \rho < 10\rho_0$), exchange corrections of ρ -meson soften the equations of state very much(Fig. 13). But at high densities($\rho > 10\rho_0$) the self-consistent exchange corrections from π and ρ -meson stiffen the equations of state apparently(Fig. 13). The equations of state for the Hartree approximations are relatively soft at high densities. The self-consistent effective mass for neutron matter is shown in Fig. 1. In the HF2 it approaches zero drastically and it seems to be self-contradicting to the behaviour of the self-energy(Fig. 15). In the HF2 one remarkable result is the exchange contributions of ρ -meson to the scalar component of the self-energy and the Fock term contributions of ρ -meson turns out to be positive in contrast to the results from other meson(Fig. 15). However, in the self-consistent HF calculations this has the small effects on the results of Σ_{HF}^B . In Fig. 1, effective momentum in the HF2 shows the different patterns at low densities, where the exchange contributions in the HF2 are positive(Fig. 15). In Fig. 18 all components of the self-energy for different models are illustrated. We now turn to the single particle energy spectrum, which is defined as

$$E^B(p) = T^B(p) + V^B(p), \quad (4.7)$$

where $T^B(p)$ and $V^B(p)$ are the kinetic and potential energy of a particle respectively and are given by

$$T^B(p) = \frac{m_B m_B^*(p) + p p^*(p)}{\sqrt{m_B^{*2}(p) + p^{*2}(p)}}, \quad (4.8)$$

$$V^B(p) = \Sigma_0^B(p) + \frac{m_B \Sigma_s^B(p) + p \Sigma_v^B(p)}{\sqrt{m_B^{*2}(p) + p^{*2}(p)}}, \quad (4.9)$$

with

$$m_B^*(p) = m_B + \Sigma_s^B(p) \quad (4.10)$$

and

$$p^*(p) = p + \Sigma_v^B(p). \quad (4.11)$$

As shown in Fig. 6 - Fig. 9 in Appendix A at normal densities ($PF = 1.42 fm^{-1}$), $E^B(p)$ in the HF1 and HF2 is similar to the Hartree results. As the density increases, the effect of exchange corrections on the spectrum becomes apparent. Unlike the Hartree model there is inversion of the energy spectrum in the Hartree-Fock Theories. The inversion of the single particle spectrum in the HF approximations is caused by two main factors: the behaviors of the vector component Σ_v^B and timelike component Σ_0^B of the self-energy in Eq.(4.8) and Eq.(4.9). The behaviours of the self-energy are illustrated in Fig.16 - Fig.17 as a function of momentum at high densities. Near the Fermi surface the Fock term reduces the repulsive contribution Σ_0^B and increases the attractive contribution Σ_v^B . As a result the energy spectrum is inverted at $PF = 3.8 fm^{-1}$ for the HF1 and at $PF = 4.0 fm^{-1}$ for the HF2 respectively. Above these densities the spherical distribution of the states may be unstable and a phase transition may occur from the spherical structure to a new stable ground state, which may be the shell structure. Such a phase transition has effects on the equation of state and energy spectrum. It softens the equation of state slightly at above critical density. It disturbs the inversion of energy spectrums and lowers them (Figs. 7 and 9). For that reason the shell structure may be a stable ground state at high densities. We can understand the phase transition more explicitly from the behaviour of the energy density as a function of P_{min} (Figs. 10 - 11). At the transition point the energy density curve is flat as P_{min} changes. Above the critical point there is a local minimum in the energy density. Other interesting results are the fluctuation of the kinetic and potential energy in certain momentum ranges at high densities. In Figs. 6 - 9 the kinetic and potential energy spectrums of single particle are illustrated. The fluctuation of the single particle kinetic energy is related directly to the behavior of $m^*(p)$ and $p^*(p)$. In the Hartree models there is no such fluctuation pattern in the kinetic energy. At above certain high density exchange terms reduce baryon mass and momentum very strongly near rest momentum. As a result they certainly yield the unphysical results. For instance, at certain density baryon's effective mass, $m^*(p)$, begins negative at near rest. They happen at $PF = 3.7 fm^{-1}$ in the HF1 and at $PF = 4.5 fm^{-1}$ in the HF2. The ρ -meson contributions show less effect on the reduction of baryon mass at near rest at certain density. Momentum dependent effective momentum, $p^* = p + \Sigma_v^B$, also has negative value at $PF = 3.6 fm^{-1}$ in the HF1 and at $PF = 3.4 fm^{-1}$ in the HF2. In contrast to the results of m^* , the ρ -meson contributions has strong influence on the reduction of p^* . In the HF1 m^* is the main cause for the fluctuation of kinetic energy but in the HF2 p^* is more responsible for the fluctuation, because in the HF2 the attractive exchange contribution of the vector component of the self-energies play the dominant role at high densities. But potential energy spectrum shows rather strong fluctuation near the Fermi surface where potential energy decreases rapidly. The strong reduction of timelike component Σ_0^B near the Fermi surface causes mainly the fluctuation of potential energy(Figs. 16 - 17). Such fluctuations for the kinetic and potential energy are still poorly understood and the standard models, e.g. the Hartree-Fock theory, may have the limitation on studying the physical properties of superdense matter.

4.2 Asymmetric nuclear matter

For asymmetric nuclear matter the results are illustrated in Fig. 19 - Fig. 25 in Appendix B. Here asymmetric parameter is defined by

$$\delta = \frac{\rho_n - \rho_p}{\rho_B}. \quad (4.12)$$

For $\delta = 1$ the results are the same as that of pure neutron matter. For $\delta \neq 1$ the symmetrization process has the effects on the change of the physical properties of the system. For instance, in contrast to pure neutron matter the equations of state for models, which are taken into calculation, shows the same pattern around the saturation density in the symmetrization process (Figs. 20 and 22). One of interesting results is the behavior of effective chemical potential in Fig. 19.

Here we define the effective chemical potentials (ECP) for proton and electron in the following way

$$\mu_p^{eff} = (\mu_n - \mu_p) / \mu_n = 1 - \mu_p / \mu_n, \quad (4.13)$$

$$\mu_e^{eff} = (\mu_n - \mu_e) / \mu_n = 1 - \mu_e / \mu_n. \quad (4.14)$$

In the H1(σ, ω), HF1(σ, ω), and HF2($\sigma, \omega, \pi, \rho$) there is a local maximum in ECP. However, the local maximum is not apparent in the H2(σ, ω, ρ). The self consistent approximation and the associated behaviour of the self-energy (Fig. 18) cause such patterns for ECP. At low densities the most of contributions to μ_p and μ_n come from neutrons because of the self-consistent calculation. Until ECP reaches the local maximum at $\rho = 3.6\rho_0$ for the H1 and $\rho = 4.17\rho_0$ in the H2, μ_p is smaller than μ_n relatively because the density of neutrons is larger than that of protons in asymmetric nuclear matter and the scalar and vector component of the self-energy does not much affect on μ_p and μ_n in these density ranges. Above the local maximum in ECP μ_n suffers more depression than μ_p and the ratio μ_p / μ_n becomes slowly increasing as the density increases. But the pattern of ECP in the H2 is different from that in the H1 at high densities, since the contributions from timelike component of self-energy to ECP in the H2 play a more dominant role than that from scalar component. As the density increases μ_p and μ_n in the H2 are changing fast at the same rate, which makes the relative contribution to ECP constant. In the Hartree-Fock approximations the exchange contributions have large impact on the behavior of ECP. In the HF1 ECP mode is not too much deviated from the Hartree calculation, but in the HF2 the local maximum is shifted to higher densities. In the HF2 scalar component of self-energy has very small effect on ECP at low densities and that causes the shift of local maximum to high densities. At high densities exchange contributions from ρ -meson play a decisive role in the behavior of ECP. At lower and higher densities than the density, at which the local maximum appears in ECP of protons, μ_p is comparable to μ_n and the behaviour of ECP shows the saturation of the population of protons for each δ . As is shown in figures ECP is decreasing during the symmetrization process. Such a behaviour of

chemical potential is related to the population of chemical species. Since ECP of neutrons and protons in the HF2 undergoes symmetrization process rapidly at high densities, population of protons in the HF2 is more favorable. These results reflect more population of protons in the HF2 model in β -equilibrium(cf. Fig. 2). Another interesting result is disappearance of the shell structure in the symmetrization process. In asymmetric nuclear matter the shell structure may be a stable ground state at high densities, because for the shell structure the equation of state is slightly soft and energy density is relatively lower at high densities(Fig. 23). But in symmetric nuclear matter the shell structure disappears and the spherical structure is still a stable ground state. This effect can be seen in Fig. 24 and Fig. 25., where the energy densities are illustrated as a function of P_{min} . At below critical density the energy density increases monotonically and at critical density the flatness pattern appears in the energy density. At above critical density the shell structure has the local minimum for asymmetric nuclear matter, but local minimum disappears in symmetric nuclear matter. In this symmetrization process the critical point, at which a phase transition occurs, moves to higher densities. For instance, for asymmetric nuclear matter the HF1 results show that for $\delta = 1$ there is the phase transition at the density of $\rho \approx 12\rho_0$. For $\delta = 0.5$ the phase transition occurs at the density of $\rho \approx 14\rho_0$. But in symmetric nuclear matter, $\delta = 0$, there is no evidence for phase transition up to such densities. Another important thing is the impact of ρ -meson on the equations of state. At low densities ρ -meson contributions stiffen the equation of state in the Hartree calculation. At high densities the exchange contributions of ρ -meson stiffen the equation of state for asymmetric nuclear matter in the Hartree-Fock approximations. But during symmetrization process ρ -meson contributions soften the equation of state at all densities. For symmetric nuclear matter, in which the Hartree term of ρ -meson vanishes, there is very little difference in both models, HF1(σ, ω) and H2(σ, ω, ρ), but the equation of state is much softer in the HF2($\sigma, \omega, \pi, \rho$) model.

5 Hadronic phase in β -equilibrium and quark matter phase

In the ground state the fermion fields occupy up to the Fermi momenta according to the Pauli's exclusion principle. As a result the baryon fields in the ground state are one of the ordered systems in momentum space. But as the density increases, a new kind of order may be created. Generally, creation of a new order is related to the stability condition of the system. Apart from the shell structure, which is discussed in Chapter 4, there may be other possibilities to create new orders in the density evolution. At low densities the system is supposed to be composed of pure neutron matter. But increasing density leads to the population of other species, because creation of the new particles makes the system more stable. In this process the shell structure may not be created, since the spherical distribution is still a stable ground state if the symmetrization effect (see Section 4.2), creation of protons, is taken into account. The other possibility may be phase transition from confined hadronic matter to deconfined quark-gluon mixed phase.

5.1 Hadronic Phase

Now we suppose that the system is composed of almost pure neutron matter with small amounts of electrons at low densities. For increasing density β -decay does occur:

$$n \rightleftharpoons p + e^- + \bar{\nu}_{e^-}, \quad (5.1)$$

$$\mu^- \rightleftharpoons e^- + \bar{\nu}_{e^-} + \bar{\nu}_{\mu^-}. \quad (5.2)$$

We can compute the physical properties of such a mixture of electrons, muons, protons, and neutrons by assuming that they are in generalized β -equilibrium. The equilibrium is imposed through the chemical potentials corresponding to baryon and lepton:

$$\mu(n) = \mu(p) + \mu(e), \quad (5.3)$$

$$\mu(\mu) = \mu(e). \quad (5.4)$$

The constraint of charge neutrality leads to

$$\rho^p = \rho^e + \rho^\mu. \quad (5.5)$$

The conservation of baryon number is defined by

$$\rho = \rho^n + \rho^p. \quad (5.6)$$

The chemical compositions of neutron stars can be calculated by a density evolution equation.

The density evolution equation may be written as the coupled nonlinear equations in the following way

$$\frac{dx_i}{d\rho} = F_i(x_1, \dots, x_i, V_{iBjB}(\rho), \rho). \quad (5.7)$$

Here x_i denotes the ratio of the density of the i -th chemical element to the total baryon density, that is $x_i = \frac{\rho_i}{\rho_B}$. The quantity, $V_{i_B j_B}(\varrho)$, is the interaction contributions from baryons of i_B and j_B .

This nonlinear evolution equation can be solved only under certain physical boundary conditions. But under certain circumstances it is more simple to determine the chemical composition by the coupled nonlinear algebraic equations, which is given by

$$f_i(x_1, \dots, x_i, V_{i_B j_B}(\varrho), \varrho) = 0. \quad (5.8)$$

For instance, in the Hartree and Hartree-Fock approximations the chemical evolution of neutron star matter can be determined directly by Eq.(5.8) and it leads to the following relations

$$x_p + x_n - 1 = 0, \quad (5.9)$$

$$x_p - x_e - x_\mu = 0, \quad (5.10)$$

$$\frac{\Sigma_0^n(\varrho) + \sqrt{(m_n + \Sigma_s^n)^2 + ((3\pi^2 x_n \varrho)^{1/3} + \Sigma_v^n)^2} - \Sigma_0^p(\varrho) + \sqrt{(m_p + \Sigma_s^p)^2 + ((3\pi^2 x_p \varrho)^{1/3} + \Sigma_v^p)^2} - \sqrt{m_e^2 + (3\pi^2 x_e \varrho)^{2/3}}}{\sqrt{m_e^2 + (3\pi^2 x_e \varrho)^{2/3}} - \sqrt{m_\mu^2 + (3\pi^2 x_\mu \varrho)^{2/3}}} = 0, \quad (5.11)$$

$$\sqrt{m_e^2 + (3\pi^2 x_e \varrho)^{2/3}} - \sqrt{m_\mu^2 + (3\pi^2 x_\mu \varrho)^{2/3}} = 0. \quad (5.12)$$

Energetically the phase of pure neutron matter is not favorable with increasing densities, and at certain density protons are populated with the same amount of electrons. Generally the threshold condition for population of baryons including protons is given by

$$\mu^n - q_B \mu^e > \mu_B^0. \quad (5.13)$$

Here q_B is the electric charge of baryon B and μ_B^0 denotes the threshold chemical potential of baryon B . In the case of protons in the Hartree and Hartree-Fock approximations the threshold chemical potential is given by

$$\mu_B^0 = \Sigma_0^B(\omega^B(\vec{p}), \vec{p}) + I_{3B} \Sigma_{03}^B(\omega^B(\vec{p}), \vec{p}) + m_B + \Sigma_s^B(\omega^B(\vec{p}), \vec{p}) \quad (5.14)$$

Since above the nuclear saturation density electrons are highly relativistic, population of muons is more favorable. The threshold condition for muons is given by

$$\mu^e > \mu_\mu^0 = m_\mu. \quad (5.15)$$

Since the chemical potentials μ^n , μ^e are positive and the self-energy Σ_{03}^B is negative, it follows from Eq.(5.14) that (i) negatively charged baryons are charge-favored and (ii) baryons having the same isospin projection as the neutron (i.e. $I_3 \leq 0$) are isospin-unfavored. Another mechanism which influences the selection densities of the various state has its origin in the effective baryon mass $m_B^*(\varrho) = m_B + \Sigma_s^B(\varrho)$. Since m_B^* decreases with increasing density, it tends to depress the selection of each baryon species. In this work we investigate the simple system, which is only composed of protons and neutrons in β -equilibrium with electrons and muons. The results are shown in Fig. 2. At below sat-

uration density pure neutron matter are still in a stable phase. As density increases proton will be populated with the same amount of electrons, because of charge neutrality conditions. Near the nuclear saturation density it is energetically favorable for population of muons, since around the saturation density the chemical potential of electrons is greater than the rest mass of muons. But the population density is very sensitive to the models taken into calculations. In the simple Hartree treatment, H1(σ, ω), protons and electrons are populated at $\varrho \approx 1.35 \times 10^{-4} fm^{-3}$, and muons are populated at $\varrho \approx 0.22 fm^{-3}$. In the H2(σ, ω, ρ) model, protons and electrons are populated at $\varrho \approx 1.0 \times 10^{-4} fm^{-3}$ and muons are populated at $\varrho \approx 8.7 \times 10^{-2} fm^{-3}$. We can understand such results from the selection conditions for population. Protons fulfill the isospin-favored conditions with the ρ -meson contributions. In the Hartree-Fock calculations Fock terms modify the results which are obtained from the Hartree treatment. Protons and electrons are populated at $\varrho \approx 1.20 \times 10^{-4} fm^{-3}$ for the HF1(σ, ω) and at $\varrho \approx 1.08 \times 10^{-4} fm^{-3}$ for the HF2($\sigma, \omega, \pi, \rho$). Muons are populated at $\varrho \approx 0.15 fm^{-3}$ for the HF1 and at $\varrho \approx 0.17 fm^{-3}$ for the HF2. Because of ρ -meson contributions the isospin-favored conditions are fulfilled in the HF2. However, there are still differences in the population densities between the Hartree and Hartree-Fock theories. If we take the rest threshold conditions, which are the effective mass and timelike component of the self-energy, then we can understand such differences. The behaviour of the effective mass is shown in Fig. 1. At very low densities the exchange terms have less effect on the reduction of effective mass than the Hartree treatment. We remember that in Eq.(5.14) $\Sigma_{03}(p)$, which is contributed from ρ -meson, is negative for proton. This reduces amount of the timelike component of the self-energy for proton. But the difference of the effective mass among the models is very small. Reduction of the timelike component of the self-energy by ρ -meson contributions for proton play a decisive role in the threshold conditions. That's why protons are populated first in the H2. The difference of the population densities between two models, H2 and HF2, can be understood in the following way. In the threshold condition of Eq. (5.15) the right term of the inequality are smaller in the HF2 than in the H2. That means that in the HF2 the population of protons must be more favorable than in the H2. But the left term of the inequality is relatively much smaller in the HF2 than in the H2, because the exchange contributions reduce the chemical potential of neutrons much strongly. Therefore protons are populated first in the H2 model. For increasing densities the population of protons is more favorable in the HF2 model. At high densities they approach rapidly the same amount of neutron matter. This shows that the symmetrization effect is one of the stabilization processes. In Fig. 3 effective chemical potential(ECP) for neutron star matter is illustrated. The physical meaning of ECP for baryons is given in Section 4.2. ECP of electron decreases at low densities where they are populated. It builds the local minimum at certain density and then it increases at high densities where muons are populated. The equation of state of baryon-lepton mixed phase is shown in Fig. 4. This topic will be discussed in Chapter 6.

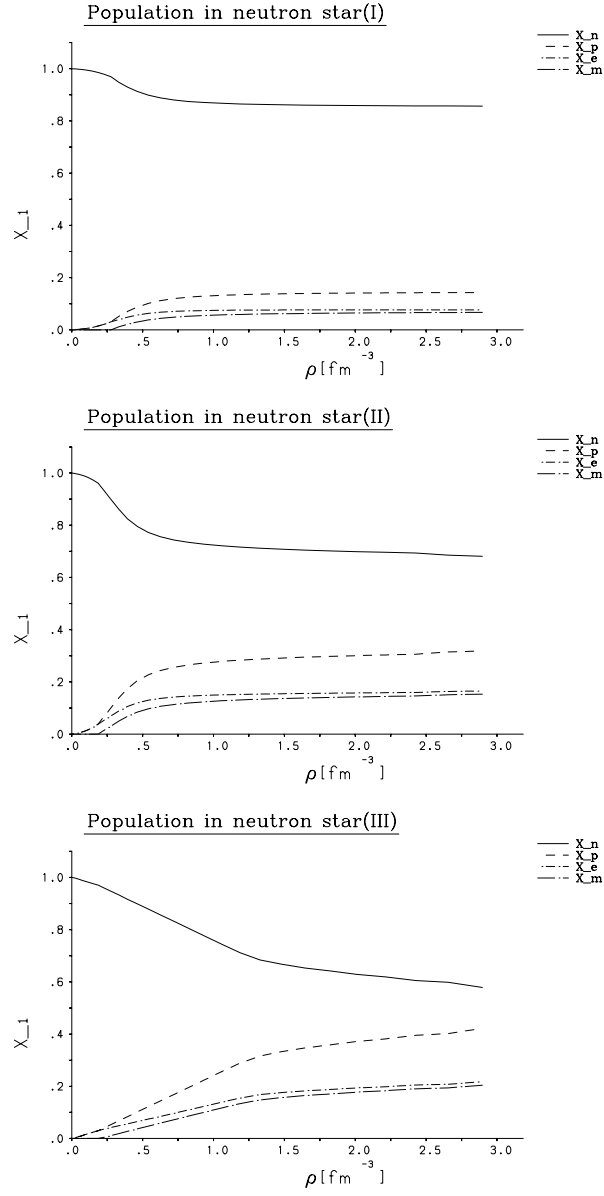


Figure 2: Evolution of the chemical compositions in neutron star. Population(I) for the Hartree(σ, ω), population(II) for the Hartree-Fock(σ, ω), and population(III) for the Hartree-Fock($\sigma, \omega, \pi, \rho$) respectively.

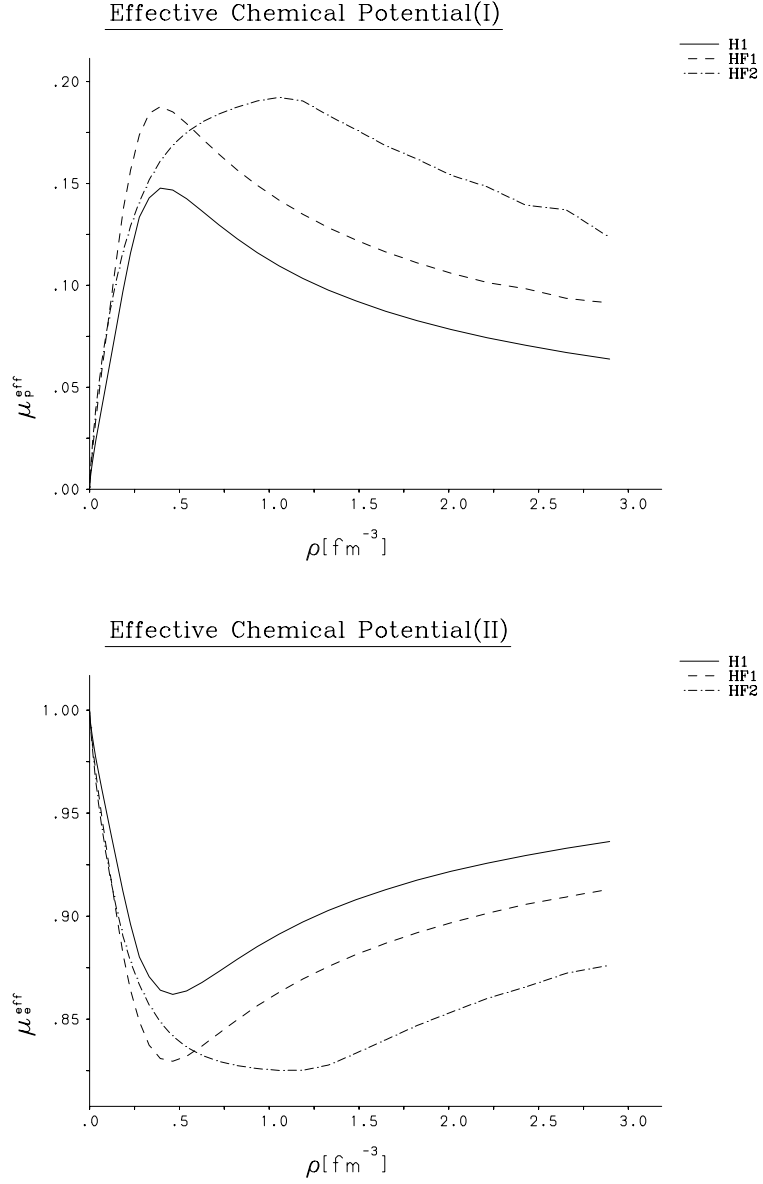


Figure 3: Effective chemical potential of neutron star matter for the same models as Fig. 2. Effective chemical potential(I) for proton's chemical potential relative to that of neutron matter. Effective chemical potential(II) for electron's chemical potential relative to that of neutron matter.

5.2 Quark-Gluon Phase

We now study another possible phase, quark-gluon plasma, in high dense regime. To study the quark-gluon phase we make a simple model based on strong interaction model in the nuclear domain. The Lagrangian density of Quark-Gluon system can be written as[11]

$$L_{Q-G}(x) = \sum_{Q=u,d} \bar{\psi}_Q(x) [i\gamma^\mu (\partial_\mu + \frac{i}{2}g\lambda^a A_\mu^a(x)) - m_Q] \psi_Q(x) - \frac{1}{4} F_{\mu\nu}^a(x) F^{a\mu\nu}(x). \quad (5.21)$$

Here $A_\mu^a(x)$ (with $a = 1, \dots, 8$) are the gluon fields, λ^a are the standard $SU(3)$ matrices of Gell-mann. The matrices λ^a connect the color indices $R, G,$ and B of the quark field ψ_Q . The quantity $F_{\mu\nu}^a$ is the gluon field-strength tensor given by

$$F_{\mu\nu}^a(x) = \partial_\mu A_\nu^a(x) - \partial_\nu A_\mu^a(x) - gf^{abc} A_\mu^b(x) A_\nu^c(x) = -F_{\nu\mu}^a(x). \quad (5.22)$$

The quantities f^{abc} are the $SU(3)$ structure constants defined by

$$[\frac{1}{2}\lambda^a, \frac{1}{2}\lambda^b] = if^{abc}\frac{1}{2}\lambda^c. \quad (5.23)$$

The quantity g is the single coupling constant. The triplet quark fields are denoted by

$$\psi_Q \equiv \begin{pmatrix} \psi_Q^R \\ \psi_Q^G \\ \psi_Q^B \end{pmatrix}. \quad (5.24)$$

In the nuclear domain we confine our attention only to the u and d quarks and interactions in the quark-gluon phase will be neglected. However the model must satisfy the confinement property and this is achieved by introducing a constant, the positive energy per unit volume in the vacuum, $(\frac{E}{V})_{vacuum} = b$. This constant can be interpreted as the energy needed to create a bubble in the vacuum, in which the noninteracting quarks and gluons are confined. Analogously to leptonic case we can calculate the equation of state of free quark phase and bubble fields. The energy-momentum density tensor for free quark and bubble can be written by[11]

$$T_{\mu\nu}(x) = \sum_{Q=u,d} \bar{\psi}_Q(x) [i\gamma_\mu \partial_\nu - g_{\mu\nu}(i\gamma^\sigma \partial_\sigma - m_Q)] \psi_Q(x) + T_{\mu\nu, bubble}(x). \quad (5.25)$$

The propagator for free quark is defined by

$$S_{\zeta\zeta'}(x, x') = i \langle \phi_0 | T(\psi_\zeta(x) \bar{\psi}_{\zeta'}(x')) | \phi_0 \rangle \quad (5.26)$$

where ζ, ζ' denote the Dirac (α, α') , flavor (l, l') and color (m, m') indices, i.e. $\zeta = (\alpha, l, m)$ and $\zeta' = (\alpha', l', m')$. The momentum-space representation of the propagator is given by

$$S_{\zeta\zeta'}(p) = \delta_{l'l'} \delta_{mm'} G_{\alpha\alpha'}(p). \quad (5.27)$$

Table 4.1: Masses, spin quantum numbers and electric charges of the quarks and gluons. Bag constant used here, $b = 131.2 \text{ MeV}/f m^3$.

Quark(Q)	$m_Q(\text{MeV})$	J_Q^π	q_Q	Strangeness
u	2 – 8	$\frac{1}{2}^+$	$\frac{2}{3}e$	0
d	5 – 15	$\frac{1}{2}^+$	$-\frac{1}{3}e$	0
s	100 – 300	$\frac{1}{2}^+$	$-\frac{1}{3}e$	-1
g	$m_G = 0(\text{MeV})$	$J_G^\pi = 1^-$	$q_G = 0$	

The baryon density and equation of state in this model can be calculated analogously to the leptonic case. The results are

$$\varrho_B = \frac{1}{3} \frac{\gamma_Q}{(2\pi)^3} \sum_{Q=u,d} \int d^3\vec{q} \Theta(\mu^Q - \omega^Q(\vec{q})), \quad (5.28)$$

$$E = b + \frac{\gamma_Q}{(2\pi)^3} \sum_{Q=u,d} \int d^3\vec{q} \sqrt{m_Q^2 + \vec{q}^2} \Theta(\mu^Q - \omega^Q(\vec{q})), \quad (5.29)$$

$$P = -b + \frac{1}{3} \frac{\gamma_Q}{(2\pi)^3} \sum_{Q=u,d} \int d^3\vec{q} \frac{\vec{q}^2}{\sqrt{m_Q^2 + \vec{q}^2}} \Theta(\mu^Q - \omega^Q(\vec{q})), \quad (5.30)$$

where the degeneracy factors in this model are $\gamma_Q = 2 \times 3 = 6$. The quarks carry baryon number $B = \frac{1}{3}$ and the contribution of gluon to the energy-momentum tensor has been omitted. $P = 0$ now corresponds to self bound quark-gluon gas, in which the Fermi pressure of the quarks just balances the bubble pressure. This occurs for

$$\left[\frac{d}{d\varrho_B} \left(\frac{E}{\varrho_B} \right) \right]_{\varrho_B = \varrho_B^{min}} = 0. \quad (5.31)$$

In this simple model quarks are assumed to be massless. The equation of state of the quark-gluon phase and the energy per baryon for massless quark model are given respectively by

$$P = \frac{1}{3} E - \frac{4}{3} b, \quad (5.32)$$

$$\frac{E}{\varrho_B} = \frac{3\pi^2 b}{2P^{\frac{2}{3}}} + \frac{9}{4} P. \quad (5.33)$$

Hadronic phase is interpreted as the confined state of quark matter. This confined state may change at high temperature or at high densities and a phase transition may occur from baryon-meson phase to deconfined quark-gluon matter. But the critical density, at which the phase transition occurs, and the real mechanism of phase transition are still poorly understood. In this simple model the phase transition occurs at the density range of $\varrho \approx (1.5 - 2.0)\varrho_0$ where ϱ_0 is the nuclear saturation density. The results are illustrated in Fig. 4. The equation of state of quark matter is softer than that of hadronic phase at high densities. At low and high densities energy per particle shows enormous difference between two phases. Such a difference can be understood by the confinement of quark matter in hadronic phase at low densities and non-interacting free phase of quark matter at high densities.

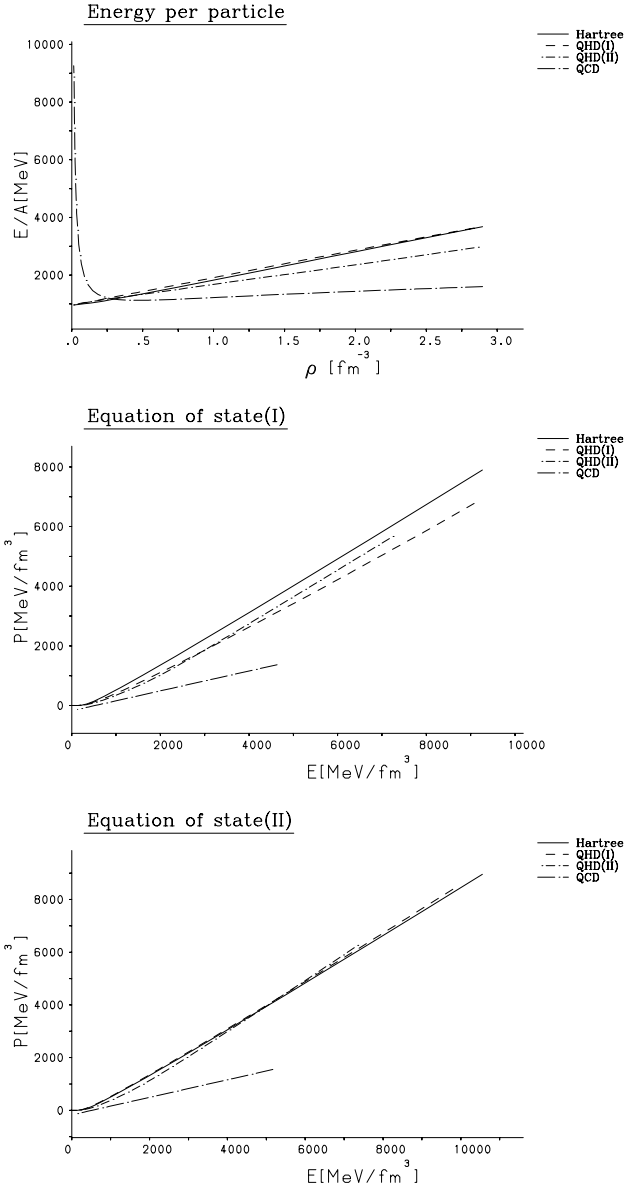


Figure 4: The equation of state and energy per particle of baryon matter in β -equilibrium with leptons in the Hartree(σ, ω), QHD(I)(Hartree-Fock(σ, ω)), and QHD(II)(Hartree-Fock($\sigma, \omega, \pi, \rho$)). Quark matter results in the nuclear domain are also determined in the framework of quantum chromodynamics. THE Equation of state(I) is the results for baryon matter with leptons and the equation of state(II) is calculated only for baryon matter.

6 Application to celestial objects

Generally the fact is accepted that compact objects are the last stage of stellar evolution. Neutron stars, which contain matter in one of the densest forms found in the universe, are one kind of the compact objects ever found. The understanding of matter under such extreme conditions of the density is one of the central issues at present. Because of extrem high density gravitational potential is very strong even on the surface of the star so that the geometry of space-time is changed considerably from flat space. Thus for the construction of realistic stellar models of neutron stars Einstein's theory of general relativity will play the key role.

6.1 General theory of relativity

The Einstein's field equation is defined by[10,3]

$$R_{\mu\nu} - \frac{1}{2}(\Lambda + R)g_{\mu\nu} = 8\pi GT_{\mu\nu} \quad (6.1)$$

where G is the gravitational constant. The terms involving $R_{\mu\nu}$ and R constitute the Einstein curvature tensor. The cosmological constant Λ is, according to the best astronomical evidence, very close to zero in our universe and may generally be omitted. The tensor $T_{\mu\nu}$ is derivable from the star's matter Lagrangian $L_m(x)$,

$$\frac{\partial L_m(x)}{\partial \psi(x)} - \partial_\mu \frac{\partial L_m(x)}{\partial (\partial_\mu \psi(x))} = 0 \quad \text{for field } \psi(x). \quad (6.2)$$

The matter Lagrangian $L_m(x)$ of Eq.(6.2) is in the case of neutron star matter contributed from various baryon, meson and leptonic fields. From Eq.(6.1) it follows that the field equations for empty space, everywhere outside the star, are

$$R_{\mu\nu} = 0 \quad (6.3)$$

The corresponding unique solution of Eq.(6.3) is known as the Schwarzschild metric.

6.2 Non-rotating neutron star

For a static metric describing a spherically symmetric space, the solution of the Einstein Eq.(6.1) is known to have the form[21,3]

$$ds^2 = -e^{2\Phi(r)} dt^2 + e^{2\Lambda(r)} dr^2 + r^2(d\theta^2 + \sin^2 \theta d\phi^2), \quad (6.4)$$

where $\Phi(r)$ and $\Lambda(r)$ are the metric functions. By denoting the spherical star's radius and mass by R_s and M_s , respectively, and introducing the abbreviation

$$\Gamma(r) = \begin{cases} \frac{2Gm(r)}{r} & \text{if } r < R_s \\ \frac{2GM_s}{r} & \text{if } r > R_s \end{cases} \quad (6.5)$$

the metric functions of Eq.(6.4) are then given by

$$e^{2\Lambda(r)} = \frac{1}{1-\Gamma(r)} \quad (6.6)$$

$$e^{2\Phi(r)} = e^{-2\Lambda(r)} = 1 - \Gamma(r) \quad (\text{outside the star}). \quad (6.7)$$

The structure of spherical neutron stars is determined by the Oppenheimer-Volkoff equations[22] of hydrostatic equilibrium:

$$\frac{dP}{dr} = -Gr^{-2}(\varrho(r) + P(r))(m(r) + 4\pi r^3 P(r))(1 - \Gamma(r))^{-1}, \quad (6.8)$$

with the boundary condition $P(r=0) \equiv P(\varrho_c) \equiv P_c$ [22]. The mass contained in a sphere of radius r ($\leq R_c$), denoted by $m(r)$, follows from the density $\varrho(r)$

$$m(r) = 4\pi \int_0^r dr' r'^2 \varrho(r'). \quad (6.9)$$

The metric function $\Phi(r)$ satisfies the differential equation

$$\frac{d\Phi(r)}{dr} = -\frac{1}{\varrho(r)+P(r)} \frac{dP(r)}{dr}, \quad (6.10)$$

with the boundary condition

$$\Phi(r = R_s) = \frac{1}{2} \ln[1 - \Gamma(R_s)]. \quad (6.11)$$

The Oppenheimer-Volkoff Eqs.(6.9) - (6.11) can only be solved once the equation of state of matter, $P = P(\varrho)$, has been specified.

One of important neutron star properties is the redshift of photons emitted at the star's surface. For non-rotating neutron star the shifts in spectral line frequency of photons are caused by the strong gravitational field.

In the non-rotating limit it is written by

$$z = e^{\Phi(R_s)} - 1 = \sqrt{1 - \frac{2M_s G}{R_s}} - 1. \quad (6.12)$$

Here M_s and R_s denote the spherical star's mass and radius, respectively.

6.3 Rotating neutron star

The gravity of the normal stars is not strong enough to hold their matter against rotational shedding if they rotate fast. Only compact objects, whose gravity is strong enough, can rotate fast. Since the first pulsar, very fast rotating star, has been detected, the existence of such objects has had a profound impact on subsequent astrophysical research. To identify such objects several possibilities have been suggested, but only a rotating neutron star meets all theoretical objections[10]. The rotational effect causes the deformation of the star. As a result the metric is not spherically symmetric. There are two main approaches, exact solution and perturbation solution, to determine the physical properties of the deformed stars. In this work we perform our investigations in the framework

of an improved version of Hartle's perturbative method.

6.3.1 Perturbation solution

The basic idea in Hartle's treatment is the development of a perturbation solution based on the Schwarzschild metric of Eq.(6.4). The assumption that under the influence of rotation the star distorts and the pressure, energy, and baryon number density change by amounts of ΔP , $\Delta\epsilon$, $\Delta\varrho$, respectively, the energy-momentum density tensor of Eq.(6.1) changes by $\Delta T_{\mu\nu}$ and becomes ($g_{\mu\nu} = (-1, 1, 1, 1)\delta_{\mu\nu}$)[23,24,3]:

$$T_{\mu\nu} = T_{\mu\nu}^0 + \Delta T_{\mu\nu}, \quad (6.13)$$

$$T_{\mu\nu}^0 = (\epsilon + P)u_\mu u_\nu + P g_{\mu\nu}, \quad (6.14)$$

$$\Delta T_{\mu\nu} = (\Delta\epsilon + \Delta P)u_\mu u_\nu + \Delta P g_{\mu\nu}. \quad (6.15)$$

The quantity $T_{\mu\nu}^0$ of Eqs.(6.13) and (6.14) denotes the perfect fluid energy momentum tensor where P , ϵ , and ϱ are measured by an observer in a locally inertial frame comoving with the fluid at the instant of measurement.

The normalization of the fluids four-velocity u of Eqs.(6.14) and (6.15) is $g^{\mu\nu}u_\mu u_\nu = -1$. For the distortion functions of Eqs.(6.13) and (6.15) a multipole expansion is performed. Assuming axial symmetry, one can write

$$\Delta P = (\epsilon + P)(p_0 + p_2 P(\cos\theta)), \quad (6.16)$$

$$\Delta\epsilon = \Delta P \frac{\partial\epsilon}{\partial P}, \quad (6.17)$$

$$\Delta\varrho = \Delta P \frac{\partial\varrho}{\partial P}. \quad (6.18)$$

The quantities p_0 , p_2 , and $P(\cos\theta)$ of Eq.(6.16) are the monopole and quadrupole pressure perturbation function, and the second order Legendre polynomial respectively. The perturbed metric, expanded through second order in the star's rotational velocity, Ω , has the form[25]

$$ds^2 = -e^{2\nu(r,\theta,\Omega)} dt^2 + e^{2\psi(r,\theta,\Omega)} (d\phi - \omega(r, \Omega)dt)^2 + e^{2\mu(r,\theta,\Omega)} d\theta^2 + e^{2\lambda(r,\theta,\Omega)} dr^2 + O(\Omega^3). \quad (6.19)$$

The metric functions in the disturbed line element of Eq.(6.19) have the form[23,25,3]

$$e^{2\nu(r,\theta,\Omega)} = e^{2\Phi(r)} [1 + 2(h_0(r, \Omega) + h_2(r, \Omega)P_2(\cos\theta))], \quad (6.20)$$

$$e^{2\psi(r,\theta,\Omega)} = r^2 \sin^2\theta [1 + 2(v_2(r, \Omega) - h_2(r, \Omega))P_2(\cos\theta)], \quad (6.21)$$

$$e^{2\mu(r,\theta,\Omega)} = r^2 [1 + 2(v_2(r, \Omega) - h_2(r, \Omega))P_2(\cos\theta)], \quad (6.22)$$

$$e^{2\lambda(r,\theta,\Omega)} = e^{2\Lambda(r)} [1 + \frac{2}{r} \frac{m_0(r,\Omega)G + m_2(r,\Omega)P_2(\cos\theta)}{1 - \Gamma(r)}]. \quad (6.23)$$

They are independent of time and azimuthal angle ϕ , assuming stationary rotation and axial symmetry about the axis of rotation. Here, ω is the angular

velocity of the local inertial frame and is proportional to Ω . It is known as dragging of the local inertial frame. The functions p_0 , h_0 , m_0 , p_2 , h_2 , m_2 , and v_2 are all functions of r proportional to Ω^2 which are obtained from the field equations. The critical angular velocity for which this approach should be valid is given by[23]

$$\Omega_c = \sqrt{\Gamma_s/(2R_s^2)} = 36\sqrt{[M_s/M_\odot]/[R_s/km]^3} \times 10^4 s^{-1}, \quad (6.24)$$

which expresses Newtonian balance of centrifuge and gravity.

The angular velocity relative to the local inertial frame, $\bar{\omega}$, is defined by

$$\bar{\omega} = \Omega - \omega. \quad (6.25)$$

in terms of which the fluid inside the star moves.

The stellar equilibrium condition of Eq.(6.8) is now supplemented by the centrifugal forces and yields a condition for $\bar{\omega}$ from the field equation

$$\frac{d}{dr}(r^4 j(r) \frac{d\bar{\omega}}{dr}) + 4r^3 \frac{dj(r)}{dr} \bar{\omega} = 0, \quad (6.26)$$

where

$$j(r) = e^{-\Phi(r)} \sqrt{1 - \Gamma(r)}. \quad (6.27)$$

Equation (6.26) is to be solved subject to the boundary conditions that (i) $\bar{\omega}$ is regular at $r = 0$ and (ii) $d\bar{\omega}/dr|_{r=0} = 0$.

Outside the star one has

$$\bar{\omega}(r, \Omega) = \Omega - \frac{2G}{r^3} J(\Omega), \quad r > R_s, \quad (6.28)$$

where $J(\Omega)$ is the total angular momentum of the star, defined by

$$J(\Omega) = \frac{R_s^4}{6G} \left(\frac{d\bar{\omega}}{dr} \right)_{R_s}. \quad (6.29)$$

The moment of inertia, I , is then defined to be[3]

$$I = \frac{J(\Omega)}{\Omega} = \frac{8\pi}{3} \int_0^{R_s} dr r^4 \frac{\epsilon+P}{\sqrt{1-\Gamma}} \frac{\bar{\omega}}{\Omega} e^{-\Phi}. \quad (6.30)$$

Relativistic corrections to the Newtonian expression for I come from the dragging of local inertial frames($\bar{\omega}/\Omega < 1$) and the redshift (e^Φ) and space-curvature factors($1/\sqrt{1-\Gamma}$).

The set of coupled monopole ($l = 0$) equations can be integrated once $\bar{\omega}$ is known from Eq.(6.26). The differential equations for the monopole mass and pressure perturbation functions, m_0 and p_0 (for $r < R$), are given by[23,24,3]

$$\frac{dm_0}{dr} = 4\pi r^2 \frac{\partial \epsilon}{\partial P} (\epsilon + P) p_0 + \frac{1}{12G} j^2 r^4 \left(\frac{\bar{\omega}}{dr} \right)^2 + \frac{8\pi}{3} r^4 j^2 \frac{\epsilon+P}{1-\Gamma} \bar{\omega}^2, \quad (6.31)$$

$$\frac{dp_0}{dr} = -G \frac{1+8\pi r^2 GP}{r^2(1-\Gamma)^2} m_0 - 4\pi G \frac{(\epsilon+P)r}{1-\Gamma} p_0 + \frac{1}{12} \frac{r^3 j^2}{1-\Gamma} \left(\frac{\bar{\omega}}{dr} \right)^2 + \frac{1}{3} \frac{d}{dr} \left(\frac{r^2 j^2 \bar{\omega}^2}{1-\Gamma} \right). \quad (6.32)$$

The boundary conditions are that $m_0 \rightarrow 0$ and $p_0 \rightarrow 0$ for $r \rightarrow 0$. Outside the

star one has

$$m_0(\Omega) = \Delta M(\Omega) - \frac{G}{r^3} J(\Omega)^2, \quad (6.33)$$

where ΔM is the change in gravitational mass due to rotation. Evaluation of Eq.(6.33) at the star's surface leads for ΔM to

$$\Delta M(\Omega) = m_0(R_s) + \frac{G}{R_s^3} J(\Omega)^2. \quad (6.34)$$

The spherical function h_0 of Eq.(6.20) can be solved from the algebraic relations

$$h_0 = -p_0 + \frac{r^2}{3} \bar{\omega}^2 e^{-2\Phi} + h_{0c}, \quad r < R_s, \quad (6.35)$$

and

$$h_0 = -\frac{\Delta MG}{r(1-\Gamma)} + \frac{J^2 G^2}{r^4(1-\Gamma)}, \quad r > R_s, \quad (6.36)$$

where h_{0c} is chosen to make $h_0(r)$ continuous at $r = R_s$.

Inside the star the quadrupole perturbation functions v_2 and h_2 of Eqs.(6.20) - (6.22) satisfy the following coupled set of differential equations[23,24,3]:

$$\frac{dv_2}{dr} = -2 \frac{d\Phi}{dr} h_2 + \left[\frac{1}{r} + \frac{d\Phi}{dr} \right] \left[-\frac{r^3}{3} \frac{dj^2}{dr} \bar{\omega}^2 + \frac{j^2}{6} r^4 \left(\frac{d\bar{\omega}}{dr} \right)^2 \right], \quad (6.37)$$

and

$$\begin{aligned} \frac{dh_2}{dr} = & -2 \frac{d\Phi}{dr} + \frac{2G}{1-\Gamma} \left(\frac{d\Phi}{dr} \right)^{-1} [2\pi(\epsilon + P) - \frac{m}{r^3}] h_2 - \frac{2}{r^2(1-\Gamma)} \left(\frac{d\Phi}{dr} \right)^{-1} v_2 + \\ & \frac{1}{6} \left[r \frac{d\Phi}{dr} - \frac{1}{2r(1-\Gamma)} \left(\frac{d\Phi}{dr} \right)^{-1} \right] r^3 j^2 \left(\frac{d\bar{\omega}}{dr} \right)^2 - \frac{1}{3} \left[r \frac{d\Phi}{dr} + \frac{1}{2r(1-\Gamma)} \left(\frac{d\Phi}{dr} \right)^{-1} \right] (r\bar{\omega})^2 \frac{dj^2}{dr}. \end{aligned} \quad (6.38)$$

Their boundary conditions are $h_2(0) = v_2(0) = 0$ and $h_2(\infty) = v_2(\infty) = 0$.

Outside the star the solutions are

$$h_2 = \left(\frac{GJ}{r^2} \right)^2 \left(1 + \frac{2}{\Gamma} \right) + A Q_2^2 \left(\frac{2}{\Gamma} - 1 \right), \quad (6.39)$$

and

$$v_2 = -\left(\frac{GJ}{r^2} \right)^2 + A \frac{\Gamma}{\sqrt{1-\Gamma}} Q_2^1 \left(\frac{2}{\Gamma} - 1 \right). \quad (6.40)$$

Here $Q_n^m(\cos\theta)$ are the associated Legendre polynomials of the second class.

The constant A which is chosen to make h_2 and v_2 continuous at $r = R_s$ is given by

$$\begin{aligned} A = & \left[\left(\frac{GJ}{R_s^2} \right)^2 \left(1 + \frac{\Gamma_s}{2} \right)^{-1} - h_2^{(P)} \right] \frac{1}{h_2^{(H)}(R_s)} \frac{dh_2^{(H)}(R_s)}{dr} + \frac{dh_2^{(P)}(R_s)}{dr} - \\ & \left(\frac{GJ}{R_s^2} \right)^2 \frac{1}{R_s} \left(1 + \frac{\Gamma_s}{2} \right)^{-1} \left[\frac{\Gamma_s/2}{1+\Gamma_s/2} - 4 \right] \times \left[\frac{dQ_2^2(2/\Gamma_s-1)}{dr} - \frac{Q_2^2(2/\Gamma_s-1)}{h_2^{(H)}(R_s)} \frac{dh_2^{(H)}(R_s)}{dr} \right]^{-1}. \end{aligned} \quad (6.41)$$

Here the quantities $h_2^{(H)}(R_s)$ and $h_2^{(P)}(R_s)$ are the homogeneous and particular solutions of Eq.(6.38) respectively.

The quadrupole mass and pressure perturbation functions m_2 and p_2 are given

by

$$m_2 = r(1 - \Gamma)[-h_2 - \frac{r^3}{3}(\frac{dj^2}{dr})\bar{\omega}^2 + \frac{r^4 j^2}{6}(\frac{\bar{\omega}}{dr})^2], \quad (6.42)$$

and

$$p_2 = -h_2 - \frac{1}{3}(r\bar{\omega})^2 e^{-2\Phi}. \quad (6.43)$$

From the functions p_0, p_2, v_2, h_2 and the constant A the properties of the rotationally deformed star can be calculated.

The star's spherical surface of constant density is distorted by rotation into the spheroid

$$r \rightarrow r + \xi_0(r) + \xi_2(r) + r[v_2(r) - h_2(r)]P_2(\cos\theta), \quad (6.44)$$

where

$$\xi_0(r) = -p_0(\epsilon + P)(\frac{\partial P}{\partial r})^{-1} \quad (6.45)$$

and

$$\xi_2(r) = -p_2(\epsilon + P)(\frac{\partial P}{\partial r})^{-1}. \quad (6.46)$$

The star's eccentricity, defined by Hartle, is

$$e^{HT} = \sqrt{(\frac{R_{eq}}{R_p})^2 - 1} \approx \sqrt{-3[v_2(r) - h_2(r) + \frac{\xi_2(r)}{r}]|_{r=R_s}}. \quad (6.47)$$

An alternative definition of the star's eccentricity is given by [25]

$$e = \sqrt{1 - (\frac{R_p}{R_{eq}})^2}. \quad (6.48)$$

The quadrupole moment of the rotating star can be calculated from

$$Q = \frac{8}{5}A(\frac{\Gamma_s}{2})^2 + G(\frac{J}{R_s})^2. \quad (6.49)$$

6.3.2 Kepler frequency

An upper limit on neutron star rotation is set by the Kepler frequency Ω_k , beyond which instability sets in because of mass shedding at the star's equator. For the metric function of Eqs.(6.20) and (6.21), the general relativistic Kepler frequency is given as the solution Ω of [25]

$$\Omega = [e^{\nu(\omega) - \psi(\omega)} V(\Omega) + \omega(\Omega)]_{eq}, \quad (6.50)$$

with

$$V(\Omega) = [\frac{d\omega(\Omega)/dr}{2d\psi(\omega)/dr} e^{\psi(\omega) - \nu(\omega)} + \sqrt{\frac{d\nu(\omega)/dr}{d\psi(\omega)/dr} + (\frac{d\omega(\Omega)/dr}{2d\psi(\omega)/dr} e^{\psi(\omega) - \nu(\omega)})^2}]_{eq}. \quad (6.51)$$

The subscript "eq" refers to evaluation at the star's equator. The quantity V denotes the orbital velocity of a comoving observer at the star's equator relative to a locally non-rotating observer with zero angular momentum in the

ϕ -direction. If one neglects the distortion functions in the metric of Eq.(6.19) and sets $\bar{\omega} = \Omega$, neglecting the dragging effect of local inertial frames, then the orbital velocity V_{eq} of Eq.(6.51) takes on the form

$$V_{eq} = \sqrt{\frac{\Gamma_{eq}}{2}} \frac{1}{\sqrt{1-\Gamma_{eq}}} \quad (6.52)$$

$$\rightarrow R_{eq}\Omega_c \quad \text{for } \Gamma_{eq} \ll 1, \quad (6.53)$$

with Ω_c given by Eq.(6.24).

As indicated here, the result of classical Newtonian mechanics for the velocity of a particle in a circular orbit is recovered from Eq.(6.52) by neglecting the curvature of space-time geometry(i.e. $\Gamma_{eq} \ll 1$), the rotational deformation of the star, and the dragging effect of local inertial frames. an approximate solution of Eq.(6.50) in the case of a rotating neutron star of limiting mass can be obtained from the empirically established expression of Haensel and Zdunik[28] ,and Friedman, Ipser and Parker[29], which reads

$$\Omega_k \approx 24\sqrt{[M_s/M_\odot]/[R_s/km]^3} \times 10^4 s^{-1} = \frac{2}{3}\Omega_c. \quad (6.54)$$

This formular has been established from the exact numerical solution of the Einstein's field equations for a rapidly rotating neutron star.

The frequency shift of light emitted at the star's equator in backward(B) or forward(F) direction is given by[25]

$$z_{B/F}(\Omega) = e^{-\nu(\Omega)}(1 \pm \omega(\Omega)e^{\psi(\Omega)-\nu(\Omega)})^{-1} \left(\frac{1 \pm V(\Omega)}{1 \mp V(\Omega)}\right)^{1/2} - 1. \quad (6.55)$$

The redshift of photons emitted at the star's pole is obtained from

$$z_p(\Omega) = e^{-\nu(\Omega)} - 1. \quad (6.56)$$

In rotating star the redshift of photons is caused by the Doppler shift as well as the presence of a strong gravitational field.

The stability parameter which is important for a proper understanding of the stability of rotating neutron star is defined by

$$t(\Omega) = \frac{T(\Omega)}{|W(\Omega)|} \quad (6.57)$$

with

$$T(\Omega) = \frac{1}{2}J(\Omega)\Omega, \quad (6.58)$$

$$W(\Omega) = M_p(\Omega) + T(\Omega) - M_s(\Omega). \quad (6.59)$$

Here $T(\Omega)$ and $W(\Omega)$ are the star's rotational energy and gravitational energy respectively. The general relativistic Kepler periods, which are derived directly from Kepler frequencies Ω_K , are given by

$$P_K = \frac{2\pi}{\Omega_K}. \quad (6.60).$$

6.4 Matter in neutron star

For neutron stars the density of matter spans an enormous range, from high densities of $\rho \approx (2.5 - 5) \times 10^{15} \text{g/cm}^3$ ($\rho \approx (10 - 20)\rho_0$, where ρ_0 is the density of normal nuclear matter, $\rho_0 = 2.5 \times 10^{14} \text{g/cm}^3$) in the cores of neutron stars obtained from a given equation of state down to zero at the star's edge. As an example we illustrate in Fig. 5 the radial dependence of the energy density in relativistic non-rotating neutron star models for the matter equations of state. One sees that the typical central energy densities in the cores of neutron stars lie in the range of $7 < \epsilon_c/\epsilon_0 < 11$ in this study. The pressure as a function of radial distance of non-rotating neutron star models is exhibited in Fig. 5. The composition of neutron star matter is presently understood to be as follows[3]:

1. Surface: Matter at mass densities $10^4 < \rho < 10^6 \text{g/cm}^3$ (which corresponds to energy densities $5.6 \times 10^{-9} < \epsilon < 3.9 \times 10^{-6} \text{MeV/fm}^3$) is composed of normal nuclei and non-relativistic electrons.
2. Outer crust: At densities $7 \times 10^6 < \rho < 4 \times 10^{11} \text{g/cm}^3$ ($3.9 \times 10^{-6} < \epsilon < 0.22 \text{MeV/fm}^3$) the electrons become relativistic (forming a relativistic e^- gas), and the nuclei (lighter metals), while becoming more and more neutron rich, form a solid Coulomb lattice.
3. Inner crust: At densities $4 \times 10^{11} < \rho < 2 \times 10^{14} \text{g/cm}^3$ ($0.22 < \epsilon < 110 \text{MeV/fm}^3$) one encounters the neutron drip regime of neutron matter: neutrons begin to populate free states outside the (neutron saturated) nuclei. Furthermore matter clusters into extremely neutron rich nuclei (heavy metals) that are arranged on a lattice and immersed in a neutron and a relativistic electron gas.
4. Neutron liquid: For $\rho > 2 \times 10^{14} \text{g/cm}^3$ ($\epsilon > 110 \text{MeV/fm}^3$) the clusters begin to dissolve and n, p , and e^- form a Fermi fluid.
5. Core region: Hyperon production sets in at densities $\rho > 5 \times 10^{14} \text{g/cm}^3$ ($\epsilon > 300 \text{MeV/fm}^3$). Unsolved issues concern meson condensation, phase transition of confined hadronic matter to quark matter.

The surface and crust regions of neutron stars are so thin that these contribute negligibly to the bulk properties (e.g. mass, radius, moment of inertia) of the more massive members (stars of gravitational masses $M_g > M_\odot$) of a neutron star sequence constructed for a given equation of state. Most of the bulk properties of the star is contributed by superdense matter. The sub-nuclear equation of state used in this work are joined with the nuclear equation of state at densities typically on the order of $\epsilon/\epsilon_0 \approx (1 - 10) \times 10^{-2}$ (see Table 6.1).

The high density (i.e. $\epsilon_c/\epsilon_0 > 1$) neutron star matter equation of state is the key uncertainty in neutron star models. It forms the basic input quantity necessary for solving both the sets of non-rotating as well as rotating structure equations. By means of solving the neutron star matter field equations subject to the constraints of charge neutrality and generalized β -equilibrium for the relativistic

Hartree-Fock approximation, it has been found that in the vicinity of nuclear matter density, $\rho \approx \rho_0 (\rho_0 = 0.15 \text{ fm}^{-3})$, neutron star matter consists almost purely of neutrons with a small admixture of electrons and protons. For increasing values of ρ , high-momentum neutrons are subject of β -decay into protons and electrons or muons. A detailed discussion of the composition of neutron star matter is given in Section 5.1. Other unsettled issues are the possibility of a phase transition from nuclear matter (confined hadronic phase of baryons and mesons) into quark matter in the cores of neutron stars and the influence of meson condensation.

In this work the neutron star models are constructed on the equations of state which fulfill the following physical constraint:

- (1) The internal energy of the star, $\epsilon^{int}(\rho) = \epsilon(\rho) - m_B \rho$, is positive.
- (2) The equations of state satisfy the microscopic stability condition $\frac{\partial P}{\partial \epsilon} \geq 0$ (Le Chatelier's principle) and the causality condition $\frac{\partial P}{\partial \epsilon} \leq c^2$.
- (3) The equations of state below some matching density is known [3,10].

Table 6.1: Neutron star matter equation of state.

Model	Equation of state	Mass density range	Composition
HW &	Harrison-Wheeler	$7.8 < \rho < 10^{11}$	Crystalline; light metals, electron gas
NV & &	Negele-Vautherin	$10^{11} < \rho < 10^{13}$	Crystalline; heavy metals, relativistic electron gas
HF1	RHF(σ, ω)	$10^{13} < \rho < 1.25 \times 10^{16}$	p, n, e^-, μ^-
HF2	RHF($\sigma, \omega, \pi, \rho$)	$10^{13} < \rho < 1.25 \times 10^{16}$	p, n, e^-, μ^-

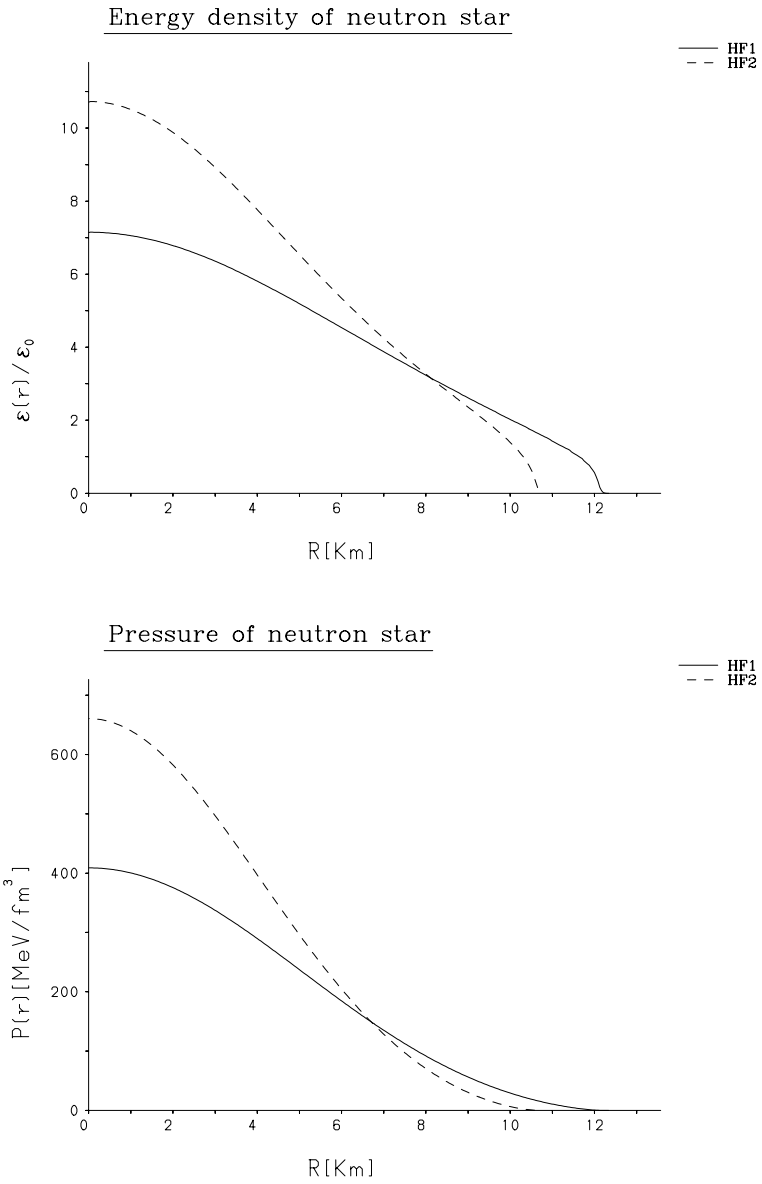


Figure 5: Energy density and Pressure as a function of radius of neutron star in the Hartree-Fock calculations, $\text{HF1}(\sigma, \omega)$ and $\text{HF2}(\sigma, \omega, \pi, \rho)$.

6.5 Neutron star properties

Astronomical observation provides more or less accurate results of the neutron star bulk properties such as masses, rotational frequencies, moment of inertia, redshifts, etc.. The gravitational mass, which is one of the most important properties of neutron stars, can be inferred directly from observation of X-ray binaries and binary pulsars (e.g. the Hulse - Taylor radio pulsar PSR 1913+16). For instance, the extremely accurately determined mass of the Hulse - Taylor binary pulsar PSR 1913+16,

$$M(\text{PSR1913} + 16)/M_{\odot} = 1.444 \pm 0.0003,$$

is given by Taylor and Weisberg[27].

The approximate range of neutron star masses which are determined from observation is $1.0 < M/M_{\odot} < 2.0$. One of the fastest so far observed pulsars, which are interpreted as rapidly rotating neutron stars, has rotational period of about $1.6ms$. The fastest known pulsar is PSR 1937 + 21, which spins on its axis every $1.56ms$. It is known that there is no method to determine the radius of neutron stars directly. But the radius can be derived from combinations of data of well-observed objects with theoretical assumptions. It yields a radius range from 10 to 15 km [3]. Another global neutron star properties are the moment of inertia and redshift. The low bound on the moment of inertia, which is estimated for the pulsar in the Crab nebular, is known to be $\approx 10^{45} gcm^2$ [34]. Redshift data, which is provided by measurements of γ -ray burst pair annihilation lines in the range of $300 - 511(MeV)$, shows range of $0.2 < z < 0.5$ [35]. In the following two sections we discuss the results of non-rotating and rotating neutron star calculations, which are carried out in this work.

6.5.1 Non-rotating neutron star

By solving the neutron star properties the basic input quantity is the equation of state. The equations of state for neutron star matter are illustrated in Fig. 4. For pure baryon matter the equation of state is very analogous to the results of asymmetric matter in the Hartree and Hartree-Fock calculations. However, the equation of state of baryon-lepton mixed phase behaves much differently. For instance the exchange contribution of ρ - meson stiffens the equation of state at high densities in the Hartree-Fock($\sigma, \omega, \pi, \rho$) calculation. However lepton matter softens the equation of state for the Hartree-Fock($\sigma, \omega, \pi, \rho$) model at all densities. This is the symmetrization effect. In this work the lepton's contributions are also taken into the calculation. The bulk properties of non-rotating neutron stars are determined in the central density ranges of $(0.8 - 50)\epsilon_0$, where ϵ_0 is the energy density of normal nuclear matter. The six different equations of state, which are determined in this work, are used as an input parameter for calculation of neutron star properties. All results are evaluated on the maximum mass condition, which is defined by $\frac{dM}{de}|_{M=M_{max}} = 0$. The results for pure neutron matter and baryon matter in β -equilibrium with leptons are illustrated in Fig. 26 - Fig. 27 in Appendix C. In pure neutron matter the core densities of the

stars reach $\epsilon_c = 5.71\epsilon_0$ in the HF1 and $\epsilon_c = 7.14\epsilon_0$ in the HF2 respectively. For baryon matter in β -equilibrium with leptons the core densities of the stars are $\epsilon_c = 7.14\epsilon_0$ for the HF1 and $\epsilon_c = 10.7\epsilon_0$ for the HF2 respectively. For baryon and lepton system maximum masses span a range of $2.14M_\odot < M < 2.4M_\odot$, and in pure neutron matter maximum masses of the star lie in the range of $2.28M_\odot < M < 2.84M_\odot$. Maximum masses, which are calculated using the realistic Hartree-Fock models, lie in the range of upper limits, which are estimated from observations. Radius, which are determined in this work, coincide with the results that are obtained from observations. Redshift data shows range of $0.50 < z < 0.61$. The moment of inertia is about to be $\approx 10^{45} \text{ gcm}^2$ and baryon numbers of the star are $\approx 10^{57}$. All global quantities, which are given above, are dependent on the behavior of the equation of state. If the equation of state is soft, then the core density of star is higher, and its mass and radius are smaller than those of the star systems, for which the equation of state is stiff. There is very little difference in maximum mass which is obtained from the spherical and shell structure calculations. The shell structure is created at the energy densities of $\epsilon > 12\epsilon_0$ (ϵ_0 is the energy density of normal nuclear matter). Such energy densities are much higher than the energy density range of $7 < \epsilon_c/\epsilon_0 < 11$, at which the bulk properties of neutron stars are estimated. The estimated bulk properties of neutron stars above the energy density range of $7 < \epsilon_c/\epsilon_0 < 11$ are unphysical. Therefore the calculations from shell structure may have no effect on neutron star results.

6.5.2 Rotating neutron star

The results for rotating neutron star calculations are illustrated in Fig. 28 - Fig. 31 in Appendix D. Rotational effect changes some bulk properties (e.g. gravitational mass, radius, etc.) of the star considerably. We now discuss the results of neutron star models that are rotating at their respective absolute maximum Kepler frequencies Ω_K . The calculations are performed for the models of the equations of state for neutron star matter of Fig. 4. The Kepler frequencies Ω_K set on absolute upper limit on stable rotation. For rotational frequencies $\Omega > \Omega_K$ the star is unstable because of mass shedding at the star's equator. The equations of state, which are determined in this work, lead to absolute limiting Kepler frequencies in the range of $1.025 \times 10^4 \text{ s}^{-1} < \Omega_K < 1.087 \times 10^4 \text{ s}^{-1}$. These Kepler frequencies yield rotational Kepler periods of $P_K = 0.63 \text{ ms}$ and 0.60 ms for the HF1 and HF2 respectively. These results are by far smaller than the smallest observed pulsar period. The rotational Kepler periods are exhibited as a function of gravitational mass in Fig. 31. The central energy densities in the cores of neutron stars at their Kepler frequencies are shown in Fig. 28 for different equations of state. The star models constructed for the HF1 and HF2 have central energy densities in the range of $6.0 < \epsilon_c/\epsilon_0 < 7.2$. This result shows that rotation causes the decrease of the central energy density. For the HF1 and HF2 rotation decreases the central energy density $\approx 11\%$ and $\approx 33\%$ respectively. The determination of rotating mass $M_{rot}(\epsilon_c, \Omega_K(\epsilon_c))$ demands for a self-consistent numerical solution of the general relativistic stellar structure equations of

rapidly rotating massive objects. The numerical outcome obtained for M_{rot} as a function of ϵ_c is graphically depicted in Fig. 28. The rotating masses obtained from this work are $M_{rot} = 2.75M_\odot$ and $2.75M_\odot$ for the HF1 and HF2 respectively. As mentioned in Section 6.5.1, the largest gravitational mass is obtained for equation of state, which is rather stiff behavior at high densities. In Fig. 29 the numerical results for gravitational masses are illustrated as a function of the core density ϵ_c . Rotational effect increases the gravitational mass $\approx 15\%$ for the HF1 and HF2. The eccentricities of the rotationally deformed neutron star models, in Eq.(6.48), depend on the ratio of polar to equatorial radius, R_p/R_{eq} . The polar and equatorial radii as a function of gravitational mass are exhibited in Fig. 29. We find $R_p/R_{eq} \approx 0.73$ for the HF1 and HF2. The calculated velocities at the star's equator are exhibited as a function of gravitational mass in Fig. 30. It amounts at most to 59.4% and 57.8% of the velocity of light for the HF1 and HF2 respectively. The smaller Kepler frequencies imply lower equatorial velocities. The stability parameter t as a function of Ω_K are shown in Fig. 31. The value of the stability parameter obtained for limiting-mass models (here HF1 and HF2) takes on values of $0.10 < t < 0.11$. The forward and backward redshifts at the star's equatorial are illustrated in Fig. 30. We can see a large rotational effect on redshift.

7 Summary

In the framework of the Hartree-Fock approximations the physical properties of superdense matter have been studied. In these models dynamics is determined by self-consistent baryon-baryon interactions which are mediated by the exchange of mesons. The density ranges of matter, which is investigated in this work, span from below the nuclear saturation density to the density of $\varrho \approx 50\varrho_0$, where ϱ_0 is the density of normal nuclear matter. The main aim of this work is the investigation of the behaviour of the ground state in the density evolution. For such an investigation one of the necessary basic quantities is the equation of state of matter. We have determined the equations of state for different kinds of matter, which are pure neutron matter, asymmetric nuclear matter and neutron star matter in the Hartree and Hartree-Fock theories. The results for neutron matter show the instability mode of the ground state above the density of $\varrho \approx 12\varrho_0$ where ϱ_0 is the nuclear saturation density. For that reason above the density of $\varrho \approx 12\varrho_0$ there may be other new stable ground states. A phase transition may occur from the standard ground state, in which states of matter are distributed in the Fermi sphere in momentum space, to a new stable ground state at high densities. For neutron matter such a phase transition has been suggested earlier and is confirmed in this work taking more realistic dynamics. For asymmetric nuclear matter this instability modes are decreasing in the symmetrization process and the instabilities disappear in symmetric nuclear matter. In symmetric nuclear matter there is no evidence for shell structure at high densities and the spherical structure is still a stable ground state. Another interesting and more realistic phase of matter is neutron star matter, in which baryons are in β -equilibrium with leptons in the density evolution. It is more realistic to suppose that neutron stars are not composed of pure neutron matter but consist of baryons in β -equilibrium with leptons. Since the equation of state of matter is the basic input parameter for determining the bulk properties of neutron stars, we have applied the equations of state, which are obtained in this work, to the neutron star calculations. But results show that there are small differences in the bulk properties of neutron stars for different models used in this work. In conclusion the equation of state of matter is still uncertain in the density range of $\varrho \approx (2 - 15)\varrho_0$, because the real dynamics of matter in this density range is poorly understood. For above densities of $\varrho \approx 15\varrho_0$ the simple standard models(e.g. Hartree and Hartree-Fock etc.) may not be applied to determine the physical properties of matter, because of appearances of unphysical results as shown in the calculation of neutron matter. More realistic dynamics is necessary to understand the physical properties of superdense matter.

A Appendix A

Neutron Matter

Fig. 6 - Fig. 18

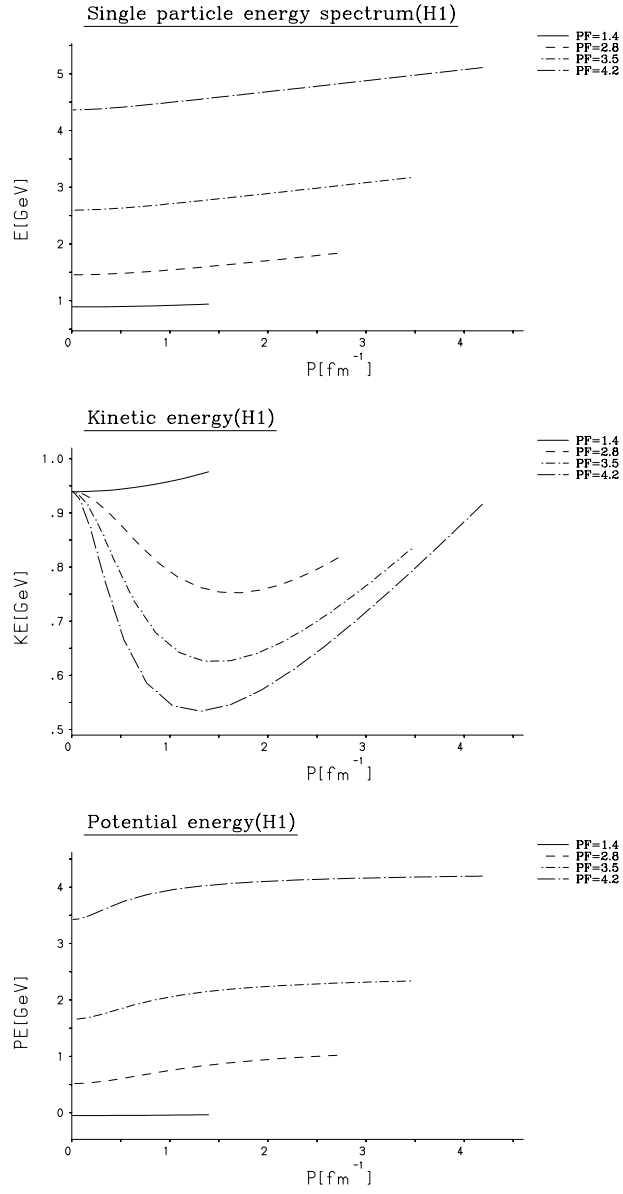


Figure 6: Single particle spectrum ,kinetic energy and potential energy as a function of momentum at given densities in the H1 (σ, ω) calculation. The results are for pure neutron matter.

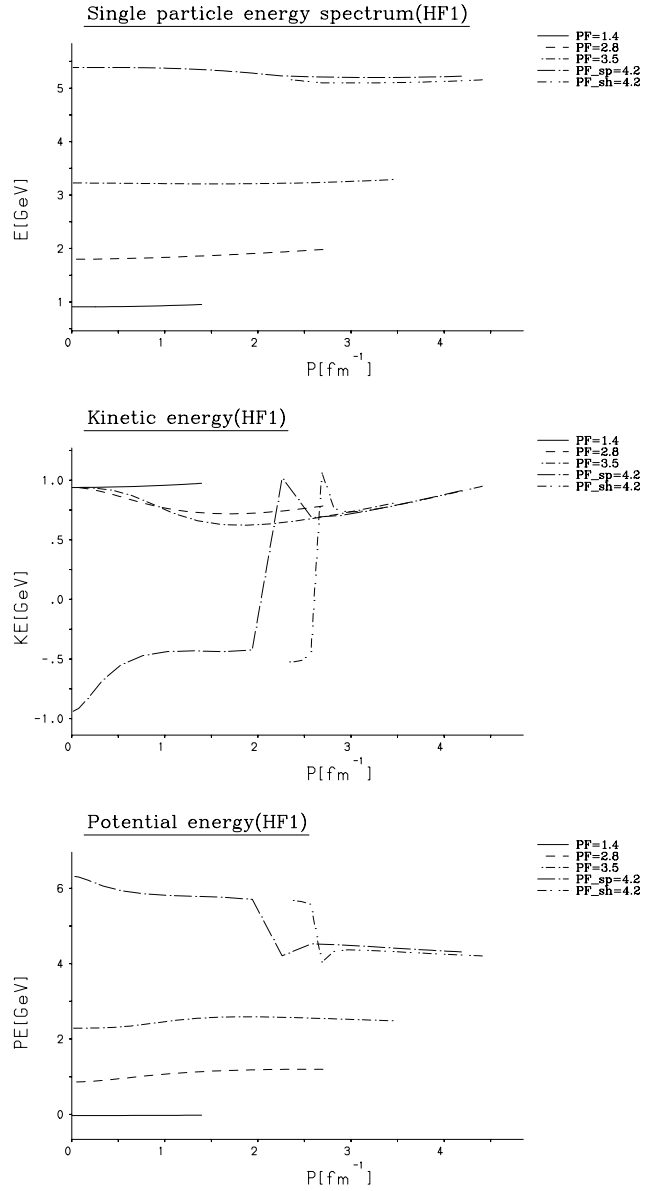


Figure 7: Single particle spectrum ,kinetic energy and potential energy as a function of momentum at given densities in the HF1 (σ, ω) approximation. The results are for pure neutron matter.

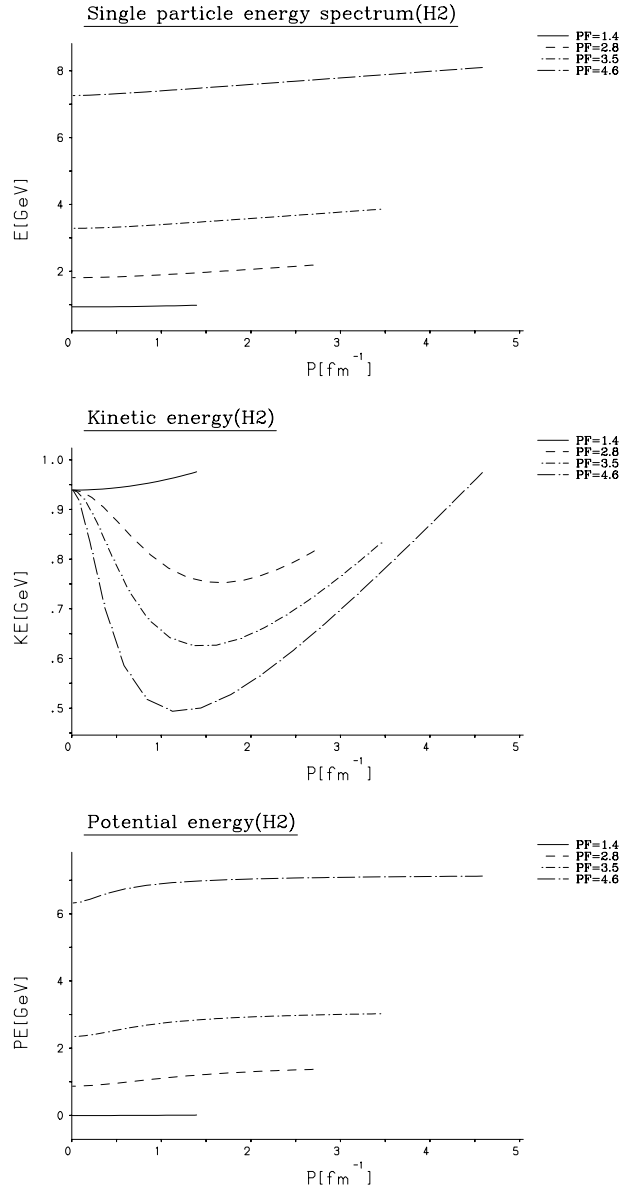


Figure 8: Single particle spectrum ,kinetic energy and potential energy as a function of momentum at given densities in the H2 (σ, ω, ρ) calculation. The results are for pure neutron matter.

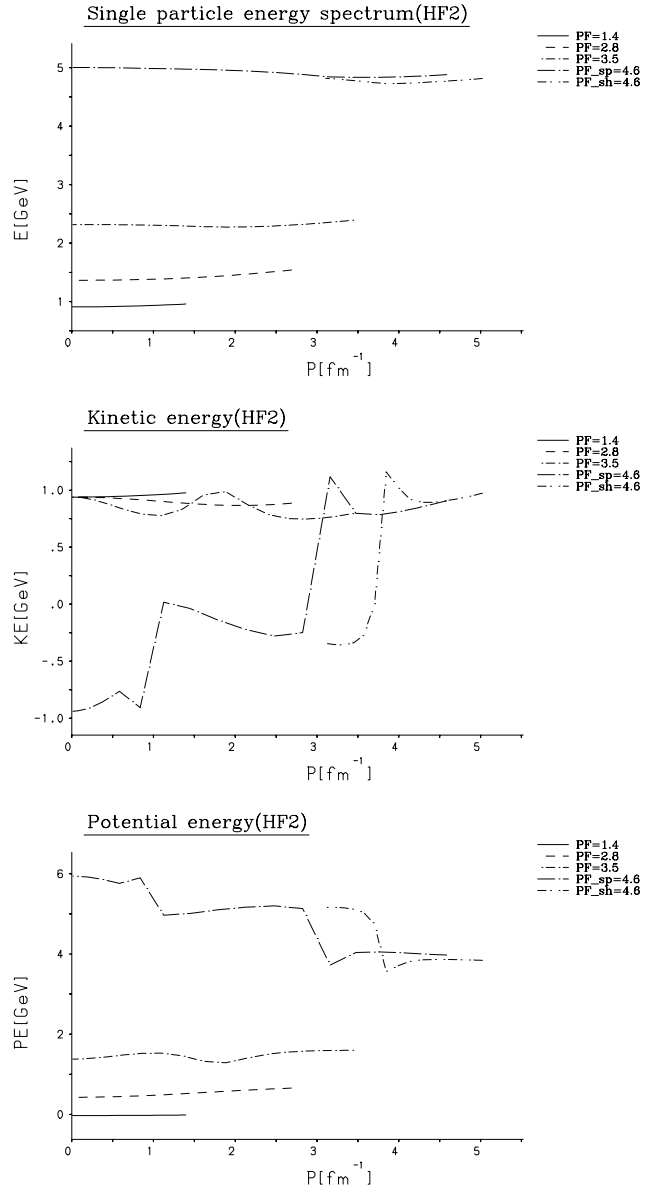


Figure 9: Single particle spectrum ,kinetic energy and potential energy as a function of momentum at given densities in the HF2 ($\sigma, \omega, \pi, \rho$) treatment. The results are for pure neutron matter.

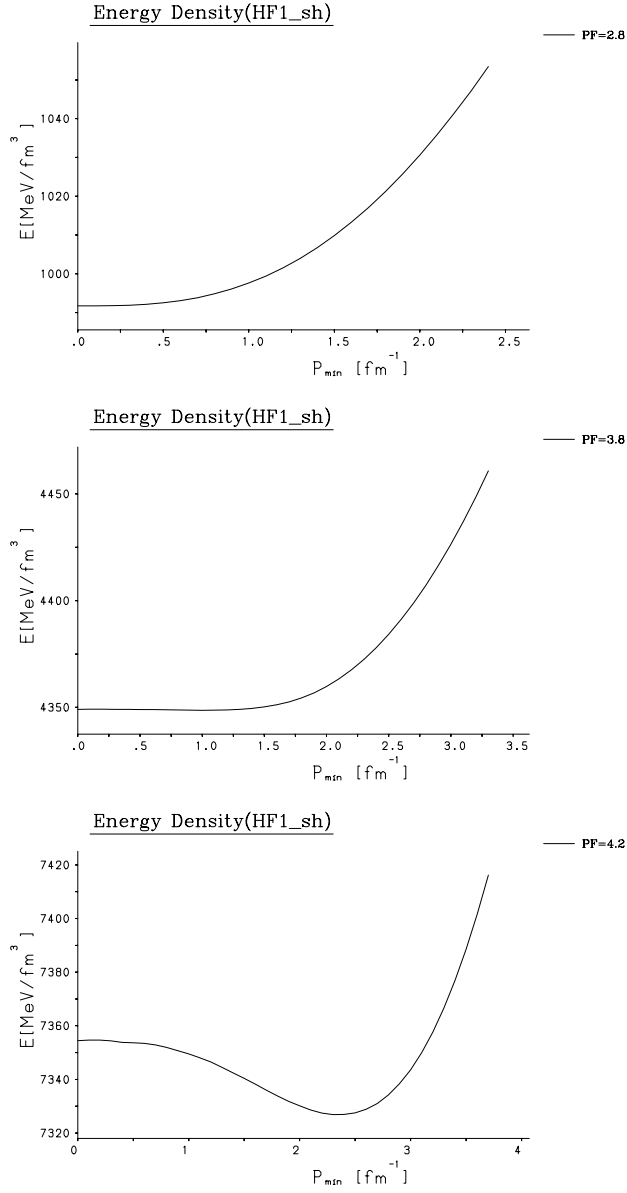


Figure 10: Energy density as a function of P_{min} for the shell distribution of neutron matter in the HF1(σ, ω) approximation.

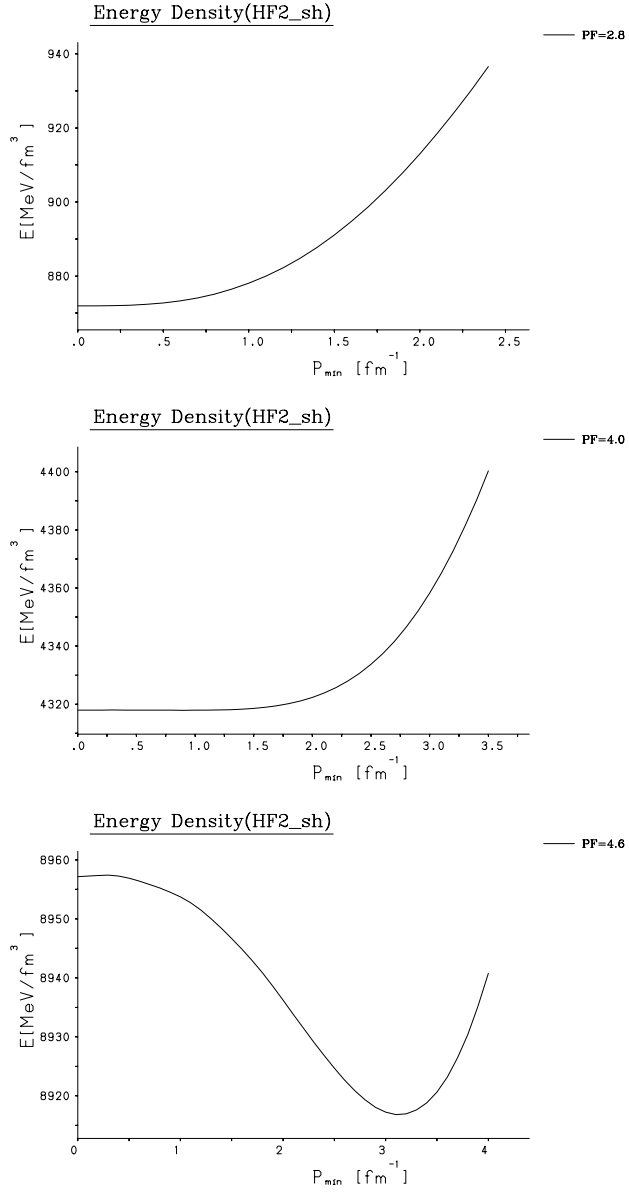


Figure 11: Energy density as a function of P_{min} for shell distribution of neutron matter in the HF2($\sigma, \omega, \pi, \rho$) approximation.

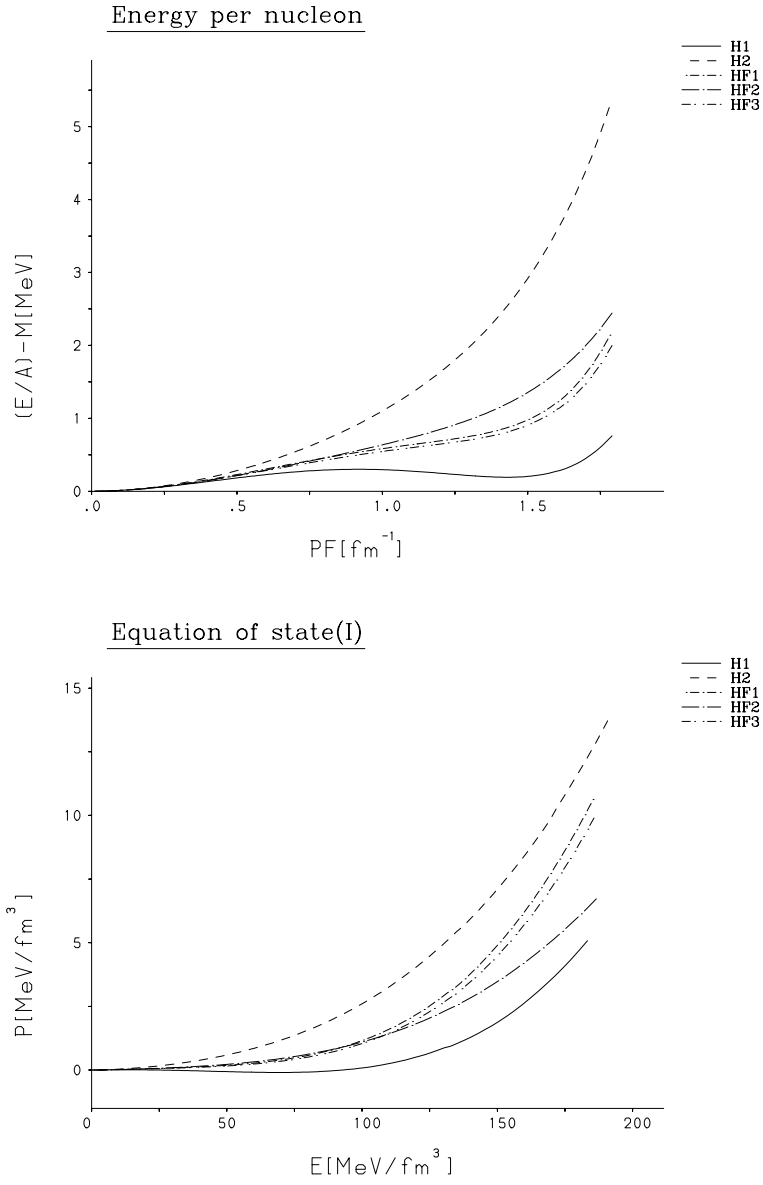


Figure 12: Energy per nucleon and equation of state for neutron matter at low densities for different models, H1(σ, ω), H2 (σ, ω, ρ), HF1(σ, ω), HF2 ($\sigma, \omega, \pi, \rho$), and HF3(σ, ω, π).

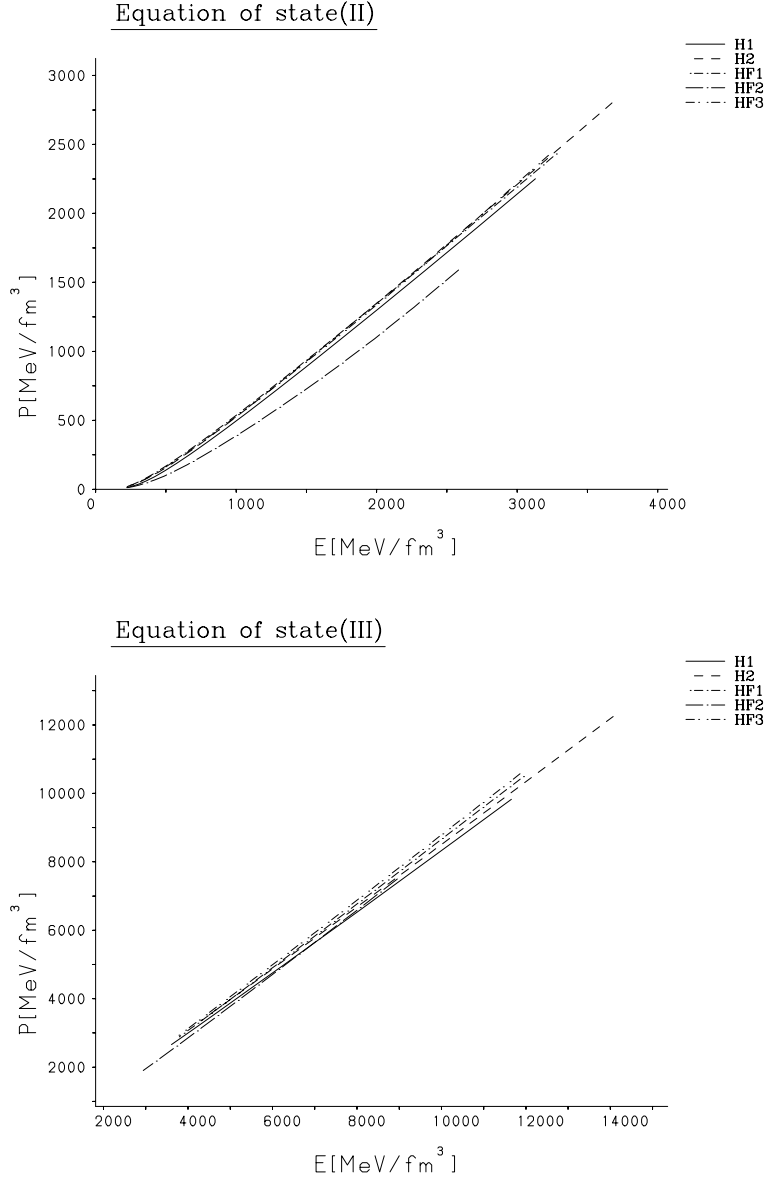


Figure 13: Equation of state of neutron matter at high densities for different models, $H1(\sigma, \omega)$, $H2(\sigma, \omega, \rho)$, $HF1(\sigma, \omega)$, $HF2(\sigma, \omega, \pi, \rho)$, and $HF3(\sigma, \omega, \pi)$.

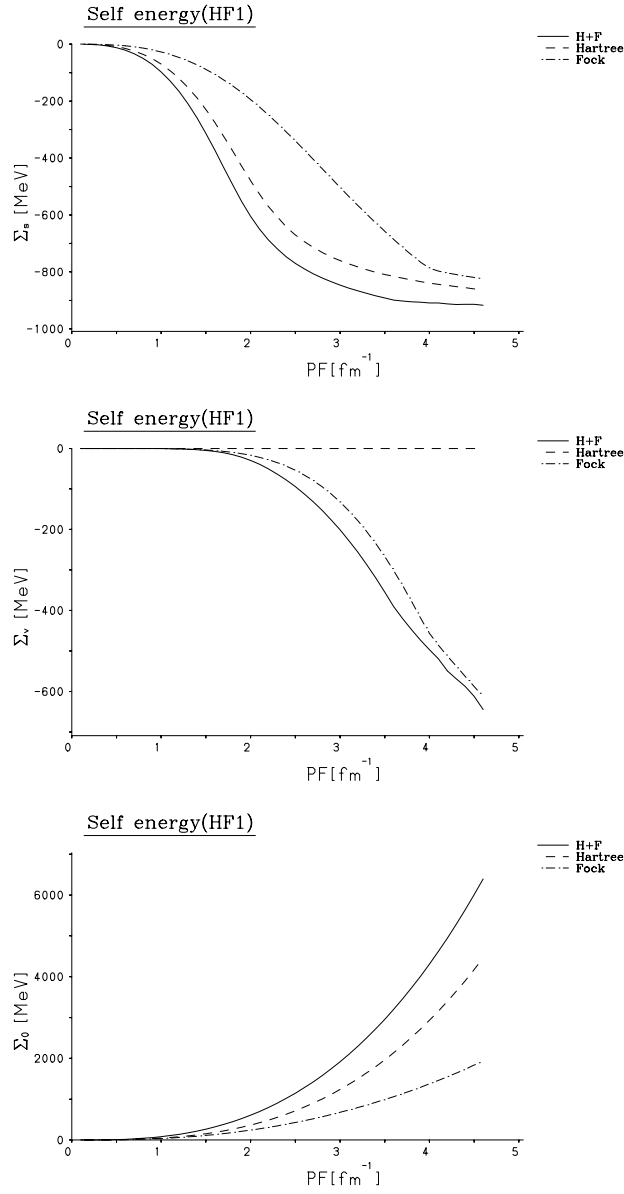


Figure 14: Hartree and Fock term contributions to self-energies of neutron matter for the HF1(σ, ω) calculations. The results are illustrated as a function of the Fermi momentum.

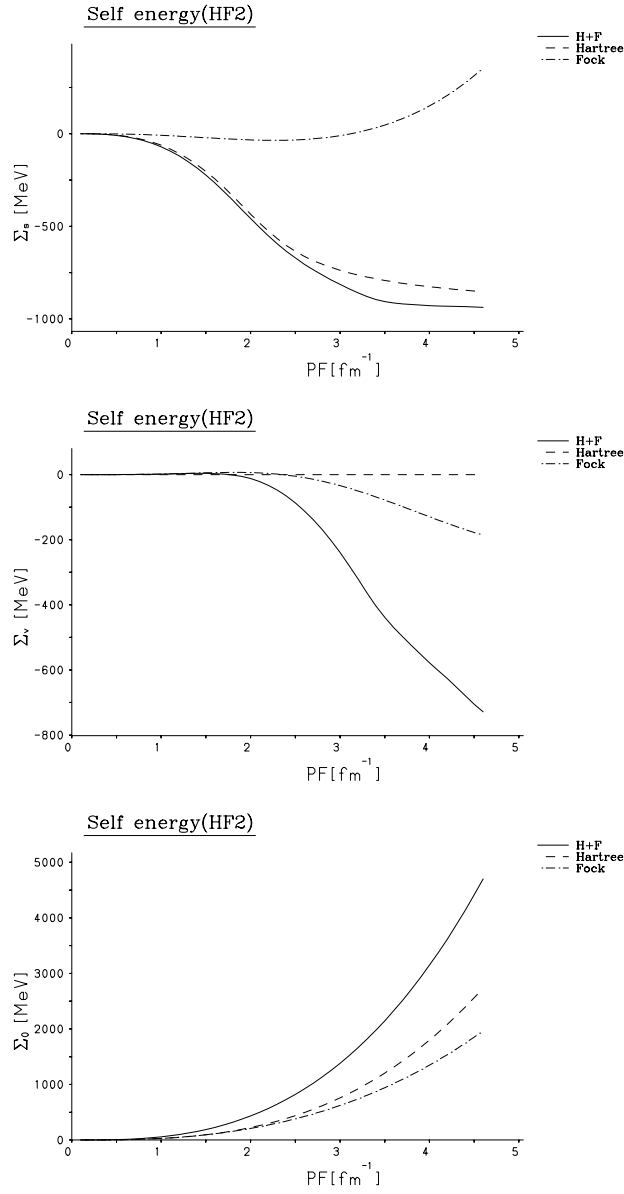


Figure 15: Hartree and Fock term contributions to self-energies of neutron matter for the HF2($\sigma, \omega, \pi, \rho$) calculations. The results are illustrated as a function of the Fermi momentum.

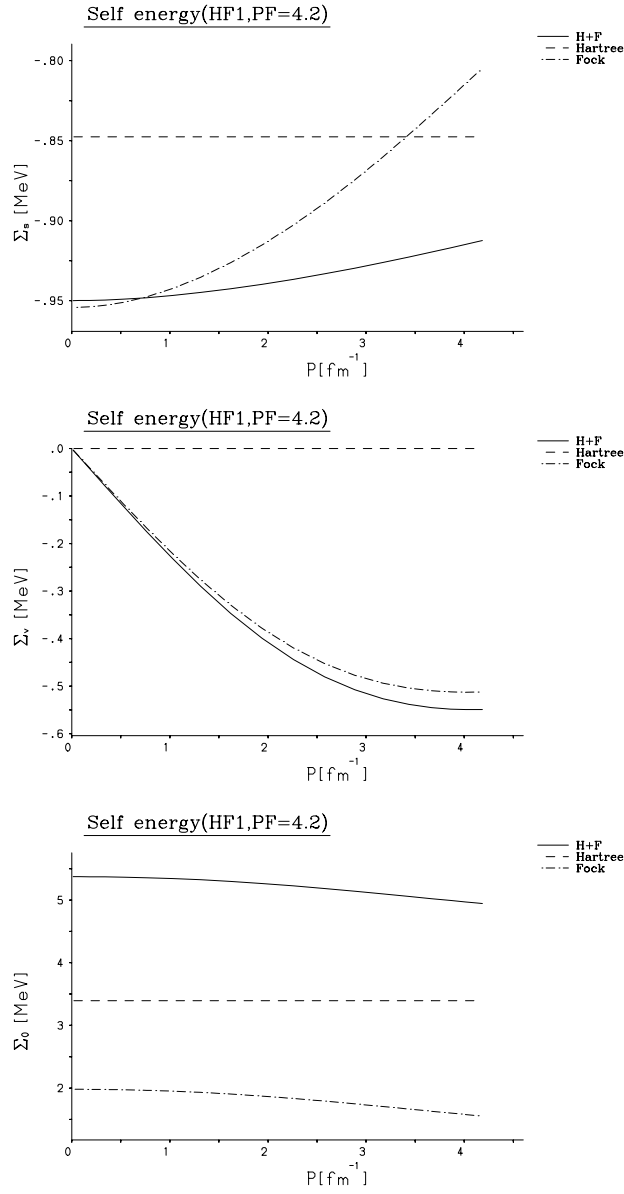


Figure 16: Hartree and Fock term contributions to self-energies of neutron matter for the HF1(σ, ω) calculations. The results are illustrated as a function of momentum.

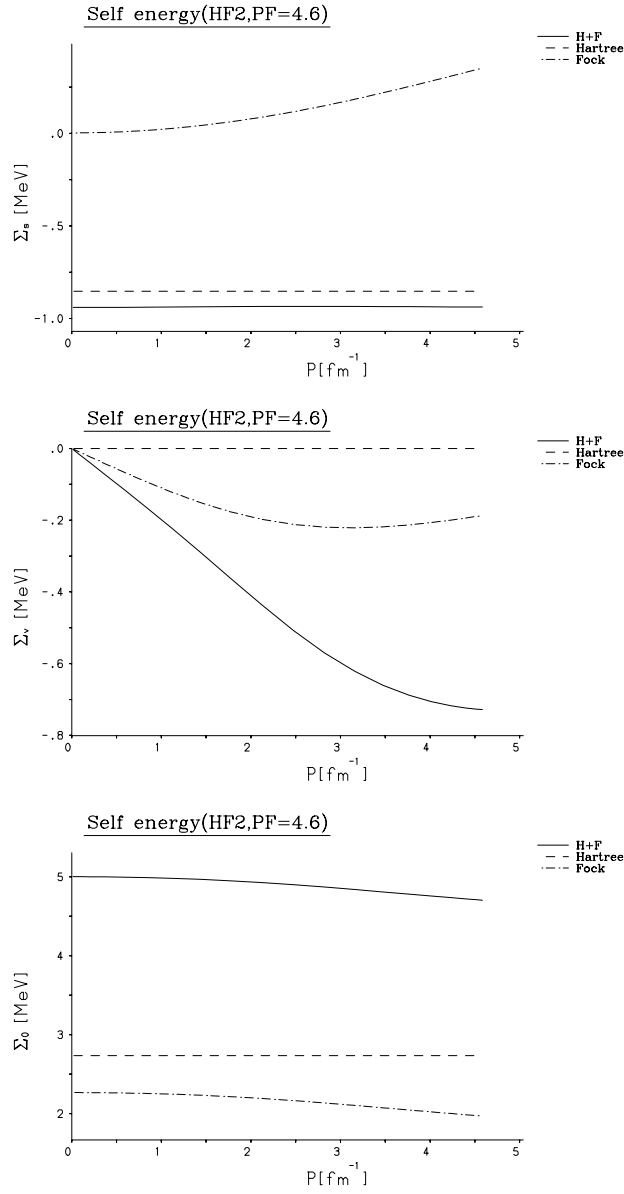


Figure 17: Hartree and Fock term contributions to self-energies of neutron matter for the HF2($\sigma, \omega, \pi, \rho$) calculations. The results are illustrated as a function of momentum.

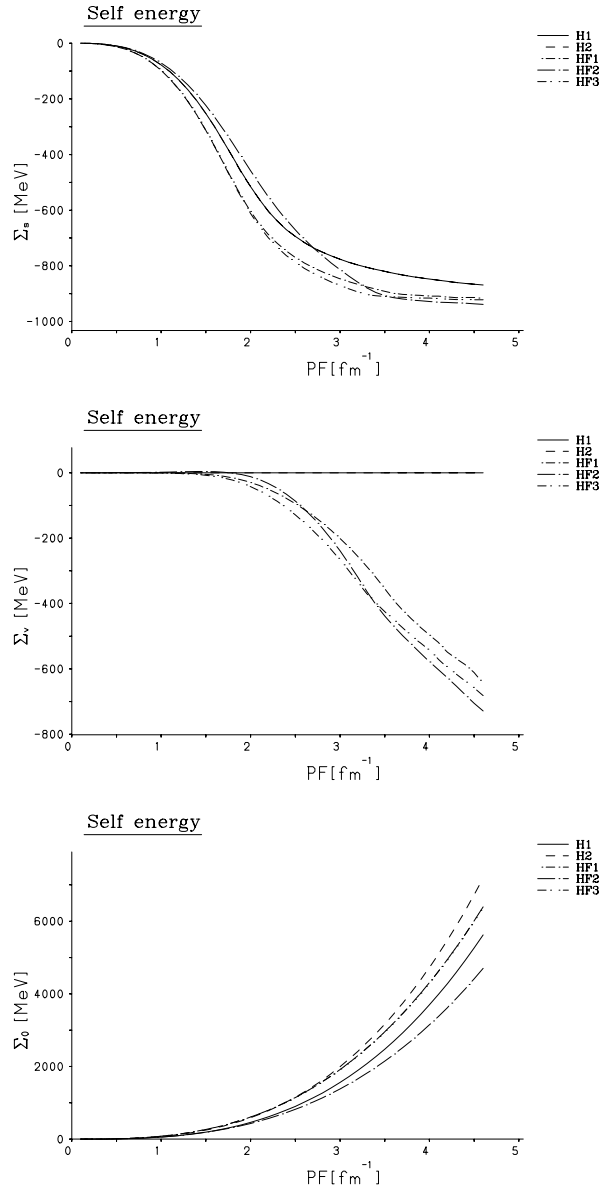


Figure 18: Self-energies of neutron matter as a function of Fermi momentum for the same models as those in Fig. 12.

B Appendix B

Asymmetric Nuclear Matter

Fig. 19 - Fig. 25

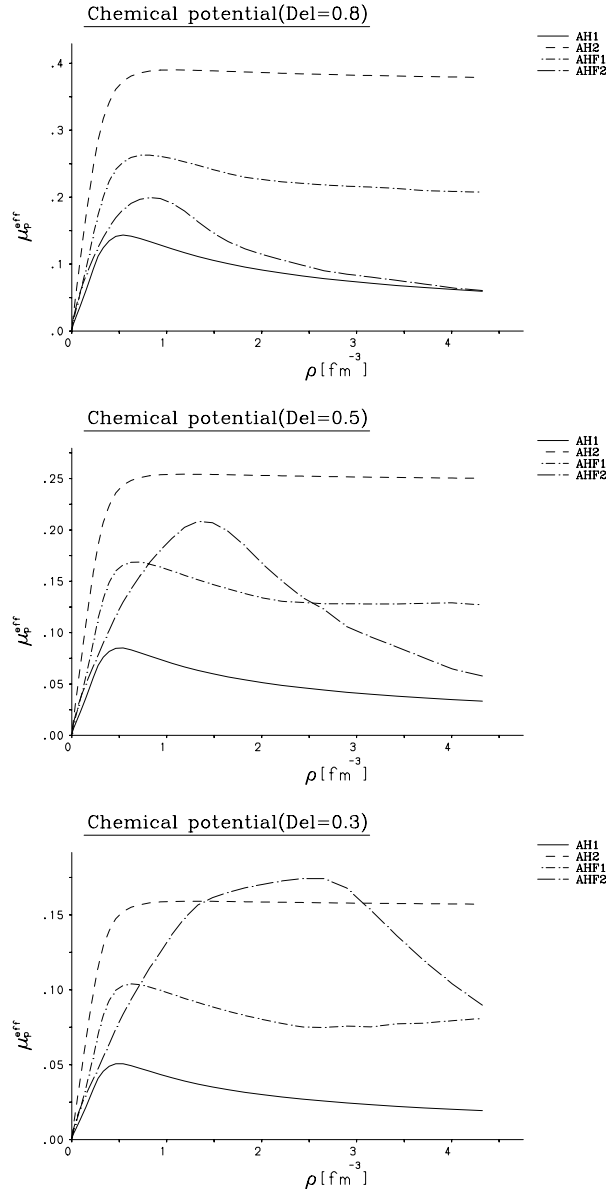


Figure 19: Behavior of chemical potential of asymmetric nuclear matter in the symmetrization process. Here the $AH1(\sigma, \omega)$ and $AH2(\sigma, \omega, \rho)$ are the Hartree treatment for asymmetric nuclear matter. The $AHF1(\sigma, \omega)$ and $AHF2(\sigma, \omega, \pi, \rho)$ are the Hartree-Fock approximations for asymmetric nuclear matter. Here $Del = (\rho_n - \rho_p)/\rho_B$.

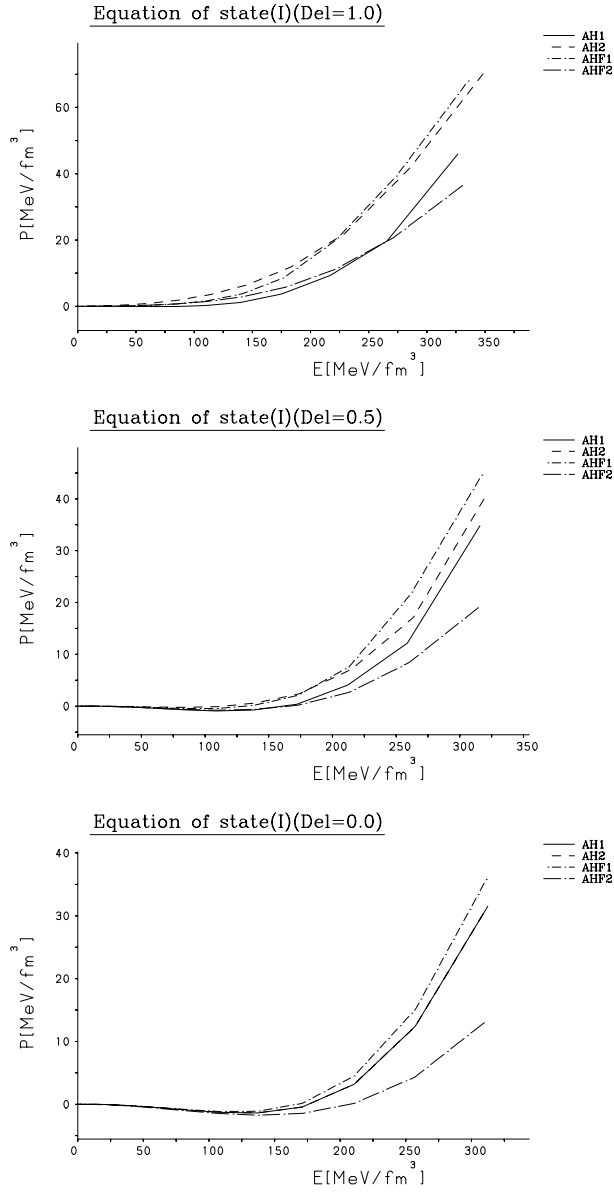


Figure 20: Equation of state of asymmetric nuclear matter at low densities for the same models as those in Fig. 19.

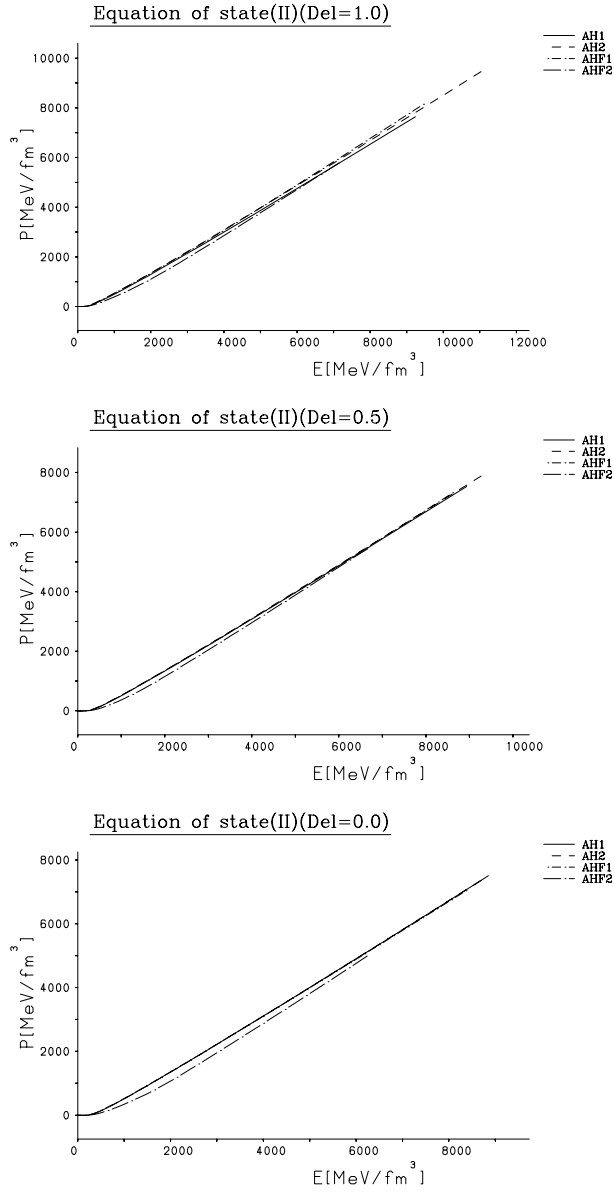


Figure 21: Equation of state of asymmetric nuclear matter at high densities for the same models as those in Fig. 19.

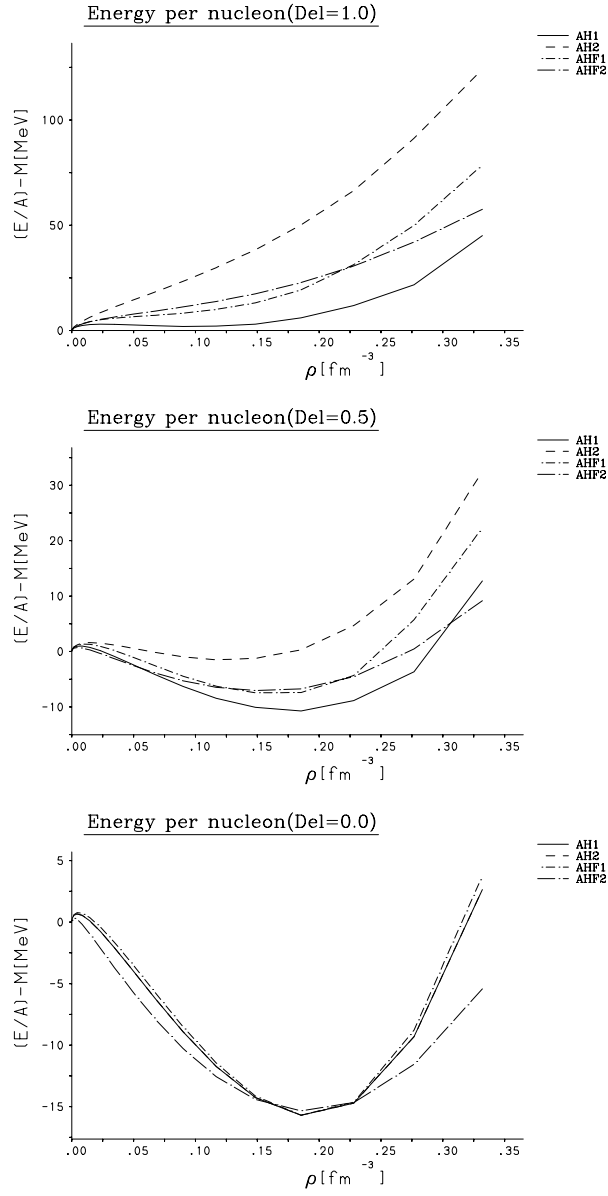


Figure 22: Energy per nucleon of asymmetric nuclear matter for the same models as those in Fig. 19.

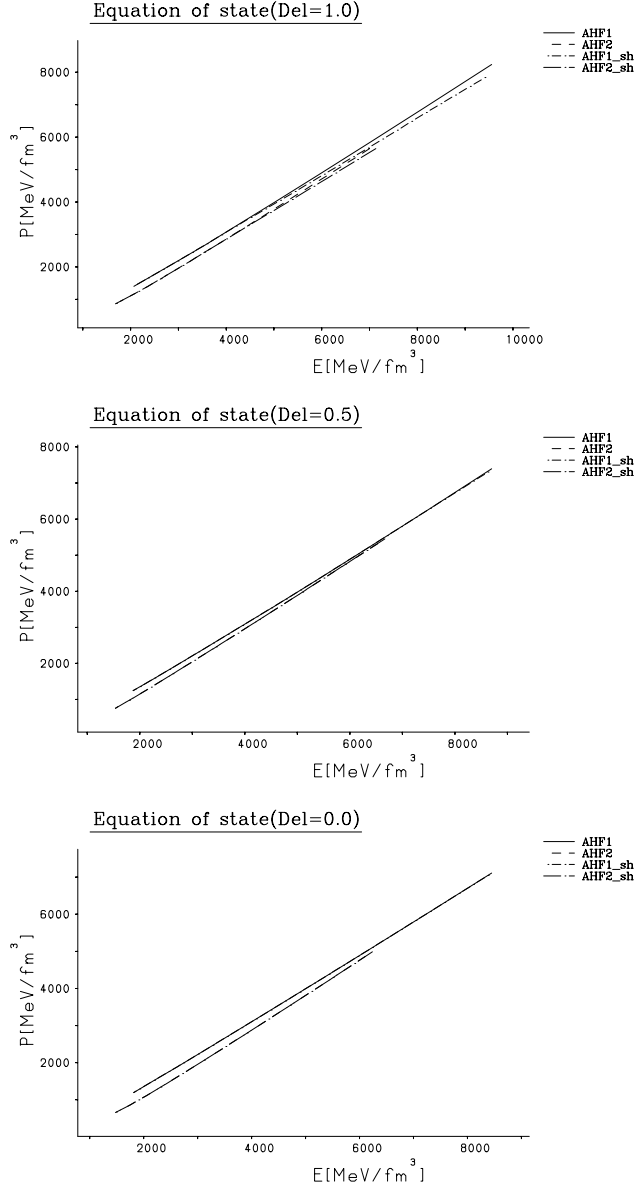


Figure 23: Equation of state of asymmetric nuclear matter for the spherical and shell structure at high densities. Here The $AHF1(\sigma, \omega)$ and $AHF2(\sigma, \omega, \pi, \rho)$ for spherical distribution, $AHF1_{sh}(\sigma, \omega)$ and $AHF2_{sh}(\sigma, \omega, \pi, \rho)$ for shell distribution respectively.

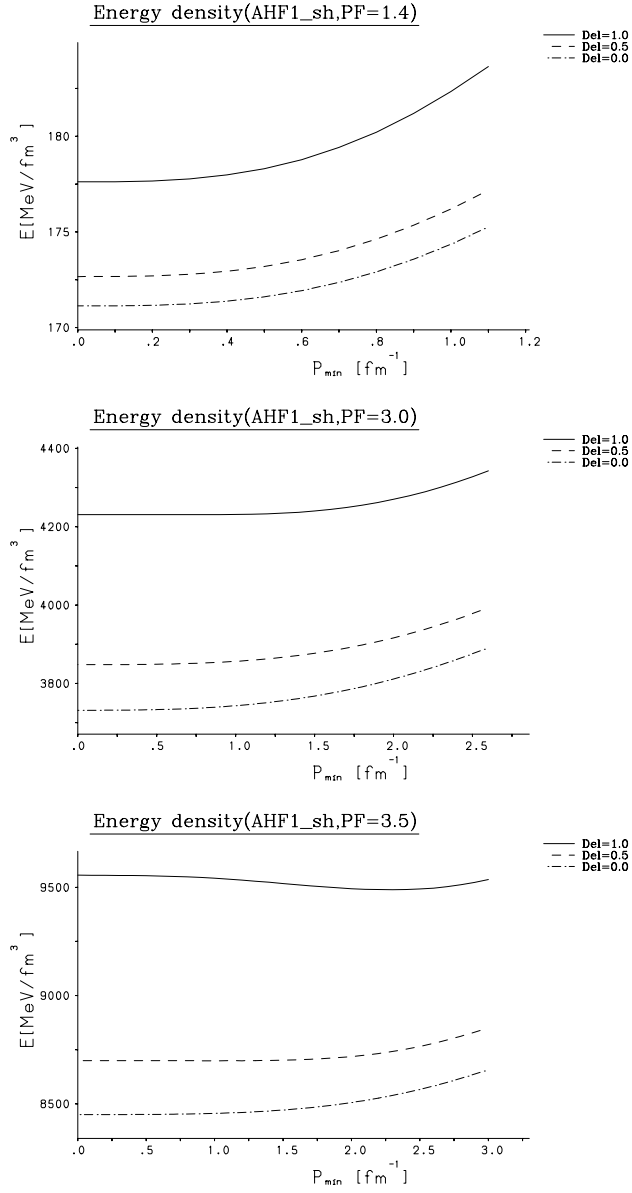


Figure 24: Energy density of asymmetric nuclear matter as a function of P_{min} for shell distribution in the HF1(σ, ω).

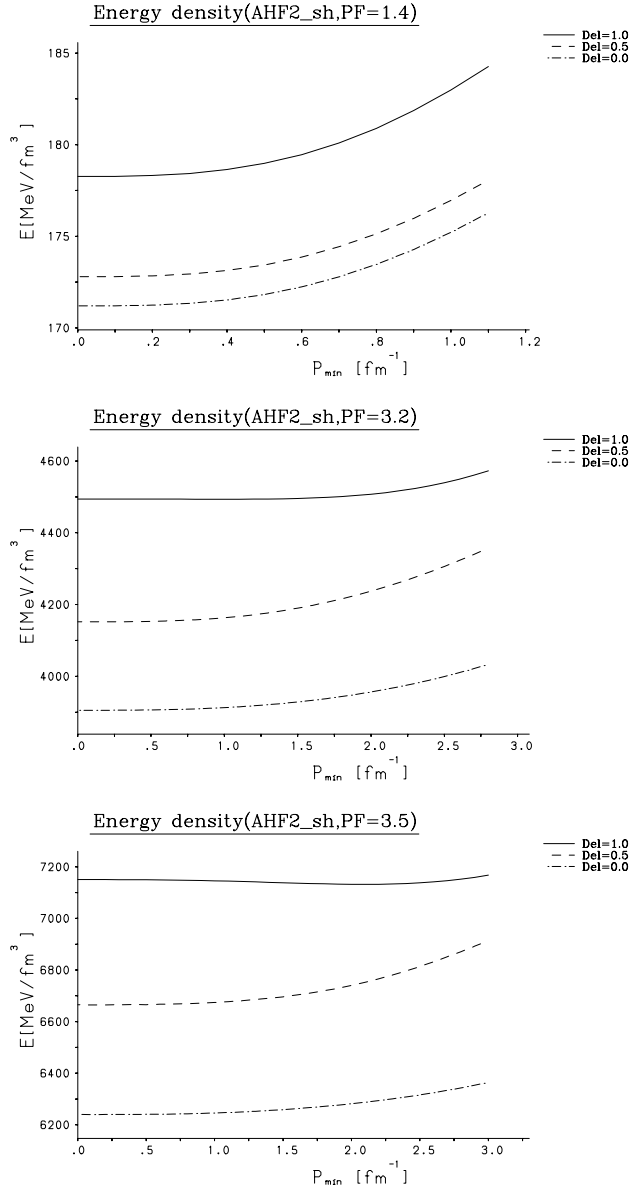


Figure 25: Energy density of asymmetric nuclear matter as a function of P_{min} for shell distribution in the HF2($\sigma, \omega, \pi, \rho$).

C Appendix C

Non-rotating Neutron Star

Fig. 26 - Fig. 27

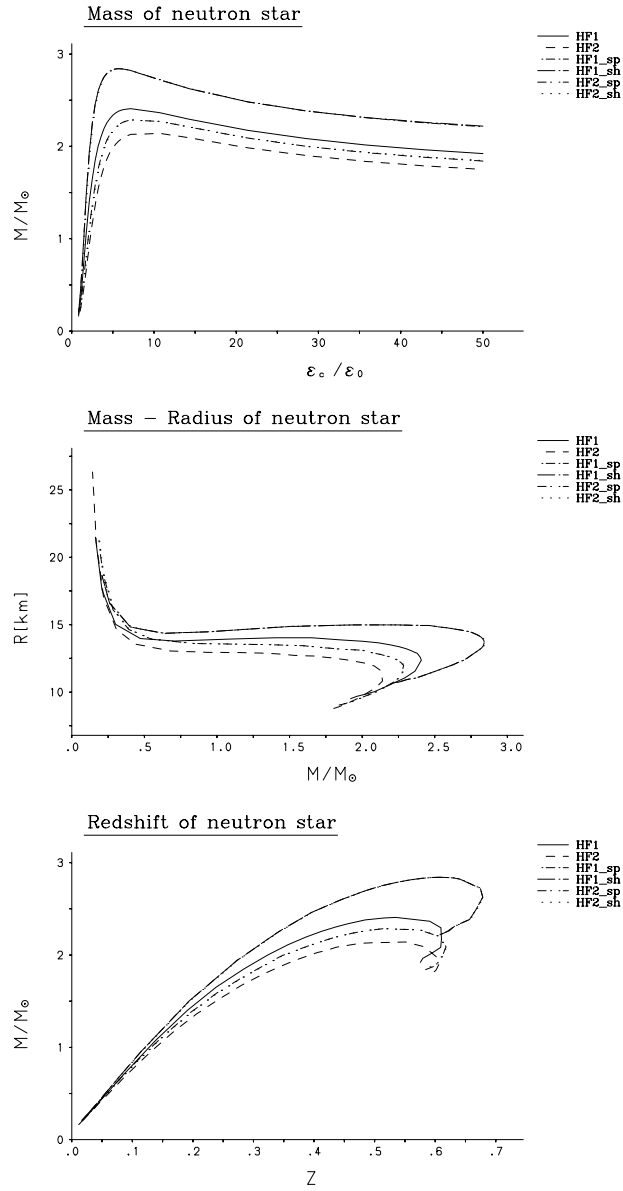


Figure 26: Mass, radius and redshift of non-rotating neutron stars in the Hartree-Fock calculations for the spherical ($HF1_{sp}, HF2_{sp}$) and the shell ($HF1_{sh}, HF2_{sh}$) structure of pure neutron matter. There are very small differences in results between the spherical and shell structure. The results for neutron star matter are also illustrated.

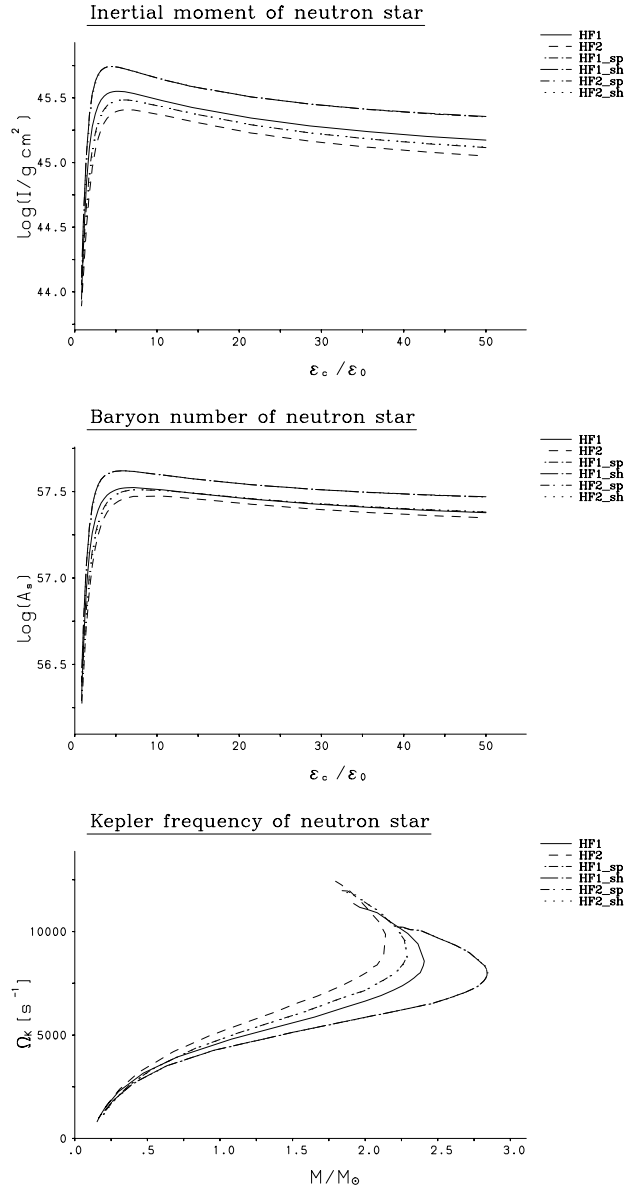


Figure 27: Inertial moment, baryon number of non-rotating neutron stars for the same models and matter as those in Fig. 26. Here Kepler frequencies are the results of Eq.(6.54).

D Appendix D

Rotating Neutron Star

Fig. 28 - Fig. 31

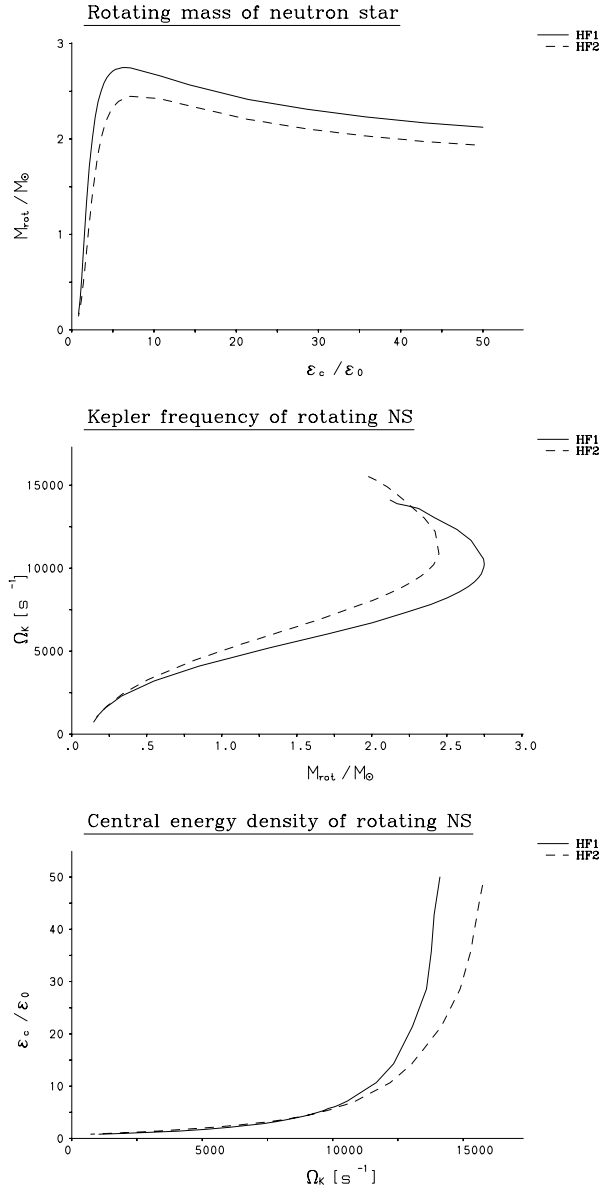


Figure 28: Maximum mass, Kepler frequency and central energy density of rotating neutron stars in the Hartree-Fock approximations, HF1(σ, ω) and HF2($\sigma, \omega, \pi, \rho$). The results are obtained for neutron star matter.

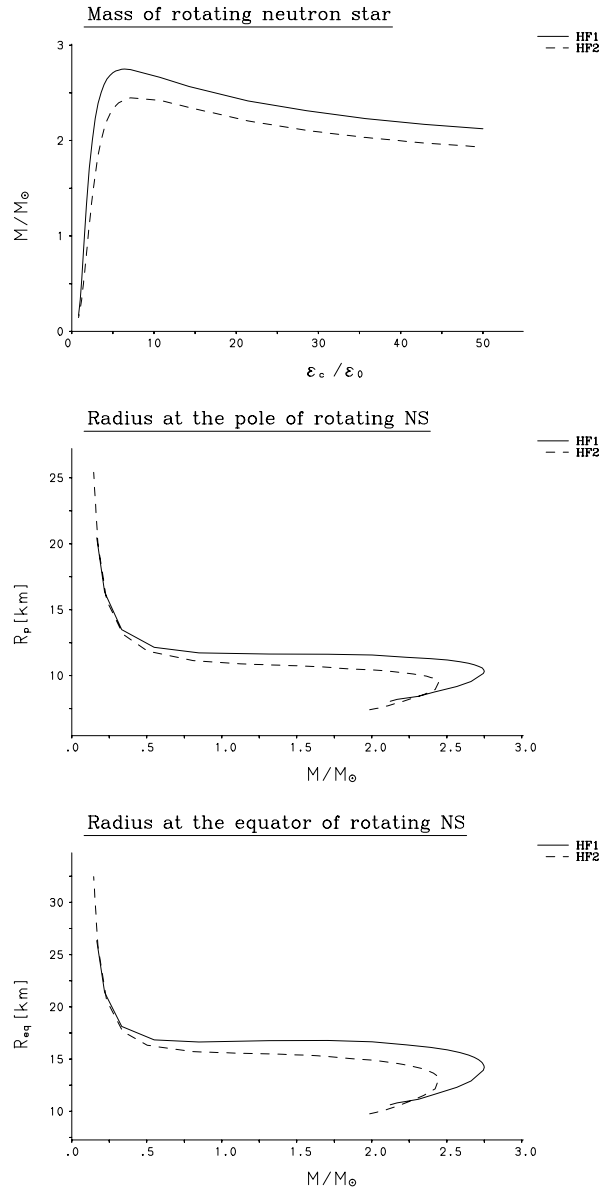


Figure 29: Gravitational mass and radius of rotating neutron stars in the Hartree-Fock approximations, $\text{HF1}(\sigma, \omega)$ and $\text{HF2}(\sigma, \omega, \pi, \rho)$. The results are obtained for neutron star matter.

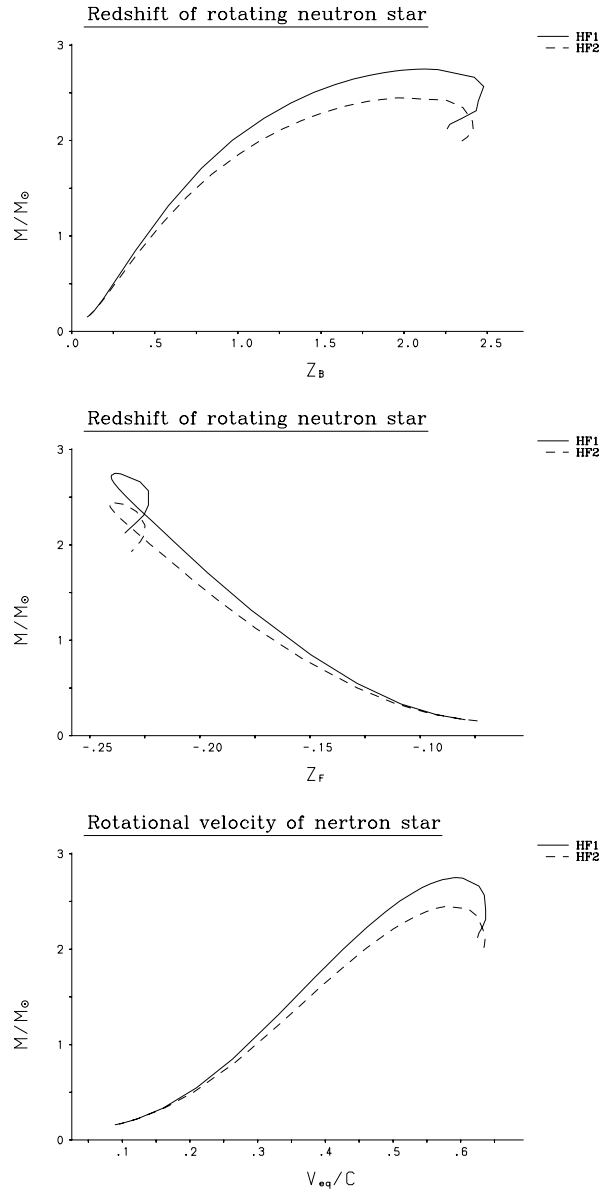


Figure 30: Redshift and rotational velocity of rotating neutron stars in the Hartree-Fock approximations, $HF1(\sigma, \omega)$ and $HF2(\sigma, \omega, \pi, \rho)$. The results are obtained for neutron star matter.

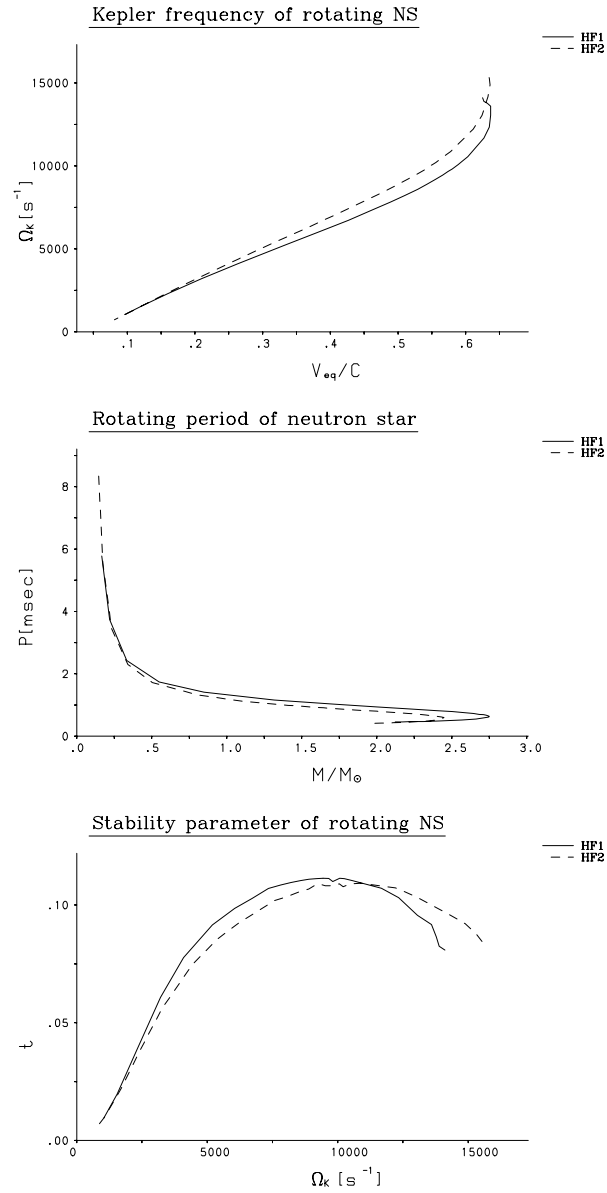


Figure 31: Kepler frequency, rotating period and stability parameter of rotating neutron stars in the Hartree-Fock approximations, HF1(σ, ω) and HF2($\sigma, \omega, \pi, \rho$). The results are obtained for neutron star matter.

References

- [1] B. K. Harrison and J. A. Wheeler, cited in B. K. Harrison et al. *Gravitation Theory and Gravitational collapse*, University of Chicago Press, Chicago, 1965.
- [2] J. W. Negele and D. Vautherin, Nucl. Phys. A207 (1973) 298.
- [3] F. Weber, Habilitation Thesis, University of Munich, 1992.
- [4] C. J. Horowitz and B. D. Serot, Nucl. Phys. A399 (1983) 529.
- [5] B. Ter Haar, R. Malfliet, Phys. Rev. Lett. 59 (1987) 1652.
- [6] F. Weber, N. K. Glendenning, and M. K. Weigel, Astrophys. J. 373 (1991) 579.
- [7] F. Weber, M. K. Weigel, Nucl. Phys. A505 (1989) 779.
- [8] C. J. Horowitz and B. D. Serot, Phys. Lett. 109B (1982) 341.
- [9] Y. Yang, S. Gao, Nucl. Phys. A514 (1990) 706.
- [10] S. L. Shapiro and S. A. Teukolsky, *Black holes, White Dwarfs, and Neutron stars*, John Wiley & Sons, N.Y., 1983.
- [11] B. D. Serot and J. D. Walecka, Adv. Nucl. Phys. 16 (1986) 1.
- [12] N. Glendenning, S. Pei, F. Weber, Phys. Rev. Lett. 79 (1997) 1603.
- [13] P. Poschenrieder, Dissertation, University of Munich, 1987.
- [14] J. D. Bjorken and S. D. Drell, *Relativistic Quantum Fields*, Mc Graw-Hill, New York, 1965.
- [15] L. Wilets, Green's functions method for the relativistic field theory many-body problem, in *mesons in nuclei*, Vol. III, ed. M. Rho, D. Wilkinson, North-holland, Amsterdam, 1979.
- [16] F. Weber, M. K. Weigel, Z. Phys. A330 (1988) 249.
- [17] L. Dolan and R. Jackiw, Phys. Rev. D 9 (1974) 3320.
- [18] M. K. Weigel and G. Wegmann, Fortschr. Phys. 19 (1971) 451.
- [19] M. Jetter, F. Weber, M. K. Weigel, Europhys. Lett. 14 (1991) 633.
- [20] R. M. Barnett *et al.*, Phys. Rev. D54 (1996) 1.
- [21] Ch. W. Misner, K. S. Thorne, and J. A. Wheeler, *Gravitation*, W. H. Freeman and Company, San Francisco, 1973.
- [22] J. R. Oppenheimer and G. M. Volkoff, Phys. Rev. 55 (1939) 374.

- [23] J. B. Hartle, *Astrophys. J.* 150 (1967) 1005.
- [24] J. M. Irvine, *Neutron stars*, Clarendon Press, Oxford, 1978.
- [25] J. L. Friedman, J. R. Ipser, and L. Parker, *Astrophys. J.* 304 (1986) 115.
- [26] J. C. Collins and M. J. Perry, *Phys. Rev. Lett.* 34, (1975) 1353.
- [27] J. H. Taylor and J. M. Weisberg, *Astrophys. J.* 345 (1989) 434.
- [28] P. Haensel and J. L. Zdunik, *Nature* 340 (1989) 617.
- [29] J. L. Friedman, J. R. Ipser, and L. Parker, *Phys. Rev. Lett.* 62 (1989) 3015.
- [30] H. Mishra, S. P. Misra, P. K. Panda and B. K. Parida, *Int. J. Mod. Phys. E2* (1993) 547.
- [31] L. Engvik, G. Bao, M. Hjorth-Jensen, E. Osnes, E. Oestaard, *Astrophys. J.* 469 (1996) 794.
- [32] Shmuel Balberg, Avraham Gal, *Nucl. Phys. A625* (1997) 435.
- [33] P. C. Martin and J. Schwinger, *Phys. Rev.* 115(1959) 1342.
- [34] V. Trimble and M. Rees, *Astrophys. Lett.* 5(1970) 93.
- [35] E. P. Liang, *Astrophys. J.* 304 (1986) 682.

Danksagung

Mein herzlicher Dank gilt Herrn Prof. Dr. M. K. Weigel.

Curriculum Vitae

I was born in a village in Chungcheong Province in Korea on Nov. 11, 1957 as the first child. I entered primary school near our village. After primary school I entered middle school in town ,Cho Chi Won. I entered high school in the city of Taejeon. I studied physics at the Chungnam National University. I received a Bachelor's of Science degree in 1980 from the Chungnam National University. Continuously I studied physics at Graduate School at the Chungnam National University. During Graduate School I served as a research assistant from 1981–1983. I received a Master's of Science degree in 1982 from the Chungnam National University. Then I served as a teaching assistant at the Chungnam National University from 1983–1985. After then I served as a Part-Time Instructor at the Chungnam National University from 1985–1988. In 1988 I have got married. I visited the German Language School at the University of Wuerzburg and at the University of Munich. I studied physics at the University of Munich. Since 1992 I have worked as a Ph.D. student at the University of Munich.